

INFORMATION TO USERS

This manuscript has been reproduced from the microfilm master. UMI films the text directly from the original or copy submitted. Thus, some thesis and dissertation copies are in typewriter face, while others may be from any type of computer printer.

The quality of this reproduction is dependent upon the quality of the copy submitted. Broken or indistinct print, colored or poor quality illustrations and photographs, print bleedthrough, substandard margins, and improper alignment can adversely affect reproduction.

In the unlikely event that the author did not send UMI a complete manuscript and there are missing pages, these will be noted. Also, if unauthorized copyright material had to be removed, a note will indicate the deletion.

Oversize materials (e.g., maps, drawings, charts) are reproduced by sectioning the original, beginning at the upper left-hand corner and continuing from left to right in equal sections with small overlaps.

Photographs included in the original manuscript have been reproduced xerographically in this copy. Higher quality 6" x 9" black and white photographic prints are available for any photographs or illustrations appearing in this copy for an additional charge. Contact UMI directly to order.

ProQuest Information and Learning
300 North Zeeb Road, Ann Arbor, MI 48106-1346 USA
800-521-0600

UMI[®]

University of Alberta

**Antibody Labeling Methods for Automated Affinity
Electrophoresis on Microchips**

By

Said Attiya



A thesis submitted to the Faculty of Graduate Studies and research in partial fulfillment
of the requirements for the degree of

Doctor of Philosophy

Department of Chemistry

Edmonton, Alberta

Spring, 2000



**National Library
of Canada**

**Acquisitions and
Bibliographic Services**

**395 Wellington Street
Ottawa ON K1A 0N4
Canada**

**Bibliothèque nationale
du Canada**

**Acquisitions et
services bibliographiques**

**395, rue Wellington
Ottawa ON K1A 0N4
Canada**

Your file *Votre référence*

Our file *Notre référence*

The author has granted a non-exclusive licence allowing the National Library of Canada to reproduce, loan, distribute or sell copies of this thesis in microform, paper or electronic formats.

The author retains ownership of the copyright in this thesis. Neither the thesis nor substantial extracts from it may be printed or otherwise reproduced without the author's permission.

L'auteur a accordé une licence non exclusive permettant à la Bibliothèque nationale du Canada de reproduire, prêter, distribuer ou vendre des copies de cette thèse sous la forme de microfiche/film, de reproduction sur papier ou sur format électronique.

L'auteur conserve la propriété du droit d'auteur qui protège cette thèse. Ni la thèse ni des extraits substantiels de celle-ci ne doivent être imprimés ou autrement reproduits sans son autorisation.

0-612-59926-4

Canada

University of Alberta

Library Release Form

Name of Author: **Said Attiya**

Title of Thesis: **Antibody Labeling Methods for
Automated Affinity Electrophoresis
on Microchips**

Degree: **Doctor of Philosophy**

Year this Degree Granted: **2000**

Permission is hereby granted to the University of Alberta Library to reproduce single copies of this thesis and to lend or sell such copies for private, scholarly, or scientific research purposes only.

The author reserves all other publication and other rights in association with copyright in the thesis, and except as hereinbefore provided, neither the thesis nor any substantial portion thereof may be printed or otherwise reproduced in any material form whatever without the author's prior written permission.

Author's Signature:  _____

Address: Apt. 23, 10745-110 st.,
Edmonton, AB
T5H 3C9
CANADA

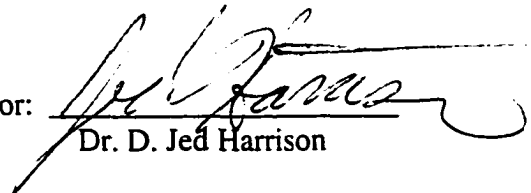
Date: March 28, 2000

University of Alberta

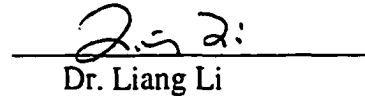
Faculty of Graduate studies and Research

The undersigned certify that they have read, and recommend to the Faculty of Graduate Studies and Research for acceptance, a thesis entitled **Antibody Labeling Methods For Automated Affinity Electrophoresis On Microchips** submitted by **Said Attiya** in partial fulfillment of the requirements for the degree of **Doctor of Philosophy**.

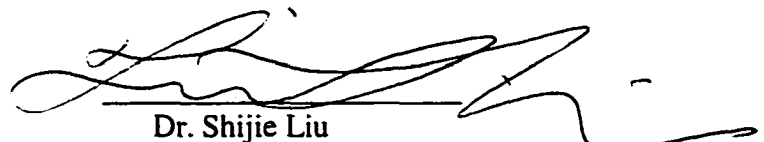
Supervisor:


Dr. D. Jed Harrison


Dr. Frederick F. Cantwell


Dr. Liang Li


Dr. Glen R. Loppnow


Dr. Shijie Liu

External Examiner:


Dr. Hélène Perreault

Date: March 3, 2000

Abstract

Development of an automated microchip-based instrument for immunoassay analysis of toxins and pathogens in environmental aerosols required (1) an ovalbumin assay for field-trial testing with this common simulant; and (2) a fluidic interface for automated sample introduction into the microfluidic chip. To develop a direct immunoassay for ovalbumin on microchip-based capillary electrophoresis (CE) with laser induced fluorescence detection (LIF), a labeled monoclonal antibody (mAb*) is needed. In this assay, the Cy5-labeled antibody reacted with ovalbumin and the products (i.e., complex and free antibody) were separated with CE and detected by LIF. However, direct derivatization of antibody with Cy5 dye renders the antibody inactive, so that the complex (ovalbumin-mAb*) was not detected by capillary electrophoresis. We developed an affinity protection technique to label the monoclonal antibody with Cy5 dye. In this approach, ovalbumin was immobilized on Cyanogen bromide-activated Sepharose 4B beads and antibody reacted with ovalbumin, thus protecting its active site. Then, the reactive Cy5 dye was added to label the antibody. Description of the procedure is given. The Cy5-labeled antibody was tested by capillary electrophoresis and the results showed that the antibody was active and homogeneously labeled.

For automation of sample introduction into the chip, a novel low flow resistance interface was constructed on-chip. A sample introduction channel (SIC), 0.3 mm deep and 1 mm wide, was fabricated into the chip. The other channels on the chip were 13 μm deep and 65 μm wide. Thus the large difference in channel dimensions was employed to demonstrate a rapid sample exchange and to introduce the sample into the SIC using a peristaltic pump at a flow rate 1 ml/min without the risk of contamination of narrower

channels. We described an interface assembly for microchip to monitor changing concentrations of fluorescein. This assembly can be connected to an aerosol collector.

.

Acknowledgments

It is very difficult to express the gratitude to everyone without feeling melancholy. I am really in debt for many people who made my life simple and enjoyable.

First, and foremost, my most sincere thanks go to Professor Jed Harrison, my research advisor, without whom none of the work presented in this thesis would have materialized. I thank him for his patience, guidance, his caring, and financing my trips abroad to attend conferences.

I thank also all the group members in Professor's Harrison research group for the fun, sharing their experience and wisdom over the years. In particular, Jessica Roberts for reading the chapters and her comments, Hossein Salimi-Moosavi for his sincere help and being available all the time, Youssouf Badal for his constant jokes, Nghia Chiem for sharing ideas and being helpful, and Abebaw Jemere for friendship.

I would like to send my thanks to Professor Fred Cantwell for his help, advice and kindness. When I was teaching assistant for environmental course that he taught I learned a lot from him.

Dr. H el ene Perreault and Dr. Glen Loppnow and other members of my examining committee, whose comments and suggestions were very useful in the preparation of this thesis.

My many thanks go to Dr. Bill Lee, principal investigator of the DARPA project, for his endless help and support. I was really lucky to work with him. Also my appreciation goes to T. Dickinson for her cooperation in measurements of affinity constant of antibody. My gratitude also goes to Dr. David Mah from Canada West Biosciences for providing me the ELISA data.

To my parents, brothers and my sister, I thank you for the love and support you have given me throughout my student years.

My wife, my daughter and my son I do not know what to do to repay all the harsh and bad times they all had to help me complete my studies. They all are and will be forever in my heart. I wish to be able to make them happy.

Table of Contents

Chapter 1

Introduction

1.1	Miniaturized total-analysis systems (μ TAS)	1
1.1.1	Examples of current research activity in μ TAS fields	3
1.2	Tools of the mission	5
1.2.1	Chip material	5
1.2.2	Micromachining	6
1.2.3	Micromachining terms	7
1.3	Capillary electrophoresis (CE)	10
1.3.1	Electrical double layer and source of EOF	12
1.4	Antigens and haptens	15
1.5	Antibodies	16
1.5.1	Antibody-Antigen interactions	18
1.6	Affinity chromatography	20
1.6.1	Chromatographic supports	22
1.6.2	Protein A and protein G affinity chromatography	23
1.7	Scope of the thesis	25
1.8	References	27

Chapter 2

Characterization of ovalbumin assay using microchip and Beckman CE

2.1	Introduction	32
2.2	Experimental	34
2.2.1	Beckman CE instrument	34
2.2.1.1	Electrophoresis on Beckman CE	35
2.2.2	Microchip devices	36
2.2.2.1	Detection system and data acquisition	40
2.2.2.2	Conditioning the chip	42
2.2.2.3	CE on chip	44
2.2.3	Chemicals	44
2.2.4	Sample preparation	45
2.2.5	Direct ovalbumin assay	45
2.3	Results and Discussion	46
2.3.1	Electrical and Fluid Interface Plates of DARPA instrument	46
2.3.2	Protein separations and immunoassay	48
2.3.3	Antibody labeling difficulties	53
2.4	Conclusions	61
2.5	References	62

Chapter 3

Affinity protection chromatography for labeling mouse monoclonal antibody (IgG1) with Cy5 dye

3.1	Introduction	64
3.2	Experimental	68
3.2.1	Material and reagents	68
3.2.2	Electrophoresis	69
3.2.3	Purification of the mouse IgG1	69
3.2.4	Direct or precolumn derivatization of mouse IgG1	70
3.2.5	Enzyme-Linked Immunosorbent Assay (ELISA)	70
3.2.6	Direct derivatization controlling the dye to protein ratio	71
3.2.7	Immobilization of ovalbumin on CNBr-activated Sepharose 4B	72
3.2.8	Labeling of immobilized mAb to ovalbumin column	73
3.3	Results and Discussion	75
3.3.1	Calculation of dye to antibody ratio(D/P)	80
3.3.2	Disadvantages of direct derivatization	81
3.3.3	Affinity protection chromatography	88
3.3.3.1	Recovery and D/P ratio of labeled antibody	91
3.3.3.2	Thermodynamics factors affecting amount of mAb bound to CNBr-ov column	92
3.3.3.3	Alternative gel matrices	95
3.4	Conclusions	96
3.5	References	98

Chapter 4

Measurement of affinity constant of anti-ovalbumin using CE

4.1	Introduction	101
4.2	Data Analysis	107
4.3	Experimental	109
4.3.1	Chemicals	109
4.3.2	Apparatus	109
4.3.3	Procedure	109
4.3.4	Data handling	111
4.4	Results and Discussion	112
4.4.1	Reaction time required to reach equilibrium	112
4.4.2	Measurements of association constant between ovalbumin and antibody in their native states	112
4.4.3	Measurements of Cy5-labeled anti-ovalbumin affinity constant	116
4.4.4	Non-linear least squares analysis (NLLS)	118
4.4.4.1	Fitting the binding data to two binding sites	121
4.5	Effect of affinity constant (K_a) on the detection limit	122
4.6	Conclusions	124
4.7	References	125

Chapter 5

Automation of sample introduction into microchip-based CE

5.1	Introduction	130
5.2	Experimental	132
5.2.1	Materials and Reagents	132
5.2.2	Instrumentation	133
5.2.3	Device fabrication	133
5.2.4	Sample exchange	135
5.2.5	On-line Monitoring	137
5.2.6	Investigations of SIC of DARPA device	139
5.3	Results and Discussion	140
5.3.1	Theory	141
5.3.2	Preferential flow design and device testing	143
5.3.3	Exchanging of Phe-FITC and Arg-FITC solutions into the chip	147
5.3.4	Calibration curve of fluorescein using on-line monitoring setup	149
5.3.5	Testing the SIC of the DARPA device	151
5.4	Conclusions	154
5.5	References	155

Chapter 6

Conclusions

6.1	Summary	157
6.2	Future directions	159
6.2.1	APC for labeling antigens	159
6.2.2	Preconcentration and labeling on microchips	159

List of Figures

Figure 1.1	Process steps in a standard one-mask micromachining procedure for an isotropically etching a channel into glass substrate. _____	8
Figure 1.2	Schematic illustrating the principle of CE. _____	11
Figure 1.3	Representation of the electrical double layer versus distance from the capillary wall. (Adapted from Ref.[41]). _____	11
Figure 1.4	Schematic diagram for an antigen with three different epitopes and hapten with one epitope. _____	16
Figure 1.5	Schematic representation of polypeptide chains in the basic immunoglobulin structure. _____	17
Figure 1.6	(A) Intermolecular attractive forces binding antigen to antibody. (B) Two examples of a good and a poor fit between the antigen and antibody. _	19
Figure 2.1	DARPA Chip layout for single channel instrument. _____	37
Figure 2.2	Layout of Faster chip with sample introduction channel. _____	39
Figure 2.3	Experimental set up with LIF detection. Cross-sectional view of the microchip is shaded. _____	41
Figure 2.4	Schematic diagram for single power supply and two relays showing the relay setup during the injection mode. _____	43
Figure 2.5	Photograph of the DARPA instrument _____	47
Figure 2.6	Electropherograms of (A) ovalbumin (50 $\mu\text{g/ml}$), (B) polyclonal antibody (50 $\mu\text{g/ml}$), and (C) nonpurified monoclonal antibody (100 $\mu\text{g/ml}$). _	51
Figure 2.7	Separation of a mixture of ovalbumin and polyclonal antibody. Molar ratio of ovalbumin to monoclonal antibody was 9:1. _____	52
Figure 2.8	Calibration curve of direct immunoassay for ovalbumin with fixed concentration 50 $\mu\text{g/ml}$ polyclonal antibody using Beckman CE system model 5010. _____	54
Figure 2.9	Bifunctional Cy5 dye absorption and fluorescence spectra. (Adapted from data sheet of Amersham with modification). _____	55

- Figure 2.10** Electropherogram of 200 nM bifunctional Cy5 dye using DARPA device and LIF detection; excitation wavelength 632.5 nm using He-Ne laser (5 mW) and emission monitoring at 675 nm, separation voltage -6kV .__ 55
- Figure 2.11** Electropherograms of Cy5-labeled monoclonal antibody (A) and mixture of nonlabeled ovalbumin and monoclonal antibody (B). (molar ratio of ov/mAb = 9:1). _____ 58
- Figure 2.12** Electropherograms of Cy5-labeled mAb, 50 $\mu\text{g/ml}$ and ov present at a molar ratio of ov/mAb*=9:1. _____ 60
- Figure 3.1** Mechanism of mouse monoclonal antibody (IgG1) purification from ascites fluid using 2 ml of gel of recombinant protein G immobilized on agarose beads. _____ 77
- Figure 3.2** Elution profiles of mouse IgG1 from protein G column. _____ 77
- Figure 3.3:** Electropherogram of purified antibody from protein G column without desalting the elution buffer. _____ 79
- Figure 3.4** Electropherogram of purified antibody eluted from PD-10 desalting. _ 79
- Figure 3.5** UV/Vis spectrum of Cy5-labeled antibody synthesized using affinity chromatography _____ 82
- Figure 3.6** Structure of bifunctional Cy5 dye. _____ 82
- Figure 3.7** ELISA results for labeled and unlabeled monoclonal antibody. _____ 84
- Figure 3.8** Electropherograms of Cy5-labeled rabbit polyclonal antibody with various D/P ratios, (Panel A). The D/P ratio is indicated next to the labeled antibody. Electropherograms of binding of ovalbumin to labeled antibody,(Panel B). _____ 87
- Figure 3.9** (A) Coupling reaction of ovalbumin to CNBr-activated Sepharose 4B beads. (B) Schematic diagram for affinity protection chromatography (APC). _____ 89
- Figure 3.10** Electropherograms Cy5-labeled mAb (mAb*) using affinity protection chromatography (A) and separation of mAb* from its complex (B).__ 94

Figure 4.1	Schematic diagram showing the three modes of Affinity Capillary Electrophoresis (ACE).	104
Figure 4.2	Multiple curve fitting for an electropherogram of a binding experiment using Igor pro.	111
Figure 4.3	Electropherograms of mixtures of native ovalbumin and its monoclonal antibody.	113
Figure 4.4	Electropherogram showing saturation of antibody.	114
Figure 4.5	CE-derived Scatchard plot for the interaction of ovalbumin and non labeled antibody.	115
Figure 4.6	CE-derived Scatchard plot of Cy5-labeled antibody and native ovalbumin.	118
Figure 4.7	Non-linear least squares analysis of the interaction of ovalbumin and antibody.	120
Figure 5.1	Sequence of sample exchange of Phe-FITC and Arg-FITC on the Faster chip.	136
Figure 5.2	Leak-free assembly for continuous monitoring.	138
Figure 5.3	Electron micrograph of Faster device showing sample introduction channel etched to ca. 1mm wide and 300 μm deep intersecting with injection channel etched to 36 μm wide and 10 μm deep.	140
Figure 5.4	Relation between F and ratio of half width and depth. (Adapted from Ref. [21]).	141
Figure 5.5	(A) Equivalent lengths of Faster layout.	144
Figure 5.6	(A) DARPA layout. (B) Equivalent fluid resistance network of the shallow channels on the DARPA chip.	145
Figure 5.7	Electropherograms of Phe-FITC and Arg-FITC acquired from the sequence in Figure 5.1.	148
Figure 5.8	Calibration curve of fluorescein.	150

Figure 5.9 (A) Electropherogram of 200 nM bifunctional Cy5 dye when pump was off. (B) Electropherogram of Cy5 dye when the pump was on under the same experimental conditions as (A). _____ 152

Figure 6.1 Drawing of cross-section of packed chamber, showing weir heights in relation to channel depth and particle size. _____ 160

Figure 6.2 Proposed microchip design to preconcentrate, derivatize, reaction, and detection of an antibody. _____ 160

List of Tables

Table 1.1	Summary of binding of different immunoglobulins to protein G and A (Pharmacia). _____	24
Table 2.1	Dimensions of DARPA chip _____	38
Table 2.2	Dimensions of Faster chip _____	39
Table 3.1	Summary of results from affinity protection column _____	90
Table 4.1	The concentration of antigen required to saturate 253 nM antibody and the dependence on the K_a of the reaction _____	123

Chapter 1

Introduction

1.1 Miniaturized total-analysis systems (μ TAS)

The concept of total chemical analysis (TAS) was first envisioned by the late Michael Widmer and coworkers [1] at the central research Laboratories of Ciba Geigy in Basel, Switzerland. The motivation was to integrate all necessary steps of an analytical process into a single automated instrumental system. A typical analytical operation for a bench top instrument includes the following steps: sampling and sample transport; sample pretreatment; separation; measurement; data analysis and interpretation. Although adherence to this code of chemical analysis enhances the accuracy and reproducibility in analytical measurements, it can also result in processes that are time consuming and/or labor intensive. To overcome this, the analytical process may be automated, which may make it more rapid and improves its reproducibility by minimizing the human involvement in the sample handling steps. Automation refers to the design of an overall flow system which facilitates automated manipulation and analysis of samples, using more complex processes than have been routinely employed in Flow Injection Analysis (FIA) [1]. From this strategy of automation for chemical analysis has evolved the concept of the total chemical analysis system or TAS [2]. Examples of TAS include: (a) gas chromatograph-based monitors for trace analysis in air [3], an on-line glucose analyzer for bioprocess control [4], a supercritical fluid chromatograph-based monitor for control process [5], and high speed capillary electrophoresis as a detector for HPLC [6].

A miniaturized total-analysis system (μ TAS) carries out all sample handling on a micrometer scale using a centimeter-sized glass, silicon, or plastic chip. Miniaturization

of instrumentation was first demonstrated in 1979 [7] when a micromachined gas chromatograph was placed on a 5 cm silicon chip. The essential difference between μ TAS and TAS is the distance over which the sample has to travel between various stages of analysis and the concomitant reductions in volume. The overall reduction in the dimensions of the flow channels should result in an enhancement of the analytical performance. For example, mass transport by diffusion is 100 times faster when a system is 10 fold smaller, so that diffusion can be used as an efficient form of mixing [8]. The same type of relationship is obtained with heat transport, improving heat dissipation in the fluid. In a chemical separation such as electrophoresis, the time scale of the separation can also be shortened because the separation lengths can be made shorter. The other practical benefits of μ TAS devices are a considerable reduction in solvent and reagent use, smaller sample volumes and high sample throughput. Throughput is a function of speed and parallelism [9-11]; that is, carrying out a number of analyses in parallel on the same microfluidic chip. For example, Mathies et al. [12] designed a microfabricated chip in a 10 cm diameter wafer which can analyze up to 96 DNA samples in parallel. The fragment sizing throughput is as fast as 1 sample/s.

CE-based μ TAS was first explored by Manz et al., and Harrison et al. [13,14]. A μ TAS chip is a microfabricated network of capillaries on a planar substrate formed using photolithographic techniques. The typical dimensions of the capillaries are 30-100 μ m wide and 10-50 μ m deep. CE-based μ TAS chips utilize electroosmotic flow (EOF) (see section 1.2) for pumping fluid during sample transport, injection and separation. EOF pumping is well-suited to μ TAS for the following reasons:

- (1) It has a plug flow profile (no-cross sectional flow velocity differences in contrast to hydraulic flow)
- (2) The linear EOF velocity is independent of the channel width.
- (3) No column back-pressure is generated by small channel dimensions.

In contrast, methods utilizing conventional pumps develop extremely high back-pressures with small capillary dimensions, and are not well-suited to delivery of such low volumes [1,15].

In the last decade, the interest in μ TAS has rapidly increased. For recent reviews, see Ref. 16-20 and also the μ TAS conference proceedings published biannually since 1994. [21-23].

1.1.1 Examples of current research activity in μ TAS fields

Ekström et al [24] were first to demonstrate a DNA separation on chip. The restriction fragments of Φ X-174 DNA (Hae III digest) were separated using 10% linear acrylamide, and the analysis was completed in less than 30 min. Since then many microsystems have been designed for genetic analysis [9-11, 25]. For example, Kopp et al. [25] used a micromachined glass chip with a single capillary channel for the polymerase chain reaction (PCR) of DNA. The device employs three well-defined temperature zones on a glass microchip. PCR theoretically doubles the concentration of a specific DNA fragment in a sample in each cycle through the three zones.

Hadd et al. [26] performed an automated enzyme assay within microfabricated chips. The enzyme β -Galactosidase (β -Gal) was assayed using resorufin β -D-galactopyranoside (RBG), a substrate that is hydrolyzed to resorufin, a fluorescent product. In this microchip system, fluid flow and reagent mixing are achieved using the electroosmotic

phenomenon, which is controlled by regulating the applied potentials at the terminus of each channel of the microchip. The relative inhibition of β -galactosidase by lactose, p-hydroxymercuribenzoic acid, and β -D-thiogalactoside was determined by using an electric field to vary the inhibitor concentration with constant enzyme and substrate concentration.

Devices for point of care clinical analyses [27,28] are also of interest to many groups. Kouny et al. [27] examined competitive immunoassay in which both labeled cortisol and the sample (nonlabeled) cortisol compete for a limited amount of antibody. The separation and quantitation of bound and free cortisol was carried out in channels micromachined into fused silica substrates. The separation was performed in less than 30 s. The assay achieves the determination of cortisol in blood serum over the range of clinical interest (1-60 μ g/dL).

Chiem et al. [28] mixed on-chip a diluted serum sample containing the drug theophylline with fluorescence-labeled theophylline and anti-theophylline antibody. Free theophylline competes with tracer-bound theophylline for a limited amount of the antibody. Electroosmotic pumping was used to control the mixing and the reaction of the reagents and serum sample. After reaction, the solution was injected into an electrophoresis channel integrated within the same chip. The separated free and bound tracers were measured by fluorescence detection, yielding data from which the concentration of the drug in the serum can be calculated.

Analytical systems for use in defense against biological and chemical weapons [28,29] represent a potential application area for μ TAS. Biological weapons would be particularly attractive to terrorist groups because of their stealthy yet powerful nature: for

example, one gram of Anthrax has the potential to kill 10 million people. Use of such weapons would likely not become apparent until several days later, when enough people started getting sick. This would make it difficult to identify the perpetrators and would leave no logical target for a military counterstrike. Although there is a treaty to prohibit the use of biological weapons, this would not deter the bio-terrorist from employing such weapons. The latest terrorist attack was from Aum Shin Rikyo, the Japanese cult that released the nerve gas in Tokyo's subway in 1995. In the worst scenario, where biological germs were spread, there would have not been enough vaccine to treat the people, even assuming the biological weapon was known.

Our group, in collaboration with Defense Research Establishment Suffield (DRES), Dycor and Alberta Microelectronic Center (AMC) has developed a robust and portable single channel CE-based bench top immunoassay instrument for the determination of biowarfare simulation agents [28]. The work in this thesis contributed to the development of the single channel microchip CE-based instrument. A brief description of the instrument is given in chapter 2.

1.2 Tools of the mission

1.2.1 Chip material

At present, the typical wafer used for a miniaturized chemical system consists of 3- or 4 inch squares of silicon, glass, quartz or plastic that are etched or molded with chambers or channels. Within this research group, the channels are typically 10 μm deep and 30 μm wide. The chips are covered with a top plate to contain the sample and reagents (see section 1.2.2).

Each material has its own advantages and disadvantages. Quartz is suitable for CE because it is a good electrical insulator and it is transparent to UV light required for absorbance. Other glasses may also be used, although they may have reduced optical qualities. Silicon is a semiconductor and the application of high voltages to a silicon microchip is virtually impossible. Silicon and glass microfluidic chips usually are fabricated using standard photolithographic methods developed for microelectronics (see section 1.2.2). Polymers such as polymethylmethacrylate (PMMA) and polycarbonate (PC) have the potential of being mass-produced inexpensively, compared to chips made from silicon or glass. Laser ablation [31], injection molding [32], silicon rubber casting [33], or embossing [34], are different microfabrication methods for the microchannel formation in the polymer substrate.

1.2.2 Micromachining

For the designs used throughout the thesis we used a two-mask process, because the chip contained two different types of channels. These were the narrow channels that were 10 μm deep and 30 μm wide, and a sample introduction channel that was 300 μm deep and 1 mm wide. In chapter 5, we describe in detail the fabrication of the devices with a sample introduction channel.

Micromachining refers to the fabrication of three dimensional micromechanical structures and related devices in silicon or other materials [35]. A standard one-mask micromachining procedure for etching a channel into a glass wafer is outlined in Figure 1.1.

1.2.3 Micromachining terms

(1) Surface micromachining is a process above the substrate, in other words mainly using the substrate as a base to build upon.

(2) Bulk micromachining is processing that removes "bulk" substrate (i.e., forming a large pits, or channels).

However, these definitions for structures tend to lose their meaning for some of the more complex (i.e., made from multiple pieces) structures. Most microfluidic chips can be categorized as being made by bulk micromachining.

(3) Photolithography is the technique by which a pattern is transferred to a layer of photoresist, the pattern itself being formed on a glass mask with dark and transparent surface regions to define the design. Masking is used to protect one area of the wafer while working on another. A photo aligner aligns the wafer to a mask and then projects an intense UV light through the mask and through a series of reducing lenses, exposing the photoresist with the mask pattern. Precise alignment of the wafer to the mask prior to exposure is critical.

(4) Etching is the process of removing layers of unwanted silicon, silicon dioxide, aluminum, and other materials from a wafer. This occurs after a wafer has a layer of photoresist, which has been exposed to UV light through a mask. The etching processes may be classified as either wet or dry. In wet chemical etching the wafer is immersed in an etching solution to etch only the desired material. For example, the chrome and gold layers are etched with a commercial Cr etch (KTI Chemicals, Sunnyside, CA, USA) and an aqueous potassium iodide/iodine solution, respectively. A mixture of concentrated HF:HNO₃:H₂O (22:14:66) is used for glass removal.

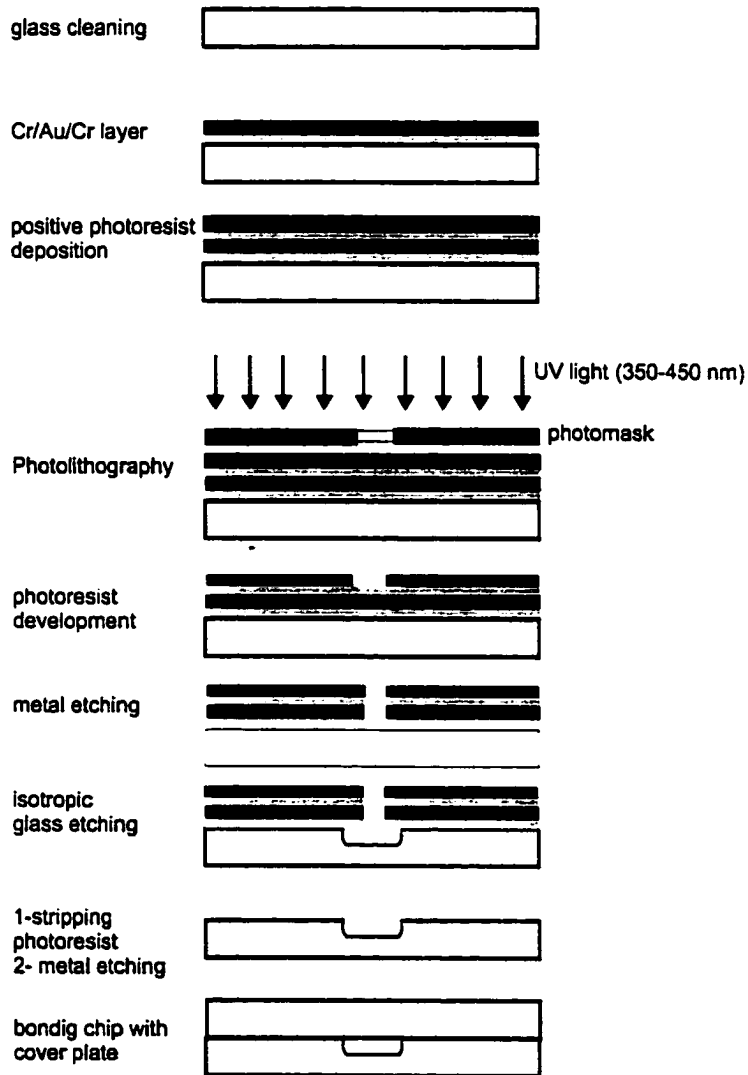


Figure 1.1 Process steps in a standard one-mask micromachining procedure for an isotropically etching a channel into glass substrate.

Isotropic etching refers to the process in which etching proceeds in all directions at the same rate, whereas, anisotropic etching occurs preferentially in one direction.

(5) In sputtering, the material to be deposited is literally thrown at the silicon wafer at a high velocity and the material displaces part of the silicon in the wafer. Sputtering is accomplished by ionizing Argon gas into a plasma and directing the plasma against a metallic target which may contain the aluminum, gold, or some other material to be deposited. The plasma causes some of the material to break off, or sputter. The plasma, which now contains some foreign material in it, is directed against a sample wafer. The material is then deposited onto the surface of the wafer.

This process occurs in a high vacuum chamber containing Argon gas at a pressure of 8×10^{-6} atmospheres. The sample wafer is placed in an electrode at one end in the chamber. Quite often it is necessary to deposit a thin (100-300 Å) adhesion layer of a reactive metal such as Ti or Cr beneath a relatively non-reactive metal such as Au or Pt that is used for photolithography. A bilayer of Cr/Au or a tri-layer of Cr/Au/Cr (200Å /1000Å /200Å) is sputtered onto glass substrates.

(6) Bonding refers to the assembly of wafers, whether this be silicon-to-silicon, glass-glass, silicon-to-glass or some other combination of materials. Because of the planarity of chip substrates, bonding usually results in fusion of etched channels and a perfectly tight seal. Bonding can be achieved either thermally [36], or anodically [37] depending upon the material.

1.3 Capillary electrophoresis (CE)

In early 1980, Jorgenson and Lukacs investigated and began to popularize capillary electrophoresis [38,39], which was called capillary zone electrophoresis (CZE) or high-performance capillary zone electrophoresis [40]. CZE is the most popular mode of capillary electrophoresis modes [41, 42]. The main features of CZE are low sample consumption, high resolution, and efficient separation. As shown in Figure 1.2, CE is performed in a capillary tube with a typical inner diameter of 10-100 μm and a total length of 27-100 cm. Capillaries are made of fused silica. Both ends of the buffer-filled capillary are immersed in buffer reservoirs that contain platinum electrodes. A high voltage in the range of 10-30 kV is applied to the electrodes. On-column detection is performed to avoid loss of separation efficiency caused by detector dead volume.

Fundamentally, two processes are associated with CZE: electrophoresis of charged species and electroosmosis of bulk solution. The electroosmosis occurs because of the surface charge, which controls the zeta potential of the wall of the capillary. At $\text{pH} > 3$, the silanol groups (Si-OH) are ionized to SiO^- and attract the cationic species in the buffer. Obviously, the fraction of the silanol groups that will be ionized will be determined by the pH. When the surface is negatively charged the ionic layer formed has a positive charge density that decreases approximately exponentially as the distance from the wall increases.

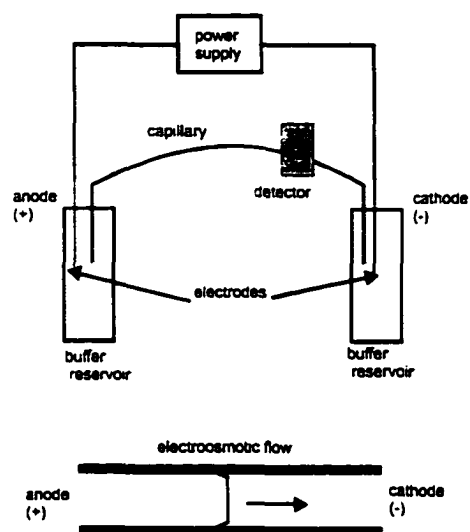


Figure 1.2 Schematic illustrating the principle of CE.

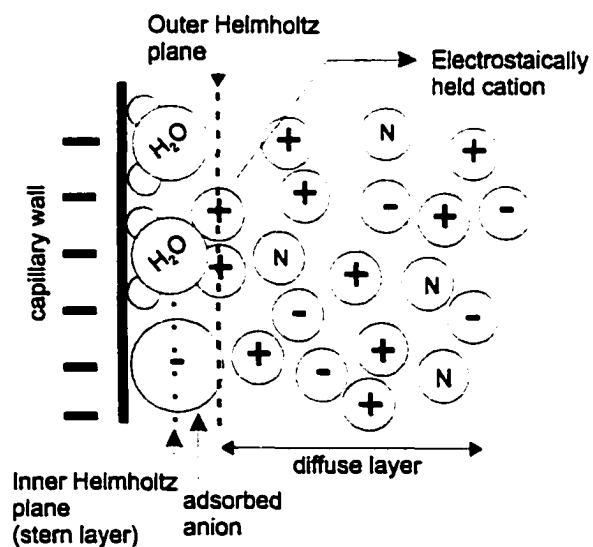


Figure 1.3 Representation of the electrical double layer versus distance from the capillary wall. (Adapted from Ref. [41]).

1.3.1 Electrical double layer and source of EOF

Figure 1.3 illustrates the structure of the electrical double layer formed at the capillary wall. When only electrostatic interactions operate, ions of the solution phase may approach the capillary wall so far as their inner solvation shells will allow. The surface array of ions is thus 'cushioned' from the electrode surface by a layer of solvent molecules (Figure 1.3). The line drawn through the center of such ions at this distance of closest approach marks a boundary known as the 'outer Helmholtz plane'. The region within this plane constitutes the compact part of the double layer or the Helmholtz layer. The remaining charge needed to balance the surface potential is held with increasing disorder as the distance from the electrode surface increases, where electrostatic forces become weaker and where dispersion by thermal motion is more effective. This less ordered arrangement of charges with sign opposite to that on the electrode constitutes the diffuse layer (Gouy-Chapman layer) of the double layer. Thus, all the charge which neutralizes that of the capillary wall is held in a region between the outer Helmholtz plane and the bulk of the electrolyte solution. The potential at the edge of the outer Helmholtz layer, where the diffuse layer begins, is usually considered to be the zeta potential (ζ).

The above is the case for purely electrostatic interactions between the surface and the ions in solution. In other cases, specific adsorption of ions (Figure 1.3) may occur, in which van der Waals and other chemical forces participate. Many anions are specifically adsorbed, losing most, if not all, of their inner hydration shell. Specifically adsorbed species can evidently approach much closer to the surface. A line drawn through the centers of such species aligned at the surface defines a further boundary within the

Helmholtz layer-the so-called inner Helmholtz plane or Stern layer or compact layer. Under the applied electric field, the mobile cations in the diffuse layer migrate in the direction of the cathode, carrying waters of hydration with them. Thus, the entire bulk solution is pulled toward the cathode. This electroosmotic flow (EOF) or bulk flow pumps all molecules (cationic, neutral and anionic) toward the detector at the same speed. Separation is ultimately determined by the differences in the electrophoretic mobility of the individual analytes.

The overall ion mobility or apparent mobility is given by equations (1.1-1.3).

$$\mu_{ob} = \mu_{eo} + \mu_{ep} \quad (1.1)$$

$$\mu_{eo} = \frac{\epsilon \zeta_{eo}}{4\pi\eta} \quad (1.2)$$

$$\mu_{ep} = \frac{q}{6\pi\eta\gamma} \quad (1.3)$$

where μ_{ob} , μ_{eo} and μ_{ep} are the observed mobility, electroosmotic and electrophoretic mobility, respectively; ζ_{eo} is the zeta potential created by the electrical double layer at the liquid- solid interface and is the value at the plane of shear in the double layer where the ions and solvent become mobile; ϵ and η are the dielectric constant and the viscosity of the solution respectively; and q and γ are the net charge and the hydrodynamic radius of an ion [42,44].

To calculate the absolute electrophoretic mobility of an ion, the EOF mobility must be factored out. There are several practical methods to measure the EOF. One technique is to inject a neutral marker, such as dimethylsulfoxide or acetone, and measure the time

it takes to transit to the detector [45,46]. Another means of measuring EOF is called the current-monitoring method [47]. Once the μ_{eo} is measured, the μ_{ep} can be found by subtracting from μ_{ob} .

As pointed out, the separation of solutes, in principle, is governed by electrophoresis. Thus, the charge/size ratio of the solute determines the separation. The size or more importantly the hydrodynamic radius of the molecule is based on the molecular weight, the three-dimensional structure, and the degree of solvation (usually hydration). The viscosity of the buffer has the same effect on mobilities of all solutes. However, other buffer properties such as pH, ionic strength and dielectric constant are also important, because they control the effective charge on the analyte ion and for larger molecules, their shape and hydrodynamic radius.

Because of the plug flow profile of EOF, longitudinal diffusion should theoretically be the main source of band broadening [38,39]. The amount of time the solute resides in the capillary therefore affects both separation efficiency and resolution. The migration time of an ionic species is given by equation (1.4).

$$t = \frac{L^2}{(\mu_{ep} + \mu_{eo})V} \quad (1.4)$$

where V and L are the total applied voltage and capillary length, respectively. Eq. (1.4) suggests that the migration time of an ionic species depends on its electrophoretic mobility, the electroosmotic flow, the length and voltage applied.

Resolution of two components in CE is defined as [48],

$$R_s = \frac{1}{4} \frac{\Delta\mu_{ep} \sqrt{N}}{\mu_{ep} + \mu_{eo}} \quad (1.5)$$

where $\Delta\mu$ is the differences in mobility between the two species and N is the theoretical plate number of an ionic species and is given by eq. (1.6)

$$N = \frac{\mu_{ob} V}{2D} \quad (1.6)$$

where D is the diffusion coefficient of the ionic species and V is the applied voltage.

Substituting eq. 1.6 into eq. 1.5 yields [48]

$$R_s = 0.177 \Delta\mu_{ep} \sqrt{\frac{V}{(\mu_{ep} + \mu_{eo}) D_m}} \quad (1.7)$$

This expression suggests that once the voltage is large (as it is in most CE) further increases in voltage are not very effective for improving resolution. To double resolution, the voltage must quadruple. Since the voltage is usually in the 10-30 kV range, joule heating limitations are quickly approached. To improve the electrophoretic resolution, the selectivity of the separation is best addressed. The control of selectivity is first accomplished through the selection of the appropriate mode of CE. Next, proper selection of the separation buffers, buffer pH, and buffer additives are important.

1.4 Antigens and haptens

In chapter 3, we present labeling methods for monoclonal anti-ovalbumin (antibody) with cyanine (Cy5) dye, in order to determine ovalbumin (antigen) concentration in an aerosol sample taken from a field trial.

Antigens (immunogens) are substances that are able to stimulate the production of antibodies when introduced into a test animal, Figure 1.4. Antigenic structures or epitopes are mostly located in the hydrophilic part of the immunogen, each of them being capable of recognition by a specific antibody.

Haptens are small molecules such as diazonium derivatives of aromatic amines. They are not antigenic by themselves when injected into animals, but are able to induce immune system response when bound chemically to lysine or histidine residues of immunogenic proteins that are 20000 to 40000 Daltons higher in molecular weight than the haptens [49].

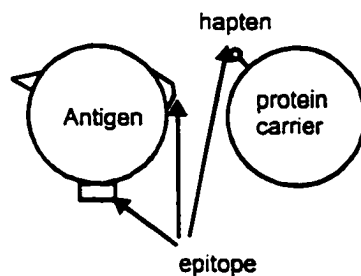


Figure 1.4 Schematic diagram for an antigen with three different epitopes and hapten with one epitope. (Epitope is a recognizable antigenic structure.)

1.5 Antibodies

Immunoglobulins, or antibodies, are a class of glycoproteins present in the serum and tissue fluids of all mammals. Chemists and biochemists have identified five immunoglobulin classes, named IgG, IgM, IgA, IgD, and IgE. Each molecule of immunoglobulin G (IgG) has a Y-shape and consists of four polypeptide chains joined together by disulfides bonds. Figure 1.5 shows the basic structure of IgG. The amino terminal end is characterized by sequence variability (V) in both heavy (H) and light (L), chains which are referred to as V_H and V_L regions, respectively.

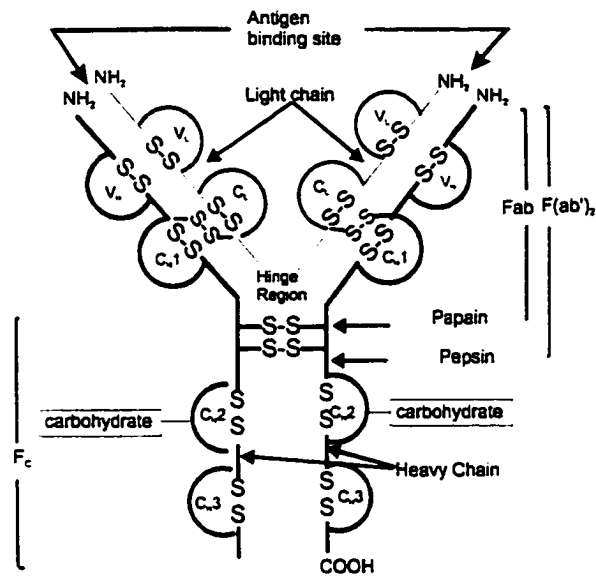


Figure 1.5 Schematic representation of polypeptide chains in the basic immunoglobulin structure.

The rest of the molecule has a relatively constant (C_{HX}) structure. The constant portion of the light chain is termed the C_L region. The constant portion of the heavy chain is further divided into three structurally discrete regions: C_{H1} , C_{H2} , and C_{H3} . These globular regions, which are stabilized by intrachain disulphide bonds, are referred to as 'domains'. Each class of immunoglobulin possesses a characteristic type of heavy chain. For example, IgG possesses γ chains; IgM, μ chains; IgA, α chains; IgD, δ chains and IgE, ϵ chains. Variation in the heavy chain structure within a class gives rise to immunoglobulin subclasses. For example the four human IgG subclasses (IgG1, IgG2, IgG3, and IgG4) have heavy chains called γ_1 , γ_2 , γ_3 , and γ_4 , respectively, which differ only slightly and so are all recognizable as γ heavy chains. The difference between the various subclasses within an immunoglobulin class is less than the differences between the different classes. The sites at which the antibody binds antigen are located in the

variable domains. The hinge region is the segment between the C_{H1} and C_{H2} regions of the heavy chain. Carbohydrate moieties are attached to the C_{H2} domains.

Papain cleaves IgG molecules in the hinge region between the C_{H1} and C_{H2} domains, to give two identical Fab (fragment antigen binding) fragments and one Fc (fragment crystalline) fragment. When the pepsin enzyme cleaves the IgG molecule it generates two major fragments: F(ab')₂ fragment which broadly encompasses the two Fab regions linked by the hinge region, and the pFc' fragment, which corresponds to the C_{H3} domain of the molecule.

A polyclonal antibody arises from several different clones of cells and is a mixture of antibody molecules that bind to different parts of the antigen with different binding affinities. An antibody produced by a single clone of cells is a monoclonal antibody: all the antibody molecules are identical and bind the same antigen site with identical binding affinities. Monoclonal antibodies can be generated in large amounts by creating a cell fusion (called a hybridoma) between an antibody-producing cell and a myeloma cell [50]. Monoclonal antibodies are a common tool in research because of their very high uniformity and specificity. For examples, many immunoassays are based on monoclonal antibodies.

1.5.1 Antibody-Antigen interactions

In Chapter 4, we describe a nonequilibrium capillary electrophoresis method for measuring the affinity constant of monoclonal anti-ovalbumin. The binding of antigen to the antibody takes place by the formation of multiple non-covalent bonds

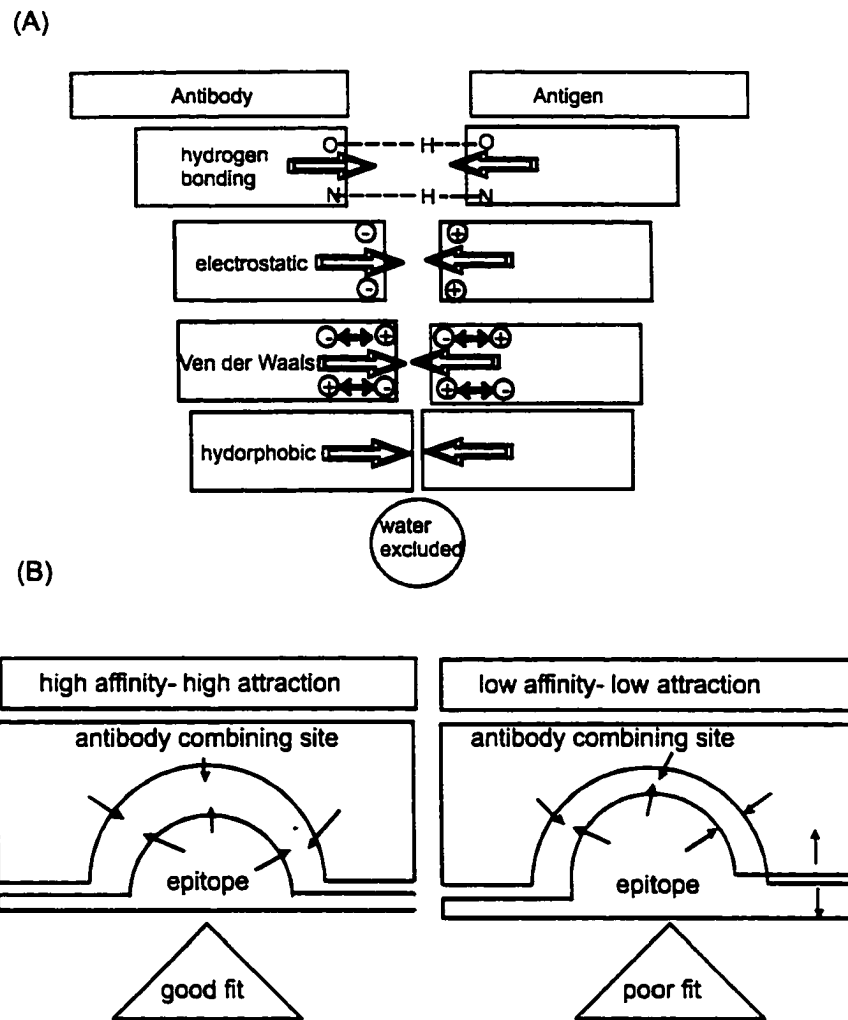


Figure 1.6 (A) Intermolecular attractive forces binding antigen to antibody. (B) Two examples of a good and a poor fit between the antigen and antibody.

between antigen and amino acids of the binding site. Although the attractive forces, (see Figure 1.6): namely, hydrogen bonds, electrostatic, Van der Waals and hydrophobic forces, involved in these bonds are individually weak by comparison with covalent bonds, the multiplicity of these interactions lead to a considerable binding energy. The strength of the non-covalent interactions depends on the distances between the interacting groups. The consequence of this is that an antigenic determinant and the antigen combining-site (epitope) must have complementary structures to be able to combine.

The strength of antibody-antigen interactions is termed the antibody affinity and is produced by the summation of the attractive and repulsive forces (see Figure 1.6). Since the non-covalent interactions between antibody and hapten are dissociable, the overall combination of an antigen and antibody must also be reversible, thus the law of mass action can be applied to the reaction. The equilibrium constant is known as the affinity constant.

1.6 Affinity chromatography

In chapter 3, we employ affinity chromatography to isolate the antibody from ascites fluid and to label the monoclonal antibody. Affinity chromatography is a type of liquid chromatography that makes use of biological-like interactions for the isolation of sample components. It was first used in 1978 with covalently attached protein A in order to achieve oriented immobilization of immunoglobulin G (IgG) [50-52]. Janis and Renier [53] used the other bacterial Fc binding protein G instead of protein A. Protein G has the advantage of binding to a wide range of IgG species and subclasses. Many bacterial strains display unique proteins on their surfaces, which bind specifically with high affinity to the tail (Fc-region) of the IgG molecule [54]. Proteins A and G are bacterial cell wall proteins produced by *Staphylococcus aureus* and group G streptococci, respectively [55-57].

Affinity chromatography is an efficient technique for the determination, and/or isolation of antibodies, antigens, haptens, cell organelles, cofactors, vitamins, enzymes, glycoproteins, saccharides, hormones, inhibitors, lectins, lipids, nucleic acids, nucleotide binding proteins, and viruses [58]. According to the International Union of Pure and Applied Chemistry [59], affinity chromatography is defined as a liquid chromatographic

technique that makes use of a “biological interaction” for the separation and analysis of specific analytes within a sample. Examples of these interactions include the binding of enzyme with an inhibitor or of an antibody with an antigen. Such binding processes are used in affinity chromatography by first obtaining a binding agent, known as the “affinity ligand”, which selectively interacts with the desired analyte, then placing this ligand onto a solid support within a column. (See Ref. 60, 61 for reviews of support and immobilization methods that can be used in making affinity columns.) Once this immobilized ligand has been prepared, it can be used for isolation or quantification of the analyte.

The immobilized ligand is the key factor that determines the success of any affinity chromatography. As implied by the definition given earlier for affinity chromatography, most of the ligands are of biological origin; however, the term “affinity chromatography” has also been used throughout the years to describe some columns that contain selective ligands of non-biological origin. Examples of these non-biological ligands are boronates, immobilized metal ions chromatography and synthetic dyes. Regardless of its origin, the type of the ligand can be used to divide affinity techniques into various subcategories, such as lectin, immunoaffinity, dye ligand, and immobilized metal affinity chromatography, to name a few [60,61].

Another method that can be used to distinguish between one affinity method and another is the type of the support used within the column. In low performance (or column) affinity chromatography, the support is a large diameter, nonrigid gel such as agarose, dextran, or cellulose. In high performance affinity chromatography, (HPAC), the support consists of small, rigid particles based on silica or synthetic polymers which

are capable of withstanding the flow rate and/or pressures that are characteristic of HPLC [60,62]. Low affinity chromatography is relatively easy to setup and inexpensive to use. However, the better flow and pressure stability of high performance supports makes HPAC easier to incorporate into instrumental systems, better speed and precision for the automated quantification of analytes. Several examples of direct analyte detection by HPAC are described in Ref. 63.

1.6.1 Chromatographic supports

Agarose (which is obtained from seaweed) is a linear polymer of D-galactose and 3,6-anhydro-1-galactose and forms a gel (a gel is a three-dimensional, solvent swollen network whose structure is usually random) that is held together without cross-links by hydrogen bonds. Agarose is not used in chromatography as a continuous gel but is formed into porous beads having various degrees of fineness. Agarose is supplied as wet beads called Sepharose 4B (Pharmacia) and Bio-gel A (Bio-Rad Laboratories). A variant of agarose has been made in which agarose chains are cross-linked to provide greater strength and stability. This substance is called Sepharose CL; it can be used with concentrated denaturing solutions (6 M guanidinium chloride, 8 M urea) and at temperatures up to 70 °C [Pharmacia].

Sepharose 4B is the most favored and widely used matrix. An open structure makes the interior of the matrix available for ligand attachment and ensures good binding capacities, even for large molecules. For example, the exclusion limit of Sepharose 4B in gel filtration is MW 20×10^6 . The bead form of the gel provides good flow properties, which is important for rapid sample loading of large samples.

The hydroxyl groups on the sugar residues can be used to activate or derivatize the matrix for covalent attachment of reagents. For example, activation of Sepharose by cyanogen bromide (CNBr) enables ligands containing primary amino group to covalently bond to the matrix by spontaneous reaction [64] in aqueous solution. We have used that activated matrix to immobilize ovalbumin (see Chapter 3). For other types of support matrix based on agarose beads see the Pharmacia or Pierce catalogues.

1.6.2 Protein A and protein G affinity chromatography

Protein A is a single polypeptide with a molecular weight of 42,000 Da. Protein A contains four high affinity ($K_a = 10^8 \text{ M}^{-1}$) binding sites capable of interacting with the Fc region of several species [65]. Protein A covalently coupled to agarose has been used for affinity chromatography for the isolation of a wide variety of IgG molecules from several mammal species. However, the interaction of protein A and IgG is not equivalent for all species [66]. Even within a species, protein A interacts with some subgroups of IgG and not others. For instance, Human IgG₁, IgG₂ and IgG₄ bind strongly, whereas IgG₃ does not bind [3]. In mice, IgG₁ has been found to bind poorly to protein A [67]. However, Protein G binds with high affinity to IgG from most species, as indicated in Table 1.1 [68]. In this study, we used recombinant protein G to isolate mouse monoclonal antibody (IgG1) from ascites fluid. Recombinant protein G (Molecular weight 17,000 Da) is produced in *Escherichia coli* and contains two IgG-binding regions. The albumin binding region of native protein G has been deleted genetically, thereby avoiding undesirable reactions with albumin. A recombinant protein A/G, which blends the activities of protein A and protein G also is available for use in affinity columns [61,69].

Table 1.1 Summary of binding different immunoglobulins to protein G and A [Pharmacia], [68]

immunoglobulin	protein A	protein G
Human IgG ₁	+++	+++
Human IgG ₂	+++	+++
Human IgG ₃	-	+++
Human IgG ₄	+++	+++
Mouse IgG ₁	+	++
Mouse IgG _{2a}	+++	+++
Mouse IgG _{2b}	+++	+++
Mouse IgG ₃	+++	+++
Rat IgG ₁	+	+
Rat IgG _{2a}	-	+++
Rat IgG _{2b}	-	+
Rat IgG _{2c}	+++	+++
Rabbit IgG	+++	+++
Bov. IgG ₁	-	+++
Bov. IgG ₂	+++	+++
Sheep IgG ₁	-	+++
Sheep IgG ₂	+++	+++
Goat IgG ₁	+	+++
Goat IgG ₂	+++	+++
Horse IgG _(ab)	+	+++
Horse IgG _(c)	+	+++
Chicken IgG	-	-

+++ = strong binding

++ = medium binding

+ = weak binding

- = no binding

1.7 Scope of the thesis

The need for detection and identification of biological weapons such as anthrax has catalyzed interest in the development of a rugged, compact, portable, and highly automated single channel microfluidic-based system. For field-trial testing, automation must include sample introduction, mixing reagents, separation and detection of reaction products. Automated sample introduction has not been reported before. The objective of this thesis is to describe microfluidic chip designs that allow us to automate sample introduction. It is known that merging immunoassay and CE, along with laser induced detection can produce a highly sensitive and selective technique. However, derivatization of either an antibody or antigen with a label is required in order to allow detection. Direct derivatization of an antibody with a fluorophore is difficult and often produces inactive antibody. This thesis reports for the first time a novel affinity chromatography method to label the antibody.

Chapter 2 gives a detailed description of the instrumentation and chip devices utilized in this thesis and provides an overview of the rationale for the effort presented in the remaining chapters. The direct assay of ovalbumin using CE with UV detection is described. The effect of derivatization of monoclonal anti-ovalbumin with Cyanine (Cy5) dye on the biological activity of the antibody is reported. Results of testing the activity of Cy5-labeled antibody using enzyme-linked immunosorbent assay (ELISA) are shown to contrast with the results obtained by CE. An explanation for such a contradiction is presented.

Chapter 3 gives the detailed procedure for purifying the monoclonal antibody from ascites fluid using a protein G affinity column. The effect of direct derivatization on the

active sites of the antibody will be described. A detailed description of the ELISA experiment for testing the activity of Cy5-labeled monoclonal antibody is presented. We will demonstrate for the first time an affinity protection chromatography method for labeling the monoclonal antibody. Immobilization of ovalbumin on cyanogen bromide-activated Sepharose 4B is presented. The factors that control yield of labeled antibody and dye/protein ratio will be discussed as well.

Chapter 4 describes the use of a Beckman CE system for studying antibody-antigen interactions. The antibody affinity constant is a measure of this interaction and is a determining factor in an immunoassay's sensitivity. Affinity capillary electrophoresis (ACE) for measuring the affinity constant of nonlabeled and Cy5-labeled antibody is described. The limitations of ACE and the effect of affinity constant on both limits of detection and sensitivity are also discussed. A comparison of values obtained from Scatchard plots and nonlinear curve fitting is reported.

In Chapter 5, we present microchip designs that incorporate two different channels. Channels for CE separations are 30-68 μm wide and 10-13 μm deep, channels for sample introduction are 300 μm deep and 1 mm wide. This drastic difference in dimensions allows pressurized samples to be introduced without contamination of the CE channels. The Sample Introduction Channel (SIC) is used for rapid sample exchange and interfacing the microchip to the real world. The throughput is about 1 sample/30 s. For the first time, we report interfacing the microfluidic chip on-line with a fluidic system for continuously monitoring increasing concentration of fluorescein solution in the beaker. With this arrangement a linear calibration curve of fluorescein is obtained.

Chapter 6 is a summary of the preceding chapters and presents possible future work.

1.8 References

- 1 N. Graber, H. Lüdi and H.M. Widmer, *Sensor and Actuator, BI* (1990) 239.
- 2 A. Manze, N. Graber and H.M. Widmer, *Sensor Actuators, BI* (1990), 244.
- 3 H.M. Widmer, J.F. Erard and C. Grass, *Int. J. Environ. Anal. Chem.*, 18 (1984) 1.
- 4 M. Garn, P. Cevy, M. Gisin and C. Thommen, *Biotechnol. Bioeng.*, 34 (1989) 423.
- 5 A. Giorgetti, N. Periclés, H.M. Widmer, K. Anton and P. Dätwyler, *J. Chromatogr. Sci.*, 27 (1989) 318.
- 6 C.A. Monnig and J.W. Jorgenson, *Anal. Chem.*, 63 (1991) 802.
- 7 S.C. Terry, J.H. Jerman and J.B. Angell, *IEEE Trans. Electron. Devices*, ED26 (1979) 1880.
- 8 A. Manz, E. Verpoorte, C.S. Effenhauser, N. Burggraf, D. E. Raymond, D.J. Harrison and H.M. Widmer, *J.High Resolut.Chromatogr.*, 16 (1993) 433.
- 9 A.T. Woolley, G.F. Sensabaugh and R.A. Mathies, *Anal. Chem.*, 69 (1997) 2181.
- 10 A.T. Woolley and R.A. Mathies, *Proc. Natl. Acad. Sci. USA*, 91 (1994) 11348.
- 11 S.C. Jacobson and J.M. Ramsey, *Anal. Chem.*, 68 (1996) 720.
- 12 R.A. Mathies, P.C. Simpson and A.T. Woolley, *Proc. μ TAS '98 Workshop*. Kluwer Academic Pub., Dordrecht, 1998.
- 13 A. Manz, D.J. Harrison, E.M.J. Verpoorte, J.C. Fettinger, A. Paulus, H. Ludi and H.M. Widmer, *J. Chromatogr.*, 593 (1992) 253.
- 14 D.J. Harrison, A. Manz, Z. Fan, H. Ludi, and H.M. Widmer, *Anal. Chem.*, 64 (1992) 1926.

- 15 A. Manz, J.C. Fettinger, E. Verpoorte, H. Ludi, H.M. Widmer and D.J. Harrison, *Trends Anal. Chem.*, 10 (1991) 144.
- 16 A. Manz, D.J. Harrison, E. Verpoort and H.M. Widmer, *Adv Chromatogra.* 33 (1993) 1.
- 17 L.J. Kricka, P. Wilding, *Handbook of Clinical Automation*, Robotica, and Optimization, John Wiley & Sons, New York, 1996.
- 18 C.L. Colyer, T. Tang, N.H. Chiem and D.J. Harrison, *Electrophoresis*, 18 (1997) 1733.
- 19 C.S. Effenhauser, G.J.M. Bruin and A. Paulus, *Electrophoresis*, 18 (1997) 2203.
- 20 A. Mans and H. Becker, *Microsystem Technology in Chemistry and Life Sciences*, Springer, Berlin, 1998.
- 21 A. Van den berg and P. Bergveld (eds.), *Proc. μ TAS '94 Workshop*, Kluwer Academic Pub., Dordrecht, 1995.
- 22 H.M. Widmer, E. Verpoorte and S. Barnard (eds.), *Proc. μ TAS '96 Anal. Methods Instrum.*, Kluwer Academic Pub., Dordrecht, 1996.
- 23 D.J. Harrison and A. Van den Berg, (eds.), *Proc. μ TAS '98 Workshop*, Kluwer Academic Pub., Dordrecht, 1998.
- 24 B. Eskröm, G. Jacobson, O. Öhman and H. Sjödin, *International Patent WO* 91/16966, 1990.
- 25 M.U. Kopp, A.J. deMello and A. Manz, *Science*, 280 (1998) 1046.
- 26 A.G. Hadd, D.E. Raymond, J.W. Halliwell, S.C. Jacobson and J.M. Ramsey, *Anal. Chem.*, 69 (1997) 3407.
- 27 L.B. Koutny, D. Schmalzing, T.A. Taylor and M. Fuhs, *Anal. Chem.*, 68 (1996) 18.

- 28 N.H. Chiem and D.J. Harrison, *Clin. Chem.*, 44 (1998) 591.
- 29 W.E. Lee, A.B. Jemere, S. Attiya, N.H. Chiem, M. Paulson, J. Ahrend, G. Burchett, D.E. Bader, Y. Ning and D. J. Harrison, *J. Capillary electrophoresis*, in press.
- 30 C.H. Ahn, T. Henderson, W. Heineman and B. Halsall, *Proc. μ TAS '98*, Kluwer Academic Pub., Dordrecht, 1998.
- 31 G. Delapierre, *Sensor and Actuators*, 17 (1989)123.
- 32 M.A. Roberts, J.S. Rossier, P. Bercier and H. Girault, *Anal. Chem.*, 69 (1997) 2035.
- 33 R.M. McCormick, R.J. Nelson, M.G. Alonso-Amigo, D.J. Benveniste and H.H. Hooper, *Anal. Chem.* 69 (1997) 2626.
- 34 C.S. Effenhauser, G.H.M. Bruin, A. Paulus and M. Ehrat, *Proc. μ TAS '96, Anal. Methods Instrum. Special Issue* (1996) 124.
- 35 L.E. Locasico, *Anal. Chem.*, 69 (1997) 4783.
- 36 G. Delapierre, *Sensors and Actuators*, 17 (1989) 123.
- 37 D.J. Harrison and P.G. Glavina, *Sensors and Actuators*, 10 (1993) 107.
- 38 J. Jorgenson and K.D. Lukacs, *Anal. Chem.*, 53 (1981) 1298.
- 39 J. Jorgenson and K.D. Lukacs, *Science*, 222 (1983) 266.
- 40 M.J. Gordon, X. Huang, S.L. Pentoney and R.N. Zare, *Science*, 242 (1988) 224.
- 41 A. Ewing, R.A. Wallingford and T.M. Olefirowicz, *Anal. Chem.*, 61 (1989) 292A.
- 42 R. Weinberger, *Practical Capillary Electrophoresis*, Academic press Inc., New York, 1993.
- 43 D.R. Crow, "*Principles and Applications of Electrochemistry*", Chapman and Hall, London, 1974.
- 44 R. Chien and D.S. Burgi, *Anal. Chem.*, 64 (1992) 489A.

- 45 Z. Dely, V. Rohlicek and M. Adam, *J. Chromatogr.*, 480 (1989) 371.
- 46 E.C. Rickard, M.M. Strohl and R.G. Nielsen, *Anal. Biochem.*, 197 (1991) 197.
- 47 P.D. Grossman, K.J. Wilson, G. Petrie and H.H. lauer, *Anal. Biochem.*, 173 (1988) 265.
- 48 D. Josić, K. Zeilinger, W. Reutter, A. Bottcher and G. Schmitz, *J. Chromatogr.*, 516 (1990) 89.
- 49 A. Paraf and G. Peltre, *Immunoassays in Food and Agriculture*, Kluwer Academic Publishers, Netherland, (1991).
- 50 S. Werner and W. Machleidt, *Eur. Biochem.*, 90 (1978) 99.
- 51 D.M. Gersten and J.J. Marchalonis, *J. Immunol. Methods*, 24 (1978) 305.
- 52 D.r. Davies, E.A. Padlan and D.M. Segal, *Annu. Rev. Biochem.*, 44 (1975) 639.
- 53 L.J. Janis and F.E. Regnier, *Anal. Chem.*, 61 (1989) 1901.
- 54 M.D.P. Boyle and K.J. Reis, *Bio/Technology*, 5 (1987) 697.
- 55 L. Bjork and G. Kronvall, *J. Immunol.*, 133 (1984) 969.
- 56 R. Lindmark, C. Biriell and J. Sjoquist, *Scan. J. Immunol.* , 14 (1981) 409.
- 57 P.L. Ey, S.J. Prowse and C.R. Jenkin, *Immunochemistry*, 15 (1978) 429.
- 58 J. Turková, *Bioaffinity Chromatography*, Elsevier, Amsterdam, 1993.
- 59 International Union of Pure and Applied Chemistry, Nomenclature for chromatography. <http://wingate.merk.de/english/services/chromatographie/iupac/chronom.htm>.
- 60 D.S. Hage, *Affinity chromatography*. In: E. Katz, R. Eksteen , P. Shoenmakers and N. Miller, (eds.) *Handbook of HPLC*, Marcel Dekker, N.Y., 1998.

- 61 G.T. Hermanson, A.K. Mallia and P.K. Smith, *Immobilized affinity ligand techniques*. Academic Press, New York, 1992.
- 62 P.O. Larsson, *Methods Enzymol.*, 104 (1987) 212.
- 63 D.S. Hage, *J. Chromatogr.*, 715 (1998) 3.
- 64 H.G. van Eijk and W.L. van Noort, *J. Clin. Chem. Clin. Biochem.*, 14 (1976) 475.
- 65 H. Hjelm et al., *Eur. J. Biochem.*, 57 (1975) 395.
- 66 G. Kronvall and R.C. Williams, *J. Immunol.*, 103(4) (1969) 828.
- 67 G. Kronvall et al., *J. Immunol.*, 105 (1970) 1116.
- 68 B. Åkerström and L. Björck, *J. Biol. Chem.*, 261 (1986) 10240.
- 69 M. Eliasson, A. Olson, E. Palmcrantz, K. Wibers, M. Inganas and B. Guss, *J. Biol. Chem.*, 263 (1988) 4323.

Chapter 2

Characterization of ovalbumin assay

using microchip and Beckman CE

2.1 Introduction

Recent work has shown that a wide range of chemical processing can be incorporated into microchip platforms [1,2]. These technological advancements are directed toward developing complex and automated processing on a single chip. However, to utilize microfluidic technology for analytical instruments, there are two requirements for system integration. The first requirement is the integration of chemical function on the chip. Since an analytical process is a set of defined steps that must be carried out in a fixed order, each step must lead into the next with respect to position on the chip and sequence of events. The second requirement is the addition of peripheral system components for control and operation of the chip. This requires having the peripherals (such as high voltage supplies, optical detection unit, external peristaltic pump) under computer control, and ready to respond to a predetermined set of software-based commands. In this way, the operator can initiate the analysis and the peripheral components will respond by making the analysis on-chip, collecting the data from the analysis, and then resetting the system for the next run.

The objective of this thesis is to develop some of the components of an automated microchip-based platform for immunoassay analysis. We developed an immunoassay for the protein ovalbumin, which is used in field trial testing to evaluate aerosol collectors and environmental monitoring systems. In this assay, a fluorescently-labeled monoclonal antibody was reacted with ovalbumin and the product was separated by capillary

electrophoresis and detected by laser-induced fluorescence (LIF). Capillary electrophoresis (CE) has emerged as a useful tool for immunoassays [3-4] and is well suited for microchip applications. This thesis examines the methods used to develop a direct immunoassay for ovalbumin, using fluorescently-labeled anti-ovalbumin.

The system, which has been developed by several researchers in a DARPA-funded project, enables on-chip operation of the key elements in analysis: injection, mixing, separation, detection, and quantitation, plus near real-time data display. Researchers who collaborated on the first prototype of a single channel microfluidic immunoassay included William E. Lee, Abebaw B. Jemere, Said Attiya, N. H. Chiem, Murray Paulson, Jack Ahrend, Gary Burchett, Douglas E. Bader, Yuebin Ning and Professor Jed Harrison. The unit was designed to connect to a large volume aerosol sample collector for environmental monitoring, although any low-pressure fluid delivery apparatus would be suitable for use with the microchip system. Compact peripheral subsystems were developed, so that all of the components could be engineered into a single box of 30 x 35 x 50 cm. The unit consists of a programmable high voltage subsystem for electroosmotic pumping and CE, coupled to a rapid wafer exchange, and fluidic and electrical interface to the chip. The channel networks in the microchip were fabricated on micromachined glass plates. Electroosmotic pumping was used for moving reagents on the chip at velocities up to 1 cm/s. Thus, by voltage control alone, chemical processing can be carried out within a manifold of channels on-chip through CE. Detection was accomplished with a built-in, compact, confocal epilluminescence LIF microscope equipped with a 635 nm diode laser. The operational control of the system was carried out by an on-board microprocessor under the command of WindowsTM-based software in

a notepad computer. The fluid interface was designed to allow the use of a mini-peristaltic pump to deliver sample solutions from an external reservoir to the chip. In this thesis, we also investigate device designs that could be used to create such an interface.

Through the course of developing immunoassay reagents for ovalbumin determination using CE, a number of different instruments and synthetic methods were utilized. This chapter presents the devices used, and their purpose, in order to prevent confusion in later chapters, since the work is not presented in chronological order. In addition, the primary difficulty with developing a direct affinity-based immunoassay is presented here, while solutions are presented in the subsequent chapters.

2.2 Experimental

2.2.1 Beckman CE instrument

CE separations were performed by using a Beckman CE system (5010) (Fullerton, CA, USA) interfaced with a personal computer. The separation was performed within 20 cm effective length (27 cm total length), untreated fused-silica capillaries (50 μm I. D. and 365 μm O.D.) from Polymicro Technologies, Phoenix, AZ, USA. The polyimide coating was burned off using a match to form a detector window of about 0.3 cm. The capillary was assembled in a cartridge (Beckman) and thermostated at 22 $^{\circ}\text{C}$ by circulating coolant. Detection for native proteins was performed with on-column UV detection at 214-nm. A laser-induced fluorescence (LIF) detector equipped with a 675 nm band pass filter and a 2.5 mW solid state diode laser, $\lambda_{\text{excitation}}$ 635 nm, was employed to detect the labeled antibody. The system was operated in constant-voltage mode by applying 16 kV. All species of the sample injected into the capillary migrated toward the negative pole, the cathode. Samples were injected into the capillary for 3 s, unless

otherwise noted, by applying a pressure of 0.5 p.s.i. (1 p.s.i. = 6894.76 Pa) to the anodic end of the capillary.

Ultrapure water (resistance = 18.3 M Ω) was obtained from a Millipore Milli-Q water-purification system (Millipore Corp., MA, USA) and was used to prepare all solutions. Borate buffer was used as a conditioning and separation buffer, and the buffer was prepared by adjusting the pH of 5 mM sodium tetraborate (borax) containing 0.5% Tween 20 to pH 9.2 with 0.1 M NaOH. At the start of each day the capillary was flushed and activated with 1 M NaOH for 25 min, followed by water for the same period of time. Borate buffer (pH 9.2) was then flushed through for 30 min to equilibrate the capillary. The voltage control, data collection (at 5 Hz) and peak analysis of the resulting electropherograms were accomplished using P/ACE (Beckman) software, Version 2. Peak heights were used for quantification. This was done since peak areas vary due to the varying speeds (mobilities) at which different analytes pass through the detector [5.6], and because when peaks overlap it is often easier to use peak heights.

2.2.1.1 Electrophoresis on Beckman CE

Samples were loaded into a microapplication assembly. Each assembly consisted of a 30 μ l conical microvial inserted into a standard 5 ml glass vial and held for injection with an adjustable spring. The assembly was available from Beckman. In order to minimize evaporation of the sample (25 μ l), about 1-2 ml of the water was added to the microapplication glass reservoir housing the microvial as a source of humidity. Two standard vials were filled with 4.7 ml of borate buffer for electrical contact during the separation. Another vial filled with 4.7 ml of borate buffer was used for conditioning and washing the capillary for 3 min between runs. Having three reservoirs filled with buffer

ensured that the liquid level in the two separation reservoirs remained constant and eliminated pressure differences due to height differences. These steps prevented hydrodynamic flow that could accompany the electroosmotic flow. For rinsing the capillary, another standard vial was filled with 4.7 ml of 1 M NaOH.

2.2.2 Microchip devices

Chips were fabricated in 3" x 3" squares, 600 μm thick 0211 Corning glass plates (Corning Glass, NY, USA) by the Alberta Microelectronic Center (Edmonton, Alberta, CA) using a modification of bulk silicon micromachining methods [7]. Two microchips, named DARPA and Faster, were utilized. Thin line channels for the DARPA chip, Figure 2.1, were 13 μm deep and 68 μm wide at the top. The heavier lines were 13 μm deep and 275 μm wide. Sample introduction channels were 1 mm wide and 300 μm deep. The channels of the Faster chip layout, shown in Figure 2.2, were 36 μm wide at the top and 10 μm deep. Segments, with channel widths of 240 μm for a 10 μm depth, are drawn as thick lines. The channel dimensions for DARPA and Faster chips are given in Table 2.1 and 2.2, respectively. Designing various cross-sections for the device provides a built-in control of the voltage drop in each channel segment. For example, in the DARPA chip, the major potential drop can be applied in the active separation channel, from point A to point D, rather than in segments that connect the reservoirs. To make a complete device, another 600 μm , 3" x 3" square 0211 glass plate was used as a cover plate for the chip. In this cover plate, holes 1.2 mm in diameter were drilled. These holes were positioned at the ends of the channels. Before attaching, the cover plate was rinsed in acetone for 15 min in an ultrasonic bath.

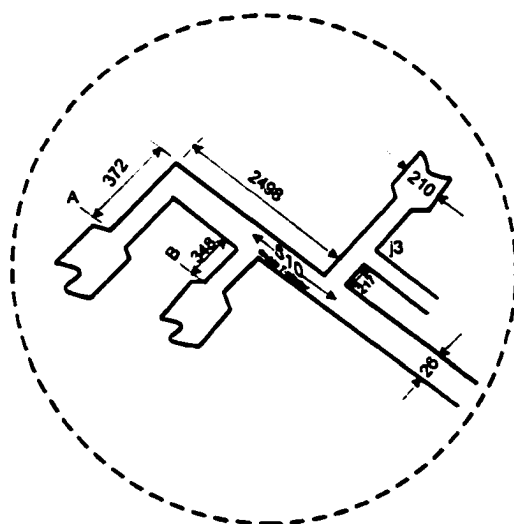
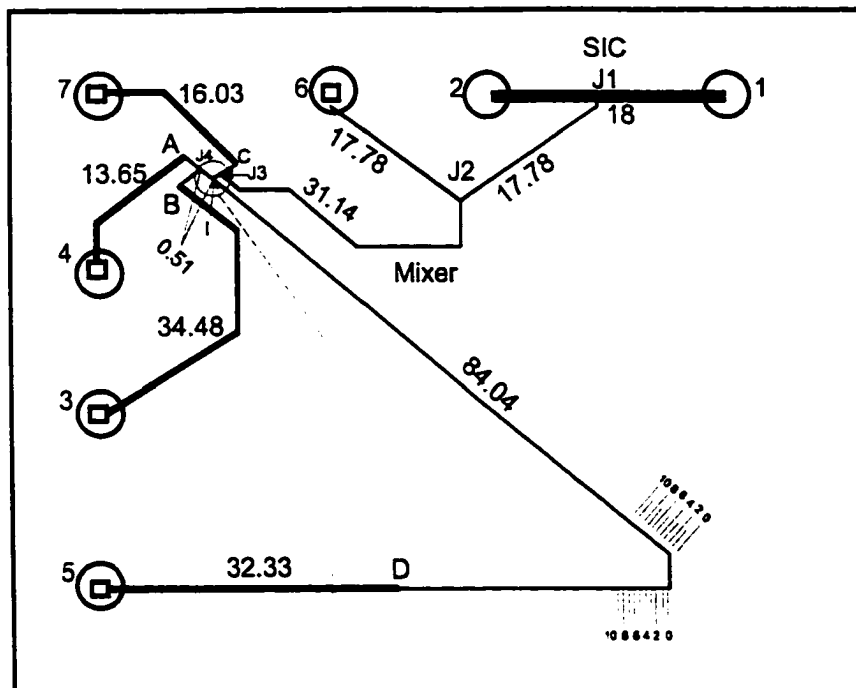


Figure 2.1 DARPA chip layout for a single channel instrument. All dimensions are in micrometers and reservoirs are numbered for reference. Different line thickness indicates relative channel widths. The double T-injector is shown in the inset. Dimensions and impedance of channels are in Table 2.1. The drawing is not to scale.

Table 2.1 Dimensions of DARPA chip

Connecting segment	To	Width, μm		Length mm	impedance	
		Feature	Etched	Actual	R/ρ^c	r/η^d
Junction (J1)	Junction (J2)	26	68	17.78	20.11	1411.45
Junction (J2)	Reservoir (6)	26	68	17.78	20.11	1411.45
Junction (J2)	Junction (J3)	26	68	31.14	35.23	2472.02
Junction (J3)	A	26	68	3.14	3.55	249.27
A	Reservoir (4)	210	275	13.65	3.82	1018.18
Reservoir (3)	B	210	275	34.48	9.64	2571.93
C	Reservoir (7)	210	275	16.03	4.48	1195.71
D	Reservoir (5)	210	275	32.33	9.04	2411.56
I	D	26	68	84.04	95.07	6671.43
A	D	26	68	86.91	98.31	6899.26
I	A	26	68	2.87	3.25	227.83
Junction (J3)	C	26	68	0.14	0.15	10.80
Junction (J3)	I	26	68	0.22	0.25	17.23
Reservoir(1)	Reservoir (2) ^e	500	1000	18.00	0.06	3.00
I	B	26	68	0.86	0.97	68.11

^aFeature width defines the dimension on the photolithographic patterning mask.

^bDevices were etched to 13 μm deep and the channel cross-sections were approximated as rectangular.

^cElectrical resistances are normalized to resistivity (ρ) and are estimated using the formula: $R/\rho=l/A$ where l is the actual channel length and A is the cross-sectional area ($A = \text{width at the top of the channel after etching} \times \text{depth of the channel}$).

^dResistances to flow are also normalized to viscosity (η) and are calculated using the formula: $r/\eta=l/abF$ where l is the actual length of the channel. F is a constant arising from the cross sectional shape of the channel (see Chapter 5) and a and b are the half width (at the top edge of the channel after etching) and half depth of channel, respectively.

^eSample introduction channel (SIC) with a depth 300 μm .

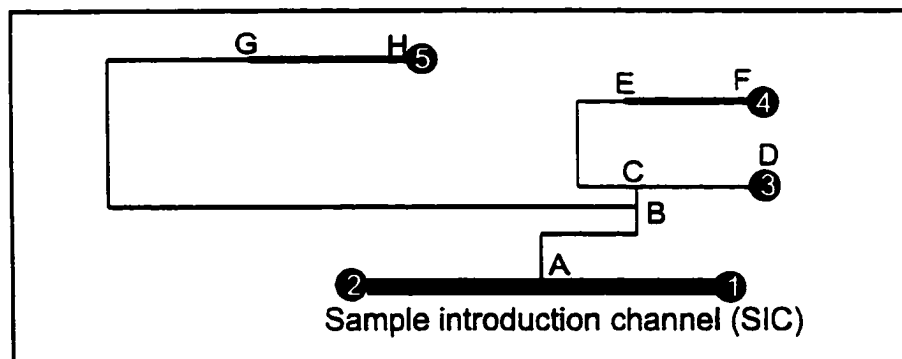


Figure 2.2 Layout of Faster chip with sample introduction channel.

Table 2.2 Dimensions of Faster chip

Connecting segment	To	Width, μm		Length (mm)	Impedance	
		Feature	Etched	Actual	R/p	r/ η
A	B	10	36	11.90	33.06	918.18
B	C	10	36	0.10	0.28	7.72
C	D	10	36	8.00	22.22	617.27
C	E	10	36	6.49	18.03	500.76
E	F	200	240	8.00	3.33	13.89
B	G	10	36	53.06	147.39	4094.02
G	H	200	240	16.00	6.67	27.78
Reservoir (1)	Reservoir (2) ^a	500	1000	20	0.07	3.33

^a Sample introduction channel with a depth 300 μm .

Then, the two plates were rinsed in Piranha etch ($\text{H}_2\text{SO}_4/\text{H}_2\text{O}_2$, 3:1) for 25 min. After rinsing with distilled water and then drying, each plate was pressure-washed in a class 100 clean hood with a MicroAutomation 2066 high pressure cleaning station. Using N_2 gas, the plates were further dried, then aligned so that the holes met the ends of the channels. When the two plates contacted a slight pressure was applied to drive out all the trapped air. Good contact was evidenced by the absence of interference fringes. Small

particles of dirt resulted in the appearance of Newton's rings around the contaminants, necessitating the separation and re-cleaning the two plates. The two plates were thermally bonded together as previously described [8], using the following temperature program: 0.5 h at 440 °C, 0.5 h at 473 °C, 6 h at 590 °C, and 0.5 h at 473 °C, and then cooled overnight to ambient temperature. Small plastic Eppendorf pipette tips were cut and glued around the holes using epoxy resin. These tips acted as reservoirs for sample and buffer. Pt wire was inserted into each reservoir for electrical contact. If the device was sandwiched between two plexiglass plates, then chromatographic fittings with 1/16" ferrules (Upchurch Scientific Inc., Ontario, Canada) were used as reservoirs.

2.2.2.1 Detection system and data acquisition

The detection system for the microchip studies consisted of a He-Ne laser (Melles Griot, Nepean, Ontario, CA) with an excitation wavelength of 632.5 nm, a microscope body (Melles Griot), fused-silica lens with a 150 mm focal length (Melles Griot), a mirror (Melles Griot), a microscope objective (Leitz NPL Fluotar, 25 x, numerical aperture 0.35, working distance 14 mm), 0.8 mm pinhole, bandpass filter 675 nm (Beckman, Fullerton, CA, USA), and a Hamamatsu R1477 photomultiplier tube (PMT). With this detection system, as shown in Figure 2.3, the 0.8 mm diameter laser beam was focused with the lens and directed at an angle of about 45° to the plane of the chip with a mirror. The objective lens collected the emission signal. The purpose of the pinhole and the band-pass filter in front of the PMT was to control the field of view and eliminate scattered laser radiation and other stray light.

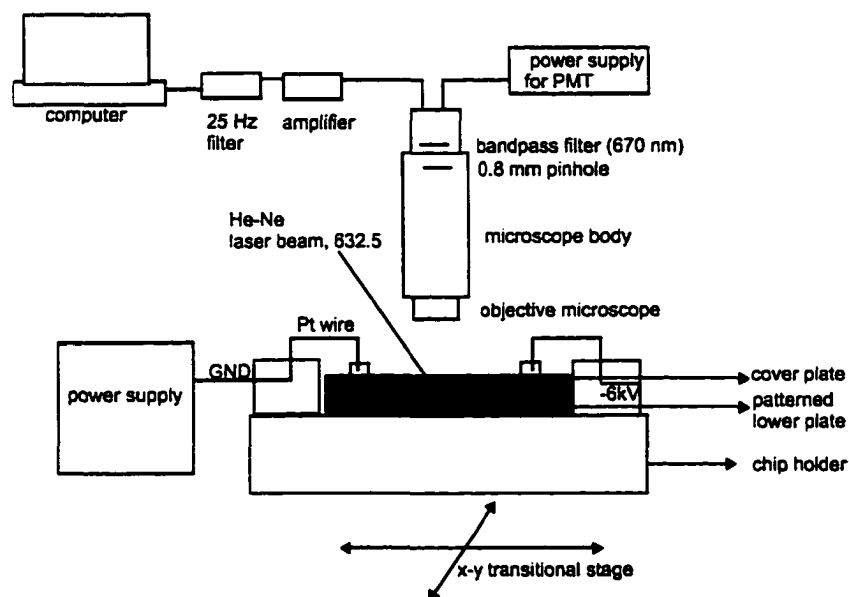


Figure 2.3 Experimental set up with LIF detection. The cross-sectional view of the microchip is shaded.

Dividing the pinhole diameter by objective magnification gave a $32\ \mu\text{m}$ viewing window for the PMT at the chip surface. The chip device and microscope were mounted on x-y translation stages. This allowed optimization of the position of the incident laser beam and channel, therefore maximizing the signal. The PMT current was converted to voltage using a 10^8 gain transimpedance amplifier, and filtered with a 25 Hz, active low pass noise filter, then digitally collected using a PC equipped with a national instrument AT-AO-6 A/D converter and LabVIEW software (National Instrument, Texas, USA). The software for data acquisition and control of the power supply and relays was written in-house using National instrument LabVIEW software V. 4. The sampling rate was 10 Hz. Only a single 30 kV power supply (Spellman Model CZE 1000R) and two 30 kV Kilovac

double-throw relays (Santa Barbara, CA, USA) were used to operate the chip, as shown in Figure 2.4.

2.2.2.2 Conditioning the chip

Like conventional fused-silica capillaries, the channels of chip devices must be conditioned with 1 M NaOH solution and the separation buffer. For a new chip device, all reservoirs were initially filled with de-ionized water, which moved by capillary action and wetted the channels. Reservoirs were then emptied using house vacuum. Then with a syringe containing 1 M NaOH, all reservoirs except one were filled with NaOH solution. House vacuum was applied to the empty reservoir for 20 min. Because the channels were interconnected the flow of NaOH solution was in the direction of the negative pressure. After 20 min, the vacuum was removed and the reservoir was filled with 1 M NaOH. Another reservoir was emptied and vacuum was applied. This process was repeated for all reservoirs. After flushing the channels with 1 M NaOH solution, reservoirs were rinsed with the separation buffer and the chip device was conditioned in the same way as with NaOH solution. At the end of the experiments, all reservoirs were emptied and de-ionized water was added to all reservoirs. The device was stored in a humid container so that water would not evaporate quickly. These conditioning steps are tedious, but necessary to obtain reproducible surface charge on the microfluidic channels or fused-silica capillary. Reproducible migration times and no leakage (i.e., mixing of the sample in the sample channel with the buffer in the separation channel during the separation step) can then be obtained.

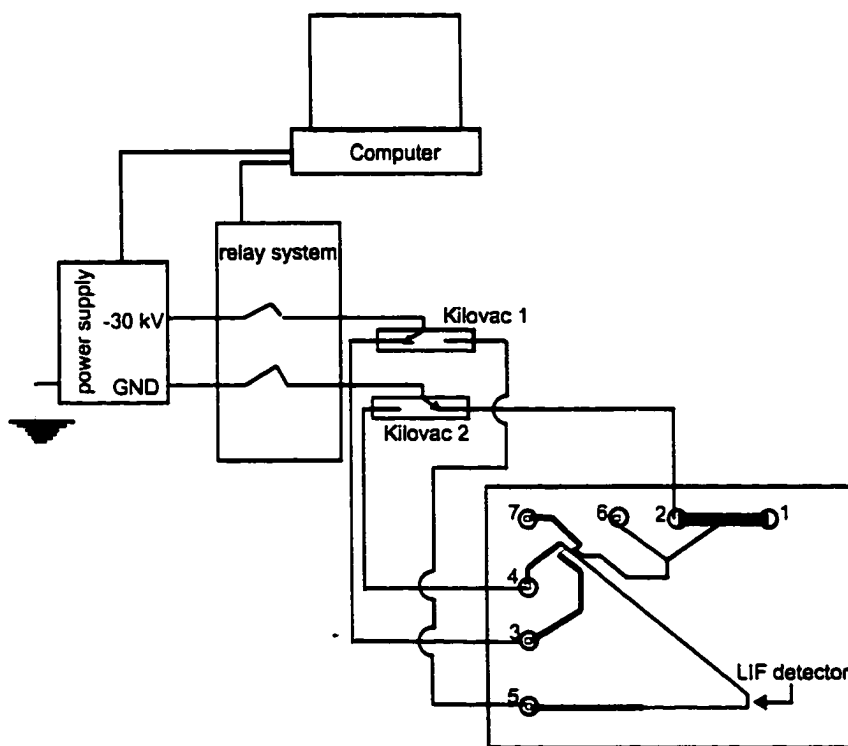


Figure 2.4 Schematic diagram for single power supply and two relays showing the relay setup during the injection mode. Both relays are switched to the other pole during the separation setup, delivering potential to reservoirs 4 and 5 on the DARPA design.

2.2.2.3 CE on chip

Similar methods were used to optimize the detector settings for both DARPA and Faster devices. A 200 nM reactive Cy5 dye solution was loaded into one reservoir of the sample introduction channel. Figure 2.4, with a micropipetter. Then -6 kV was applied between reservoirs 2 and 5 (reservoir 2 at GND) to fill up the double T-junction and the separation channel. With a mirror, the 632.5 nm He-Ne laser beam was directed toward the detection zone in the separation channel (see Figure 2.4). Observing a red spot (the emission) in the separation channel with a 675 nm band-pass filter placed above the microscope indicated that the optics were aligned. Further adjustment was achieved by moving the transition stage of either the chip device or the microscope in the x or y direction (see Figure 2.3). The PMT was placed above the microscope with the power supply of the PMT turned on and set to a value where signal was not over range. Then, -6 kV was applied between reservoir 4 and reservoir 5 (reservoir 4 at GND) to remove the dye solution from the separation channel. An injection voltage of -1500 V was applied between reservoir 1 and 3 (reservoir 1 at GND) for 15 s, followed by -6 kV between reservoir 4 and 5 to migrate the dye from the double T-junction to the detector.

2.2.3 Chemicals

Boric acid, sodium tetraborate (Borax) and sodium chloride were obtained from BDH (Toronto, Ont., CA). Tween 20 was purchased from Aldrich. Cy5 labeled monoclonal antibody against ovalbumin was obtained from Canada West Biosciences (Calgary, AB, CA). Rabbit polyclonal antibody (5.4 mg/ml, 100 μ l) against ovalbumin was obtained from DRES (Defense Research Establishment Suffield, Canada). Monoclonal anti-ovalbumin (mouse IgG1, 8.1 mg/ml, 0.5 ml) and ovalbumin grade (V)

were purchased from Sigma (St. Louis, MO, USA). The antibody was in mouse ascites fluid with a total protein concentration of 38 mg/ml. Cy5 bifunctional dye (Product No. PA 25000) was purchased from Amersham Pharmacia Biotech (Montreal, Quebec, CA).

2.2.4 Sample preparation

Stock solutions were individually prepared by dissolving ovalbumin (8.6 mg/ml), polyclonal anti-ovalbumin (1 mg/ml), monoclonal anti-ovalbumin (1 mg/ml) and bifunctional Cy5 dye (*ca.* 100 μ M) in 5 mM borate buffer (pH 9.2), containing 0.5% Tween 20. Concentrated solutions were diluted to their specific strengths with the same buffer.

2.2.5 Direct ovalbumin assay

The concentration range of ovalbumin for direct assays was between 51-135 μ g/ml. Solutions were transferred to a 250 μ l microcentrifuge tube and 47 μ l of borate buffer, pH 9.2, containing 0.5% Tween 20, and then 3 μ l of 1 mg/ml rabbit polyclonal antibody were added. The mixture was vortexed for 1 min and incubated at ambient temperature for 15 min. An aliquot was transferred to a microvial and inserted into the microapplication vessel assembly for analysis using a Beckman CE with on-column detection at 214 nm.

2.3 Results and Discussion

2.3.1 Electrical and Fluid Interface Plates of DARPA instrument

A photograph of a single channel microchip instrument that utilized the DARPA chip design [9] is shown in Figure 2.5. The instrument comprises three peripheral subsystems: a fluidic interface, a high voltage power supply, and an epiluminescence confocal microscope. The design of the fluid interface was dependent on the results of this thesis (Chapter 5).

A fixed and reusable interface plate for electrical and fluidic connections was fabricated from acrylic Plexiglas. The electrical leads from the HV power supply were connected to gold plated spring pin electrodes (Interconnect Devices Inc., Kansas City, USA) through the sides of the interface plate and were held in place by threaded screw press-fittings. Electrical contact with the fluid reservoirs was made through the gold plated electrodes. Threaded flange-free liquid chromatography mini-couplers for 1/16" o.d. tubing (Valco Instruments, Houston, TX, USA) were used as fluid reservoirs. This design provided a leak-free interconnection to the chip. The chip assembly was mounted on an X-Y-Z translation stage (Newport Instruments, Irvine, CA, USA). Sample was delivered to the chip by means of a mini-peristaltic pump (Instech Laboratories model P-625/900, Plymouth Meeting, PA). The fluid lines for delivering the sample were 0.020" i.d. silicone tubing (Instech) connected to the interface chip by the flangeless mini-couplers (Valco). A fluid interface was etched onto the chip for connection to the peristaltic pump lines.

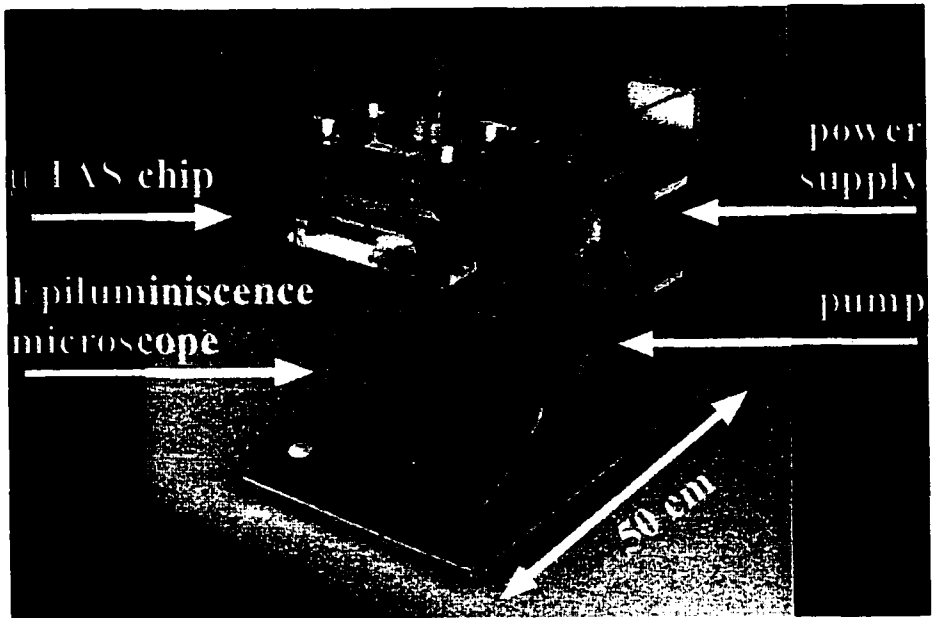


Figure 2.5 Photograph of DARPA instrument.

Initially, we employed the Faster chip (Figure 2.2) to study the interfacing of the chip to an external fluid system, e.g., a small beaker containing buffer. The chip was designed so that the microfabricated sample introduction channel (SIC) with two inlets intersected the sample inlet of the other channels. The SIC was 300 μm deep and 1 mm wide, whereas the other channels were about 10 μm deep and 36 μm wide at the top edge after etching. When a pressure was applied to one inlet of the SIC the main flow was through the SIC, because it had the lowest resistance to flow compared to the electrophoresis channels (see Table 2.1 and 2.2). Hence, the SIC allowed rapid sample exchange and continuous monitoring of external chemical events.

The DARPA chip includes all elements required for an automated immunoassay. These elements are rapid sample exchange, a sample introduction port for the world-to-chip interface, and an integrated immunoassay reactor which incorporates a method for performing on-chip mixing, reaction and separation of immunoreagents, sample and products. The exchange port design was based on the results obtained with the Faster chip.

2.3.2 Protein separations and immunoassay

A series of studies were performed to determine the feasibility of performing an ovalbumin (ov) affinity CE assay within the microchip, and to find a method to label the antibodies. We used two types of instruments, a commercial Beckman CE and the microchip devices. The Beckman CE instrument was used to evaluate the migration behavior of ovalbumin and the antibodies, optimize buffer conditions, check the biological activity of antibodies and investigate the ovalbumin assay before transferring such separation conditions to the glass chips.

Adsorption of proteins in CE in microchannels or fused-silica capillaries presents difficulties in terms of poor separation, or even no sample recovery. These problems must arise mostly from the interaction of positively charged protein molecules in the sample with the negatively charged inner wall of the fused-silica capillary [10]. Numerous efforts have been made to separate proteins by free solution CE. Some of these separation optimization methods include coating of the capillary surface, changing the pH of the separation or using additives, such as sodium chloride, in the separation buffer [11-27]. From the experimental point of view, coating is laborious and time-consuming, whereas, free solution CE in the presence of additives is simpler and separation may be more easily performed. By adjusting the pH of the running buffer to a pH higher than that of the *pI* of the proteins being separated, the charge of the capillary wall becomes negative, and the protein-capillary wall interactions are greatly minimized. We employed 5 mM borate buffer (pH 9.2) containing 0.5% Tween 20 to accomplish this. At this high pH, more silanol groups become ionized and the negative charge density on the wall surface increases, tending to repel proteins. Tween 20 is added to provide dynamic coating for the capillary walls. The other advantage of this buffer is its low absorbance of UV light [28], compared to the tricine buffer used previously in chip [27].

We first investigated the migration behavior of the polyclonal antibody (pAb), nonpurified monoclonal antibody (mAb) and ovalbumin (ov) using a Beckman CE with UV detection at 214 nm. Figure 2.6 depicts the electropherograms of the pAb, mAb, and ov. The electropherogram of mAb, Figure 2.6C shows two peaks with a smaller peak that migrates at 71 s. The first peak was identified as mAb since its migration time, 59 s.

closely matches that of pAb at 56 s, Figure 2.6B. The other two peaks in Figure 2.6C, were assigned to other components of the ascites fluid. Although the concentration of monoclonal antibody was twice than that of polyclonal antibody their relative intensity did not scale with the difference in concentrations. Such difference could be due to the presence of contaminants that could migrate with the antibody or the uncertainty of stock concentration of mAb provided by the manufacturer. We are not quite sure of the exact reason. Ovalbumin, which appeared at 72 s, Figure 2.6A, had a broader peak than its antibody. This is expected because ov is a highly heterogeneous glycoprotein [29]. The microheterogeneity arises from the two sites ASA₂₉₂ and/or ASA₃₁₂, which can be glycosylated [30, 31]. Glycosylation refers to the attachment of branched polysaccharides to a protein.

An electropherogram of a mixture of ov and pAb in a molar ratio of 9:1, respectively, is shown in Figure 2.7. The result demonstrated that pAb was biologically active, since a new molecular complex was obtained between the ovalbumin and antibody peaks. Ovalbumin binds to the antibody and the complex appears at 65 s. Ovalbumin is a smaller protein, at 45 kDa, than the antibody, at 150 kDa, so the migration shift of the antibody is due to the increase of the overall negative charge of the complex (pAb-ov) when ov binds to antibody. We carried many experiments to ensure that the complex peak is not an increased in shoulder peak of the ovalbumin as the concentration of ovalbumin increased.

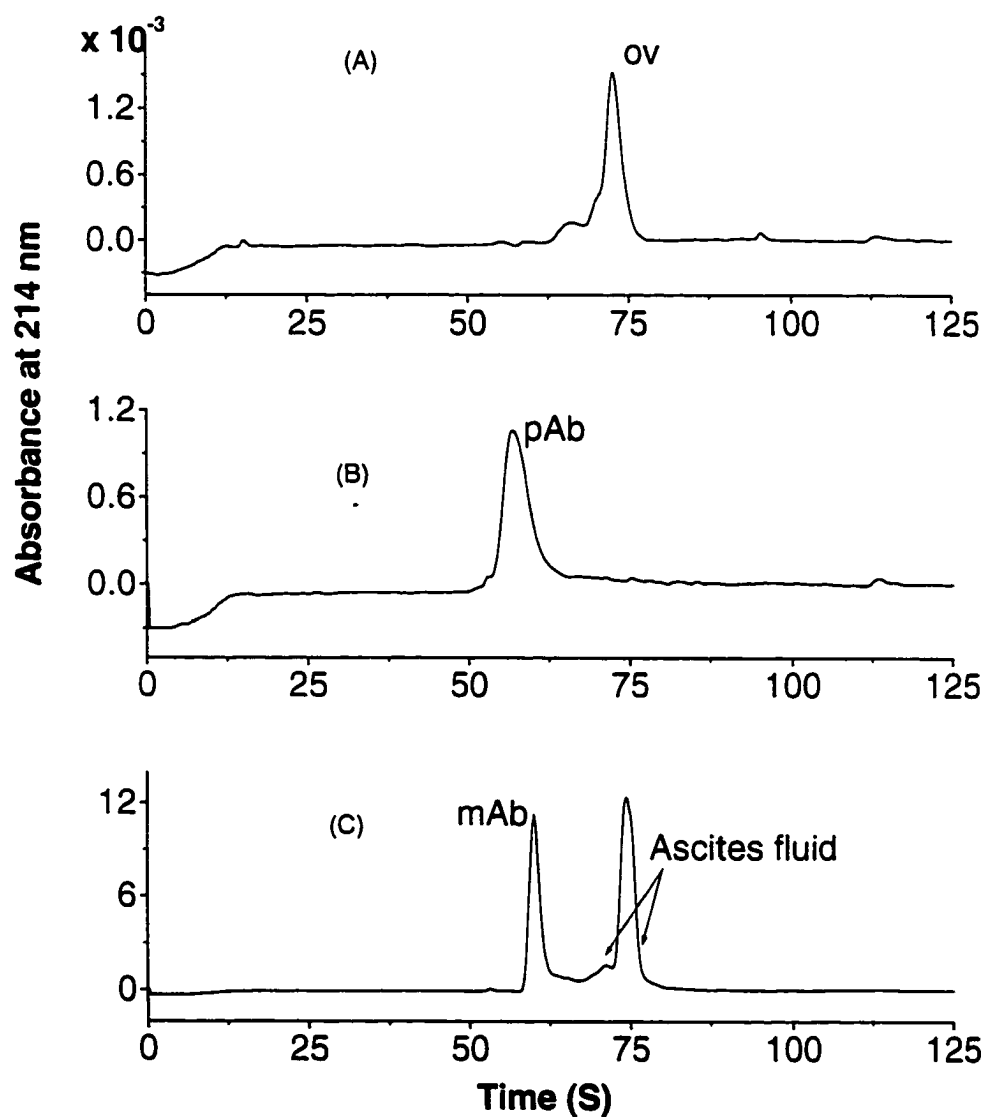


Figure 2.6 Electropherograms of (A) ovalbumin (50 $\mu\text{g/ml}$), (B) polyclonal antibody (50 $\mu\text{g/ml}$), and (C) nonpurified monoclonal antibody (100 $\mu\text{g/ml}$). Analyses were performed on Beckman P/ACE system model 5010. Separation conditions: Capillary 50 μm x 20 cm (effective length), 27 cm total length, bare fused silica; voltage-6 kV; separation buffer 5 mM borate buffer, 0.5% Tween 20, pH 9.2; injection-3s, pressure 0.5 psi; detection 214 nm.

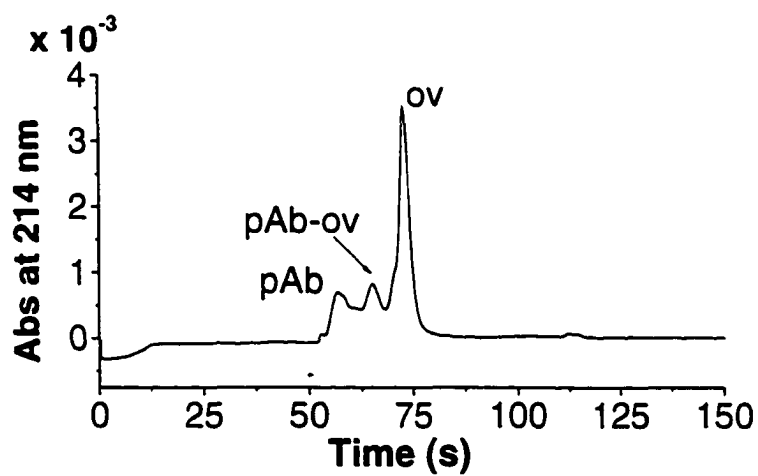
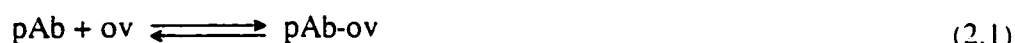


Figure 2.7 Separation of a mixture of ovalbumin and polyclonal antibody. Molar ratio of ovalbumin to monoclonal antibody was 9:1. Concentrations of pAb and ov were 30 $\mu\text{g/ml}$, and 270 $\mu\text{g/ml}$, respectively. Peak at 65 s is the complex of ovalbumin and polyclonal antibody. CE conditions were the same as in Figure 2.6.

The mixture was separated in the order of decreasing pI (isoelectric points). Ovalbumin has the lowest pI at 4.7 [32], and therefore has the longest migration time, while immunoglobulin (IgG) has a $pI > 6$ [33]. The pI value of the complex would be expected to lie between these values.

We further investigated the binding of ovalbumin to antibody (pAb) by a direct assay according to equation 2.1. The concentration of polyclonal antibody was kept constant and the concentration of ovalbumin was varied.



The antibody concentration was 50 $\mu\text{g/ml}$ and concentrations of ovalbumin were changed from 45-135 $\mu\text{g/ml}$. Figure 2.8 shows the recti-linear response as the concentration of ovalbumin increased.

2.3.3 Antibody labeling difficulties

The above results confirm that affinity CE can be used to detect ov. However, absorbance detectors on-chip are not very sensitive or very easy to make, so that fluorescence detection is preferred. This means a light source and a dye must be selected and methods to label the antibody must be available as well.

A field immunoassay detection unit will require a robust light source such as a solid state diode laser. Fluorescently-labeled compounds were chosen due to the high sensitivity of Laser induced fluorescence (LIF). When we started the project in 1997, red diode lasers were readily available at low cost, while green or blue lasers were not.

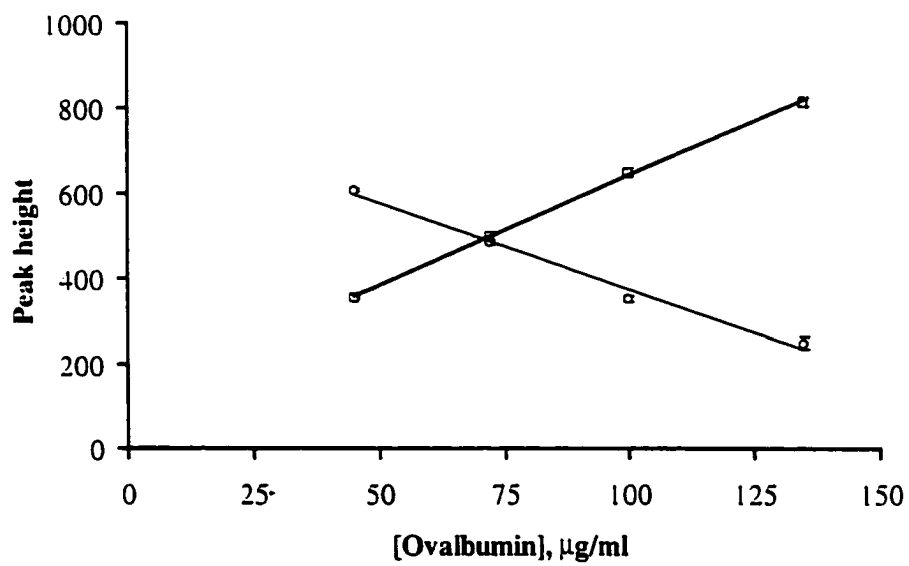


Figure 2.8 Calibration curve of direct ovalbumin immunoassay with fixed concentration 50 $\mu\text{g/ml}$ polyclonal antibody using Beckman CE system model 5010. Peak heights of antibody (circle) decrease, whereas peak heights of complex (square) increase as the concentrations of ovalbumin increase. The data points and error bars represent the mean and one standard deviation for four consecutive measurements.

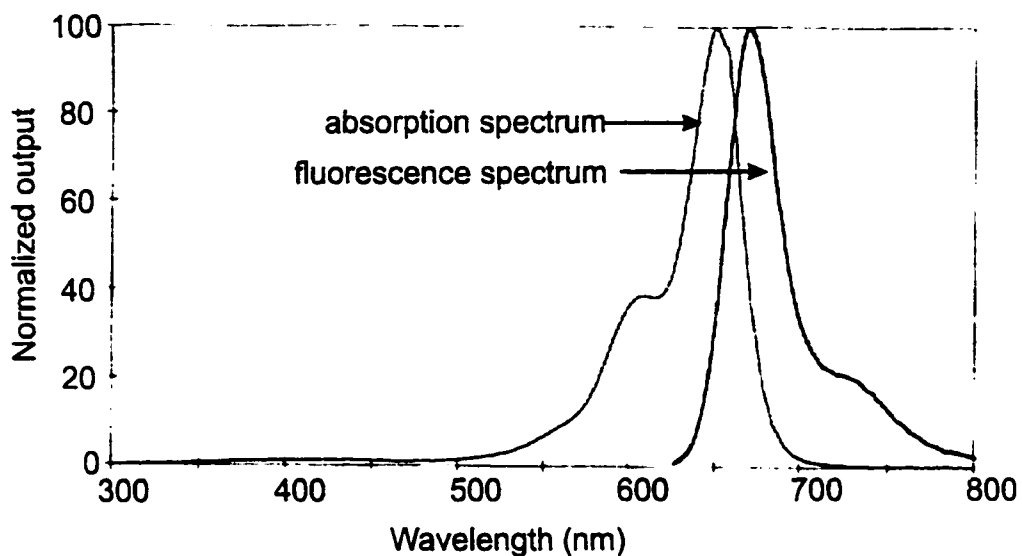


Figure 2.9 Bifunctional Cy5 dye absorption and fluorescence spectra. (Adapted from data sheet of Amersham with modification).

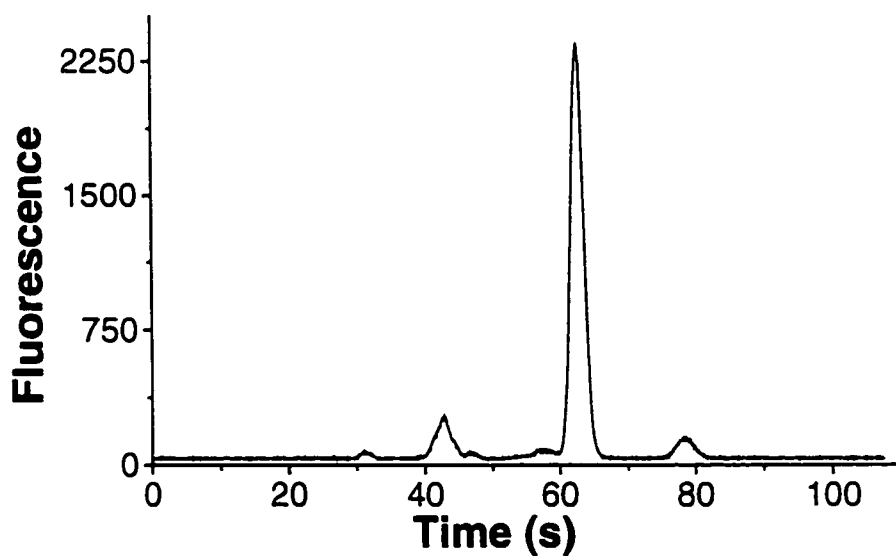


Figure 2.10 Electropherogram of 200 nM bifunctional Cy5 dye using the DARPA device and LIF detection; excitation wavelength 632.5 nm using He-Ne laser (5 mW); emission monitoring at 675 nm; separation voltage -6 kV.

This necessitated the use of a red fluorescent dye such as Cyanine 5 (Cy5) which is well matched to the 635 nm diode laser. Figure 2.9 displays the emission and excitation spectra of Cy5 dye. An electropherogram of Cy5 is shown in Figure 2.10. The labeling chemistry of commercially available Cy5 is limited to amine reactive functional groups.

In a direct assay, to test the presence of an antigen, the antibody must bear the Cy5 label to avoid the need to label samples. Therefore, we investigated a direct derivatization (labeling) procedure for the antibody with Cy5 dye by testing the activity of the Cy5-labeled antibody using CE. In direct derivatization, the antibody and dye solution were mixed at pH 8 (further details will be presented in Chapter 4), and then the labeled antibody was separated from the excess dye using a gel filtration column.

In the beginning of the project, Canada West Biosciences (CWB) provided us with labeled mAb against ovalbumin. Figure 2.11 shows the electropherogram of Cy5 labeled mAb and a mixture of ov and labeled mAb solution incubated for 20 min at room temperature. The Beckman CE with diode-LIF detection, $\lambda_{\text{excitation}}$ 635 nm, was used to analyze the samples. Separations shown in Figure 2.11B, indicated that either the labeled antibody was inactive (no complex peak was formed upon the addition of ovalbumin) or the complex co-migrated with the labeled antibody during the separation.

We investigated the possibility of variation in the migration times affecting the separation by using an internal standard. Internal standards are added to the sample to correct for quantitative losses during sample cleanup as well as instrumental imprecision, primarily caused by the injection process. We used an internal standard to check whether migration-time drifts were obscuring the formation of a complex. Figure 2.12A is the electropherogram of labeled antibody obtained using the Beckman CE with LIF

detection. We are not sure of the identity of peak 1 in Figure 2.12A. This peak was not observed in other samples either prepared in our lab or received from CWB. However, Peak 1 with migration time 53.8 s was used as the internal standard for migration time. There is also a negative deflection system peak at 88.9 s which could be used as internal standard for migration time. Peak 2 in Figure 2.12A was assigned as the labeled antibody (mAb*), with a migration time of 66.2 s. The peak identification was based on different experiments that were run under the same conditions. Peak 3 in Figure 2.12A was due to excess Cy5. To the same antibody we added excess ovalbumin (molar ratio of ov/mAb* was 9:1). Figure 2.12B displays the electropherogram of a mixture of ovalbumin and labeled antibody recorded on the Beckman CE with absorbance detection at 214 nm. The apparent mobility of the internal standard did not change, maintaining the same migration time (53.8 s). However, the system peak was slightly shifted to 86.9 s. The migration time of mAb* from Figure 2.12B was 66.8 s. The difference in migration times of mAb* before and after the addition of ovalbumin was 0.6 s. If any complex formed we would expect to see a shoulder or a partially resolved peak between the antibody and ov peaks based upon the UV data for unlabeled antibody. Alternatively, labeling might have shifted the peak position of mAb* enough to overlap the complex peak, so that conversion to complex caused a slightly broader peak or a very small shift. However, the 2 s shift in the system peak suggests that the shift in mAb* seen upon the addition of ov is within the experimental error and not indicative of reaction. Experiments with 1:3, 1:1, and 3:1 molar ratio of ov to mAb* always showed a single peak also. Consequently, we concluded a lack of activity was the most likely explanation for the results, and this was confirmed by the eventual preparation of active material.

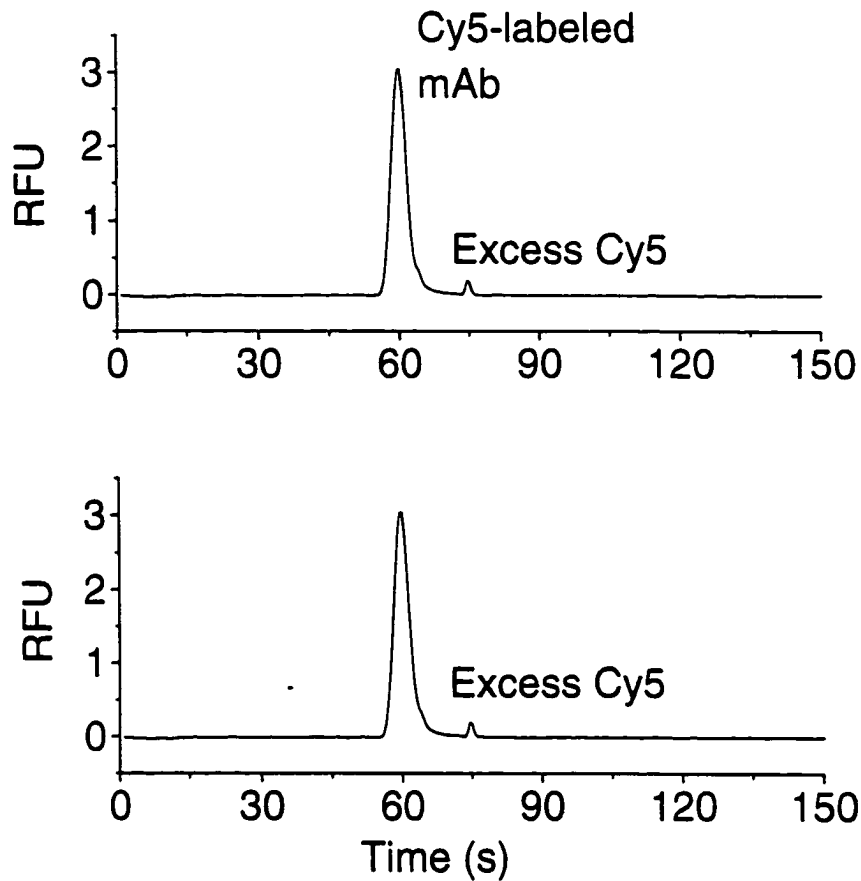


Figure 2.11 Electropherograms of Cy5-labeled monoclonal antibody (A) and mixture of nonlabeled ovalbumin and monoclonal antibody (B). (molar ratio of ov/mAb = 9:1). Concentration of mAb was 30 $\mu\text{g}/\text{ml}$. Analyses were performed on Beckman P/ACE system model 5010. Separation conditions: Capillary 50 μm x 20 cm (effective length), 27 cm total length, bare fused silica; voltage-6 kV; separation buffer 5 mM borate buffer, 0.5% Tween 20, pH 9.2; injection 3s, pressure 0.5 psi; detection LIF, excitation for detection was with 635 nm solid state diode laser (2.5 mW) and emission monitored at 675 nm..

Experiments were repeated several times with different batches of labeled antibody supplied either by the same company or by our own preparation, and the electropherograms were obtained from the Beckman CE or the chip. Complex peaks were occasionally observed with these differing batches. However, subsequent repeated synthesis of labeled antibody by the same method (i.e., direct labeling) did not often result in a product that could form a complex.

Conventional immunoassay, ELISA (Enzyme-Linked Immunosorbent Assay), performed by CWB at pH 7.1 (see Chapter 4) showed that the antibody was active, even though CE showed it to be inactive. To solve this dilemma, we had to consider that ELISA and CZE are two different techniques. In the absence of nonspecific adsorption of inactive labeled antibody, only functional antibody would bind to the immobilized ov and the inactive antibody would be washed away in later steps. This provides a built in affinity purification step for labeled antibody. Because ELISA is an amplification technique, relatively few molecules are needed to generate a signal. This effect makes ELISA sensitive to a small population of active mAb* in a larger population of inactive mAb* and puts a limitation on using ELISA to investigate the activity of mAb*.

On the other hand, CE can not discriminate between active and inactive antibody molecules since both will co-migrate. However, active antibody will form a complex that can be resolved from the mAb* peak, whereas, inactive mAb* will not. Thus, if the affinity constant is available then a known concentration of antigen can be added to at least 90% saturation of the antibody. The data set obtained may then be used to determine if the affinity constant for mAb* matches the expected value.

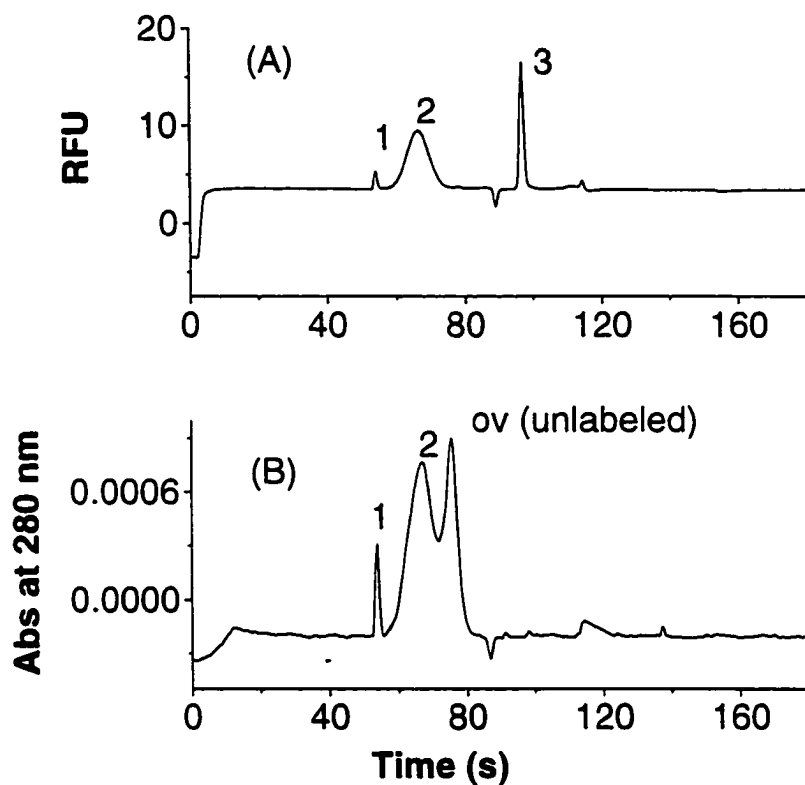


Figure 2.12 Electropherograms of Cy5-labeled mAb, 50 $\mu\text{g/ml}$ and ov present at a molar ratio of $\text{ov/mAb}^*=9:1$. Separation conditions were the same as in Figure 2.11, except that LIF detection was used for (A) and UV detection at 214 nm was utilized for (B). Peaks: (1) contaminant, labeled with Cy5, (2) Cy5-labeled antibody, and (3) excess Cy5.

If not, then some of the mAb* must be inactive. Alternatively, the conversion of all the antibody peak into the complex with enough antigen present to give saturation is an indication that all the molecules of antibody are active.

2.4 Conclusions

We described the automated instrument that was the goal of a DARPA funded project for the detection of toxin simulants. Two key elements for this instrument were identified as the contributions of this thesis. The first was an interface for the DARPA instrument to an external fluid. This interface, described in detail in Chapter 5, will allow automated sample introduction into the microchip for an analysis. Secondly, in developing an assay for ovalbumin using CE, we showed that the native polyclonal antibody had an affinity for ovalbumin and could be used for its determination. The complex and free probes (i.e., polyclonal antibody and ovalbumin) were separated using CE. However, upon labeling the antibody with Cy5 dye, it did not display any binding with ovalbumin. We conclude that the labeling deactivated the antibody. Consequently, if the desired assay of ovalbumin is to be used, then a different scheme for labeling the antibody must be developed.

2.5 References

- 1 D.J. Harrison, A. van den Berg, eds. *MicroTotal Analysis' 98*, Kluwer Academic Publishers, Norwell, MA, 1999.
- 2 A. Manz and H. Becker, eds, *Topics in current chemistry*, Vol 194, springer-Verlag, Berlin, 1998.
- 3 L. Tao and R.T. Kennedy, *Electrophoresis*, 18 (1997) 112.
- 4 C.S. Effenhauser, G.J. M. Bruin, A. Paulus and M. Ehrat, *Anal. Chem.*, 69 (1997) 3451.
- 5 O.-W. Reif, R. Lausch, T. Scheper and R. Freitag, *Anal. Chem.*, 66 (1994) 4027.
- 6 X. Huang, W.F. Coleman and R.N. Zare, *J. Chromatogr.*, 480 (1989) 95.
- 7 Z.H. Fan and D.J. Harrison, *Anal. Chem.*, 66 (1994) 177.
- 8 P.C.H. Li and D.J. Harrison, *Anal Chem.*, 69 (1997) 1564.
- 9 W E. Lee, A.B. Jemere, S. Attiya, N. H. Chiem, M. Paulson, J. Ahrend, G. Burchett, D.E. Bader, Y. Ning, and D.J Harrison, *J. Capillary Electrophoresis*, in print.
- 10 H. Engelhardt, W. Beck, T. Schmitt, *Capillary Electrophoresis: Methods and Potentials*, Viewig, Wiesbaden, 1994, pp. 102.
- 11 J.W. Jorgenson, *Trends Anal. Chem.*, 3 (1984) 51.
- 12 H.H. Lauer and D. McManigill, *Anal. Chem.*, 58 (1986) 166.
- 13 R.M. McCormick, *Anal. Chem.*, 60 (1988) 2322.
- 14 G.J. M. Bruin, J. P. Chang, R. H. Kuhlman, K. Zegers, J. C. Kraak and H. Poppe, *J. Chromatogr.*, 2 (1989) 429.
- 15 G.J.M. Bruin, R. Huisden, J.C. Kraak and H. Poppe, *J. Chromatogr.*, 20 (1989) 339.
- 16 J.S. Green and J.W. Jorgenson, *J. Liq. Chromatogr.*, 12 (1989) 2527.

- 17 M.M. Bushey and J.W. Jorgenson, *J. Chromatogr.*, 20 (1989) 301.
- 18 S.A. Swedberg, *J. Chromatogr.*, 503 (1990) 449.
- 19 J.K. Towns and F. E. Regnier, *J. Chromatogr.*, 516 (1990) 69.
- 20 K.A. Cobb, V. Dolnik and M. Novotny, *Anal. Chem.*, 62 (1990) 2478.
- 21 J.E. Wiktorowicz and J. C. Colburn, *Electrophoresis*, 11 (1990) 769.
- 22 W. Nashabeh and Z. El Rassi, *J. Chromatogr.*, 559 (1991) 367.
- 23 J.R. Florance, Z.D. Konteatis, M. J. Macielag, R. A. Lessor and A. Galdes, *J. Chromatogr.*, 559 (1991) 391.
- 24 R.L. Cunico, V. Gruhn, L. Kresin, D. E. Nitecki and J. E. Wiktorowicz, *J. Chromatogr.*, 559 (1991) 467.
- 25 I.Z. Atamna, H. J. Issaq, G. M. Muschik and G. M. Janini, *J. Chromatogr.*, 588 (1991) 315.
- 26 N.A. Guzman, J. Moschera, K. Iqbal and A. W. Malick, *J. Chromatogr.*, 608 (1992) 197.
- 27 N. Chiem and D. J. Harrison, *Anal. Chem.*, 69 (1997) 373.
- 28 M.A. Friedberg, M Hinsdale, Z.K. Shihabi, *J. Chromatogr.*, 781 (1997) 35.
- 29 Y. Chen, J. -V. Holtje and U. Schwarz, *J. Chromatogr.*, 685 (1995) 121.
- 30 C.-C. Huang, H.E. Mayer and R. Montgomery, *Carbohydr. Res.*, 13 (1970) 127.
- 31 C.G. Glabe, J.A. Hanover and W.J. Lennarz, *J. Biol. Chem.*, 255 (1980) 9236.
- 32 J. Turková, L. Petkov, J. Sajdok, J. Káš and M.J. Beneš, *J. Chromatogr.*, 500 (1990) 585.
- 33 M. Mammen, F.A. Gomez and G.M. Whitesides, *Anal. Chem.*, 67 (1995) 3526.

Chapter 3

Affinity protection chromatography for labeling mouse monoclonal antibody (IgG1) with Cy5 dye

3.1 Introduction

In bioanalysis, low concentrations of analytes usually must be determined in the presence of high concentration of interfering endogenous and exogenous compounds. One analytical technique that provides both selectivity and sensitivity is capillary electrophoresis with laser-induced fluorescence detection, (CE-LIF). Capillary electrophoresis has become a routine technique, and is characterized by short run times, and high efficiency. The method is applicable to analysis of small molecules and biopolymers such as peptides, proteins, and oligonucleotides. Detection in CE can be performed by fluorescence, chemiluminescence or electrochemically. The limitation of the above-mentioned techniques is their inherent limits in selectivity, which means that frequently a derivatization reaction should be incorporated into the analytical procedure [1,2] in order to make the analyte measurable. By incorporating a derivatization procedure and LIF detection, analyte concentration detection limits in the zmol range have been achieved [3].

Although, in principle, almost any detection mode can be enhanced by a derivatization procedure, fluorescence (LIF) monitoring is normally favored. The obvious reason is that it is applicable to a variety of solvent systems compared to electrochemical detection. An additional problem associated with electrochemical detection is the contamination of the electrodes during analysis of complex matrices.

Recently, infrared (IR) and near-IR diode lasers have become available [4-6]. Diode laser-induced fluorescence (DIO-LIF) is considered a promising technique for analytical detection because of the following advantageous characteristics: (1) they emit radiation with wavelengths longer than 620 nm, where background signals due to fluorescence from optical impurities are reduced; (2) they are stable (intensity fluctuations <0.003 %); (3) inexpensive (<US\$100.0 for a 10 mW laser emitting at 670 nm); (4) small (<10 mm³ for the total package) and (5) have a life time of over 25000 h. In contrast, a deep UV laser, < 300 nm, which is used to excite the native fluorescence of proteins molecules is much larger than a diode laser.

The greatest limitation of the DIO-LIF- CE is that it is limited to red fluorescing compounds excited in the near IR region, therefore a derivatization procedure is usually required [7]. While various types of derivatization are conducted for many different purposes, our interest is in reactions that produce a covalent bond to a fluorescent label. During labeling procedures a covalent bond is formed between the analyte and the labeling agent.

One classification of derivatization procedures is based on their location in the analytical set-up: before (pre-column) [8], during (on-column) [9] or after (post-column) [10] the electrophoretic separation. The most suitable method of derivatization depends on the reason why the derivatization is introduced, the number of samples that must be analyzed, and the physicochemical properties of the analytes and reagents. Proteins can be converted into fluorescent derivatives by attaching amine-reactive fluorescent probes [11]. These probes contain an amine reactive moiety and are covalently attached to the proteins through their primary amines, such as the N-terminus or lysine residues.

For small molecules, e.g. amino acids and ethyl alcohol, labeling reactions are less complicated than with proteins, antibodies or peptides and have been optimized for several decades [12,13]. Small molecules usually have a single site of attachment and a single product is often formed in high yield. Mank and Yeung [14] utilized dicarbocyanine fluorophore with single succinimidyl ester functionality to label 18 amino acids. The electropherogram of the 18 labeled amino acids does not show much background and the labeled amino acids are separated. However, the derivatization must be performed at concentrations of 2.5×10^{-7} M or higher, because in aqueous solution hydrolysis of the label competes with the derivatization procedure. Dovichi et al., previously demonstrated something similar with fluorescein isothiocyanate, FITC, [3].

Derivatization procedures are, however, different for proteins, antibodies and peptides. This is because proteins often have several sites of reactivity, especially amino groups. These nitrogen groups could be N-terminal, lysine derived, arginine derived or heterocyclic. In general it is the N-terminal and lysine free amino groups which compete for the reagent [15]. Thus for a simple protein like insulin, that has many different functional groups, multiple tagged products will be produced; singly tagged at different amino acids, di-tagged, tri-tagged and so forth [15]. These products are usually formed at different reaction rates, with different efficiencies of conversion and in different yields. Evangelista and Chen [16] labeled morphine with a commercially available Cy5 (Cyanine) dye. Morphine-Cy5 was purified from excess dye using gradient elution with methanol, then its reactivity was tested against four commercially available antibodies. Only one antibody displayed significant binding to the labeled morphine. The authors explained these results as due to the morphine-Cy5 binding site being incompatible with

that of the antibody site. This demonstrates that direct labeling is not a guaranteed procedure even for small immunogenic molecules.

In addition to not producing homogeneous tagged products, some monoclonal antibodies completely lose activity after coupling, whether it be to a macromolecule such as enzymes, or to haptens such as biotin or fluorescent molecules. That is because most couplings involve a chemical reaction to an amino group, mainly lysine [17]. Those reactions involving lysine molecules present in or very close to the antibody binding site can cause alteration of the tertiary structure of the antibody and as a result the loss of antibody activity. It is likely that this phenomenon also occurs within a population of polyclonal antibodies, but giving their heterogeneity, it involves a fraction of population and is partially masked. In contrast, when this phenomenon occurs in a homogeneous population of monoclonal antibodies, it results in nearly a complete loss of activity. For this reason it is recommended that when monoclonal antibodies are labeled their capacity to tolerate the blocking of lysine be tested beforehand. Burkot et al. [18] reported that monoclonal antibodies lost their capacity for binding antigen after conjugation with periodate-oxidized horseradish peroxidase (HPO). The authors concluded that HPO reacted with primary amines in or near the binding site yielding inactive conjugates. They suggested using fluorodinitrobenzene followed by indirect immunofluorescent antibody analysis (IFA) to screen a bank of antibodies, in order to identify those antibodies which would probably yield successful antibody-enzyme conjugates prepared with HPO. Shimura and Karger [19] avoided labeling the amino group and selectively labeled the thiol groups at the hinge region of the antibody. They used pepsin to hydrolyze mouse monoclonal antibody (IgG1) against human growth hormone (HGH)

and obtained $F(ab')_2$ fragments. After reduction of the S-S bridge between the monovalent Fab' fragments, a thiol group was formed in the C-terminal region of the fragments. The authors added tetramethylrhodamine- iodoacetamide solution to label these thiol groups. however, the chemistry of this approach was complex and yields were very low (1.8%).

In this chapter, we use a recombinant protein G affinity column to purify monoclonal antibody (mAb) against ovalbumin from mouse ascites fluid. The data for the recovery and purity of the harvested mAb will be presented. We will describe a novel method for labeling the antibody by what we call affinity protection chromatography (APC). A commercially available bifunctional Cyanine (Cy5) dye was used as a labeling agent. The dye has a high extinction coefficient ($250\ 000\ M^{-1}\ cm^{-1}$ at 649 nm), a good quantum yield (0.28 depending on dye/protein ratio), good water solubility and photostability. Its absorption and emission are in the near IR and these are suitable for use with a 635 nm diode laser. A protocol for labeling mAb with Cy5 using the APC method will be described. To the best of our knowledge, this approach has not been described in the open literature, though it has been suggested as a possible format in a review [20].

3.2 Experimental

3.2.1 Material and reagents

Monoclonal anti-chicken egg albumin (isotype IgG1) and ascites fluid (clone OVA-14) were purchased from Sigma (St. Louis, MO, USA). Rabbit polyclonal anti-chicken egg antibody was purchased from Biodesign International (Kennebunk, ME, USA). ImmunoPure immobilized protein G, 2 ml, (Product No. 20398), ImmunoPure[®] (G) binding buffer (Product No. 21011), and ImmunoPure[®] IgG elution buffer (Product No.

21009) were obtained from MJS Biolink Inc. (Brockville, Ontario, CA). To pack protein G gel, 5 ml of a polypropylene column (product No. 29922) with a 0.4" diameter and a 45 µm porous disc was obtained from MJS Biolink Inc. Bifunctional Cy5 dye (product No. PA 25000) and Cyanogen bromide, CNBr-activated Sepharose 4B (Code No. 17-0981-01) were obtained from Amersham Pharmacia Biotech (Montreal, Quebec, CA). Disposable PD-10 desalting columns were purchased from Amersham Pharmacia Biotech. A centricon concentrator with a molecular weight cut-off 30,000 was obtained from Millipore (Canada) Ltd (Nepean, Ontario, CA). All chemicals were reagent grade.

3.2.2 Electrophoresis

The instrumentation for capillary electrophoresis using glass chips and the commercial Beckman CE were described in Chapter 2.

3.2.3 Purification of the mouse IgG1

Two ml of protein G gel was poured into a disposable plastic column (MJS Biolink Inc., Product No. 29922) that had a frit at the bottom to hold the gel. The gel was washed with 20 ml of binding buffer, pH 5.0. Approximately 0.5 ml of the binding buffer was left at the top of the gel and another frit was placed just above the level of the buffer. A 0.5 ml solution of monoclonal mouse anti-ovalbumin was diluted with an equal volume of binding buffer and applied on the column using a pasteur pipette. The sample was allowed to enter the column completely. Then, the column was washed with 20 ml of the binding buffer at a flow rate of 0.6 ml/min. IgG1 (mAb) immobilized on the column was eluted with elution buffer (pH 2.8) and 1 ml fractions were collected. Fractions were neutralized with 200 µl of 0.5 M sodium phosphate buffer, pH 8.0. When the elution was complete the column was washed with 20 ml of the binding buffer followed by 15 ml of

0.02% sodium azide (NaN_3) and stored at 4 °C. The same column was used five times without deterioration in its binding properties. The absorbance of the fractions was measured at 280 nm using a photodiode array, single beam UV-VIS spectrophotometer. Fractions with high absorbance were pooled. Then, 2 ml of the purified mouse IgG1 was desalted in PBS buffer (phosphate-buffered saline, pH 7.0) or 0.1 M bicarbonate buffer, pH 8.4, containing 0.5 M NaCl using a PD-10 desalting column.

3.2.4 Direct or precolumn derivatization of mouse IgG1

One mg/ml of purified and desalted mouse mAb was added to vial containing powdered Cy5 dye (*ca.* 100 - 110 nmol). According to the manufacturer, this amount of dye is enough to label up to 10 mg of protein. The mixture was vortexed for 10 s and then allowed to stand for 30 min at room temperature and protected from light. Under these conditions, the coupling reaction proceeded to a plateau level [25]. The reaction mixture was then transferred to a Sephadex G25 column (0.7 x 15 cm) equilibrated with PBS buffer. The buffer was running at a flow rate of 0.7 ml/min. Fractionation on this column served two functions: (a) removal of unbound Cy5 dye and (b) change of the ionic strength and buffer composition prior CE analysis. The first colored band to emerge was collected and its absorbance value at 280 nm and 650 nm were measured. The dye/protein ratio was determined from the absorbance values at these two wavelengths.

3.2.5 Enzyme-Linked Immunosorbent Assay (ELISA)

The ELISA experiments were performed by Canada West Biosciences. The direct ELISA protocol on a Nunc polystyrene 96 well flat bottom plate was as follows: 50 μl volume of coating buffer (0.5 M carbonate buffer, pH 9.1) and 50 μl of 10 mg/ml

ovalbumin grade VI (Sigma) were added to each well and all wells were incubated overnight at 4 °C. The wells were washed six times with PBST (1 % Tween 20, PBS pH 7.0). In order to decrease non-specific adsorption, 200- μ l of blocking buffer (5 % skim milk + 2 % BSA in PBS) was added to each well and the whole plate was incubated for 1 h at room temperature; then the wells were washed with PBST six times. Aliquots of 100 μ l containing various dilutions of Cy5-labeled and unlabeled monoclonal anti-ovalbumin were added to the test antigen and incubated at room temperature for 1 h. As a negative control, dilutions of anti-peptide E IgG monoclonal antibody were included in the assay. After washing with PBST, each well was incubated with 100 μ l/well of 2000x diluted donkey anti-rabbit-horseradish peroxidase conjugate (Jackson Immunological) for 1 h at room temperature. After washing with PBST, color was developed using 90 μ l/well of 2,2'-azino-bis(3-ethylbenzothiazoline-6-sulfonic acid) diammonium salt (ABTS) solution (0.3 mg/ml in 0.1 M citrate buffer containing 0.01 % H₂O₂, pH 4).

3.2.6 Direct derivatization controlling the dye to protein ratio

A mM stock solution of Cy5 dye was prepared by adding to the vial containing the Cy5 dye 100 μ l of *N,N*-dimethylformamide (DMF) (99.8%, anhydrous) from Sigma. Six plastic vials containing 0.5 ml of rabbit polyclonal antibody (1 mg/ml) dissolved in 0.1 M NaHCO₃ (pH 9.0) were labeled with Cy5 solution in DMF by adding aliquots of 5 μ l, 10 μ l, 25 μ l, and 50 μ l of the stock Cy5 dye to each vial. The vials were incubated for 30 min at ambient temperature. The unbound dye was separated from the labeled polyclonal antibody using a Sepadex G50 (0.7 cm i.d. x 15 cm) column equilibrated with 20 mM borate buffer, pH 8.5, containing 0.5 M sodium chloride. The final concentration of the

labeled antibody and attached dye was estimated from UV/Vis measurements as described below.

3.2.7 Immobilization of ovalbumin on CNBr-activated Sepharose 4B

Ovalbumin (100 mg) was dissolved in 12 ml of coupling buffer (0.1 M sodium bicarbonate-0.5 M sodium chloride, pH 8.4). Ovalbumin solution (200 μ l) was removed and diluted to 1 ml with doubly distilled, de-ionized water and the absorbance ($A_{1_{total}}$) was measured at 280 nm. Two grams of freeze dried CNBr gel (Pharmacia) were re-swelled in 20 ml of 1 mM hydrochloric acid and transferred to a sintered glass funnel. The gel was filtered and washed with 500 ml of cold 1 mM hydrochloric acid. The house vacuum was adjusted so that the washing step took 30 min. Immediately prior its use, the gel was washed with 100 ml of doubly distilled de-ionized water followed by 10 ml of the coupling buffer, drained and rapidly transferred to a glass vial containing ovalbumin solution. The solution was mixed end-over-end in a 20 ml glass vial for 2 h at room temperature. The suspension was allowed to settle and 200 μ l of the supernatant containing unbound ovalbumin was pipetted and diluted to 1 ml with doubly distilled, de-ionized water. The absorbance of the unbound ovalbumin ($A_{2_{free}}$) was determined at 280 nm. The percentage of ovalbumin coupled to the CNBr-activated Sepharose beads was calculated using UV absorption of the ovalbumin solutions before and after the coupling reaction. Equation 1 was used to calculate the coupling efficiency.

$$\text{Coupling efficiency} = \frac{A_{1_{total}} - A_{2_{free}}}{A_{1_{total}}} \times 100 \quad (3.1)$$

The volume of gel in a glass vial was determined by pouring the contents of the vial to a graduated cylinder. To remove excess ovalbumin, the gel was transferred to a sintered glass funnel and washed with 100 ml of the coupling buffer. Suspending the gel in 12 ml

of 1 M ethanolamine (pH 8) buffer blocked the uncoupled sites on the CNBr matrix. The suspension was tumbled end-over-end for 2.5 h at room temperature. The gel was washed alternately six times with 20 ml of acetate buffer (0.1 M, pH 4) and 20 ml of coupling buffer, pH 8.4, to remove excess ethanolamine. The final rinse was with the coupling buffer. The gel was transferred to a glass vial and *ca.* 3 ml of purified monoclonal antibody (3.5 mg) were added to the gel. In order to determine the amount of antibody coupled to the immobilized ovalbumin, 200 μ l of the supernatant were taken immediately after adding the antibody to the gel, diluted to 1 ml with doubly distilled, de-ionized water and the absorbance at 280 nm was measured, giving A_{total} . This value is the absorbance of antibody offered for coupling to ovalbumin immobilized on the gel. The gel was tumbled end-over-end for 0.5 h at room temperature. Then another 200 μ l were removed from the supernatant and diluted to 1 ml with doubly distilled, de-ionized water. The UV absorbance at 280 nm corresponds to the concentration of uncoupled antibody, A_{free} . Equation 3.2 was used to calculate the percentage of bound antibody.

$$Bound (\%) = \frac{A_{total} - A_{free}}{A_{total}} \times 100 \quad (3.2)$$

3.2.8 Labeling of immobilized mAb to ovalbumin column

To label the mAb with reactive Cy5 dye, we used seven vials, each containing *ca.* 100 nmol of Cy5 dye. With a pasteur pipette approximately one ml of the suspension gel was added to one dry vial containing the dye, and immediately the mixture was vortexed for 10 s. Another 1 ml of the gel was added to another vial. This process was repeated until all the gel was added to the seven vials of Cy5 dye. Then the contents of all vials were poured into a clean 20 ml glass vial. The suspension was mixed end-over-end at

room temperature for 1 h. Excess dye was removed by transferring the gel into an empty column (1.5 cm x 18 cm) and subsequently washed with 20 ml of the coupling buffer or until the effluent was clear. The labeled antibody was recovered by changing the pH of the gel column. ImmunoPure[®] IgG elution buffer, pH 2.8, (from Pierce) was added to the column using a pasteur pipette and the pH of the eluent was checked with pH paper. When the pH of the effluent became acidic, the column was blocked by placing a cover at the top and bottom, in order to incubate the gel in 8 ml of the acidic buffer for about 10 min. The content of the column was occasionally mixed. The column was supported vertically and a *ca.* 4 ml fraction was collected in a test tube that contained 1.5 ml of 0.5 M di-sodium phosphate buffer (pH 8) for neutralization. The absorbance of the labeled antibody was measured at both 280 nm and 650 nm to determine the conjugation ratio (amount of the dye attached to the antibody). The incubation of the gel with 8 ml of glycine buffer was repeated. Fractions collected with a dye/protein ratio >1 were pooled and concentrated to 2 ml using a Centricon Amicon filter, with a molecular weight cutoff of 30,000. The labeled antibody was passed through a PD-10, Sephadex G25 desalting column (Pharmacia) equilibrated with borate buffer, pH 8, containing 0.5 M sodium chloride, at a flow rate of 0.7 ml/min to exchange the buffer. The concentration of the labeled antibody was determined from its absorbance at 280 nm, assuming a value of 1.35 [Pharmacia catalogue, 1999] for 1 mg/ml of antibody (IgG) at 280 nm. The immunological activity of the labeled antibody was tested by either conventional capillary electrophoresis or by using a microfluidic chip.

3.3 Results and Discussion

Affinity chromatography is a useful technique for separating biologically active substances from their contaminants. Recent advances such as identification and cloning of the gene for streptococcal protein G [21] and the development of suitable binding conditions [22] for this recombinant ligand have allowed researchers [23] to use high performance chromatographic systems for the routine purification of IgG from human serum. We purified mouse mAb from mouse ascites, since contaminants in ascites fluid would exhibit non-specific adsorption on a CNBr-ovalbumin column. These contaminants could also be labeled with Cy5 dye and co-eluted with the labeled mAb during elution from the CNBr-ovalbumin column. The electropherogram of non-purified mAb in ascites fluid is shown in Figure 2.6C (see Chapter 2). The electropherogram contains three unresolved peaks, the first peak, with a migration time of 58 s, was assigned to the monoclonal antibody. The other two peaks were due to impurities in mouse ascites fluid; they were the by-products of the mAb process [24]. Monoclonal antibody-producing hybridoma, injected into the peritoneal cavity of a mouse will secrete ascites or ascitic fluid. The ascites contains many contaminants including host proteins, lipids, and cell debris. Host proteins are the most problematic and include albumin, transferrin, and immunoglobulins. These three contaminants pose three different problems when separating from mAbs [25]: albumin because of its abundance; transferrin, because of the similarity of its charge characteristics to those of many mAbs; and host immunoglobulins, because of the similarity of their properties to those of mAbs.

Recombinant protein G (rec G) was used to purify the monoclonal antibody from ascites fluid. DNA sequencing of native protein G identifies two IgG binding domains

[21], in addition to sites for albumin and cell surface binding. The albumin and cell surface binding domains have been eliminated from rec G to reduce non-specific binding. With the albumin removed, protein G can be used to separate albumin from crude mouse IgG1. Rec G immobilized on Sepharose has a maximum of two binding sites for the Fc region of mAb. Figure 3.1 illustrates the mechanism of purification of mAb from ascites fluid. The elution profile for mAb is shown in Figure 3.2. Fractions No. 4 and 5 contained high concentrations of mAb. Those fractions were collected and their final concentration was measured by UV absorption at 280 nm. As shown in Figure 3.2, the protein G column was utilized five times without losing its binding efficiency. The recovery of the mAb using recombinant protein G was > 95%.

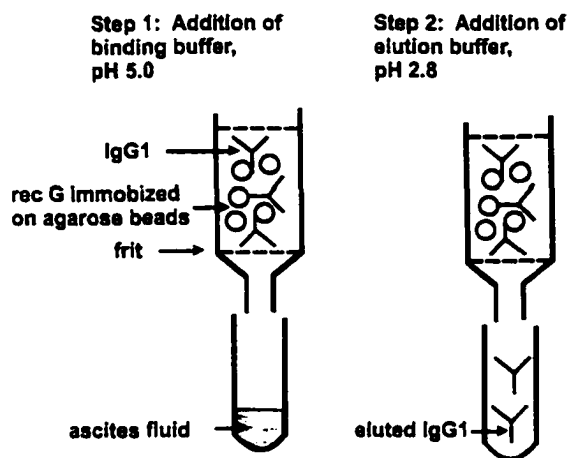


Figure 3.1 Mechanism of mouse monoclonal antibody (IgG1) purification from ascites fluid using 2 ml of gel of recombinant protein G immobilized on agarose beads.

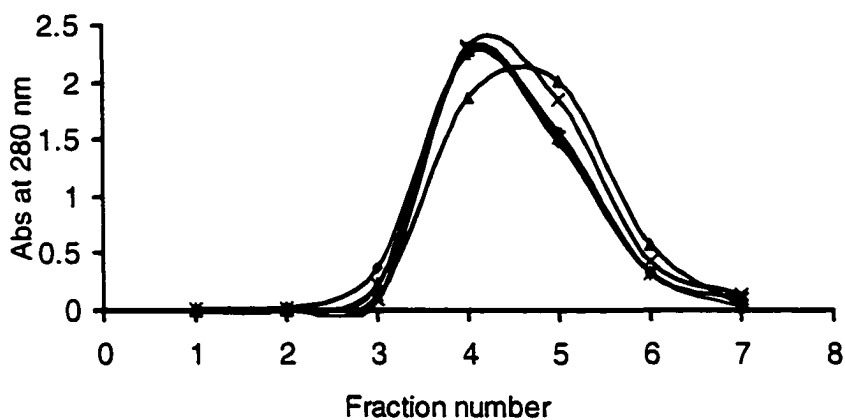


Figure 3.2 Elution profiles of mouse IgG1 from protein G column.

The purity of the recovered mAb was tested by CE with UV detection at 214 nm. CE can rapidly evaluate the purity of proteins [27] compared to slab gel electrophoresis or ELISA, which are labor-intensive and are not readily automated for analysis and quantitation of proteins. Figure 3.3 shows the electropherogram of the purified mAb. In comparison with the electropherogram of nonpurified mAb (Figure 2.6C, Chapter 2), only one peak was obtained with a migration time of 60 s. The purity of the antibody is apparently 100 %.

The peak shape shown in Figure 3.3 is distorted. The peak distortion may be due to anti-stacking [28] effects. Anti-stacking occurs when the ionic strength of the injected sample is higher than that of the background separation buffer. Because the sample eluted from the protein G column was in a mixture of buffers (elution buffer, and 0.5 M Na₂HPO₄ buffer), the ionic strength of the purified antibody was higher than the separation buffer (15 mM Borate buffer, pH 8.5 containing 15 mM NaCl).

We exchanged the ionic strength and pH of the purified mAb solution using a PD-10 desalting column, equilibrated with 20 mM borate buffer, pH 8.5, containing 0.5 M NaCl solution. Fractions with high UV absorbance at 280 nm were pooled. Increasing the ionic strength of the running buffer of the PD-10 column improves recovery. When the mAb was desalted in distilled de-ionized water without any salt added the recovery was only 40%. The best recoveries of the purified mAb from PD-10 column was >90 % in the presence of 0.5 M NaCl, borate buffer (pH = 8.5).

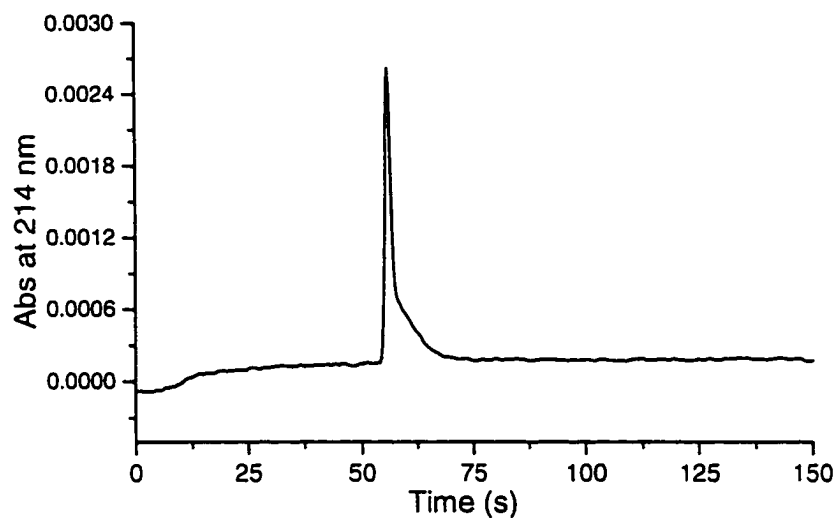


Figure 3.3: Electropherogram of purified antibody from protein G column without desalting the elution buffer. Separation conditions: 50 μm x 27 cm capillary; running buffer 15 mM borate buffer (pH 8.5) containing 15 mM NaCl; injection for 3s using low pressure, 0.5 p.s.i.; applied voltage 16 kV.

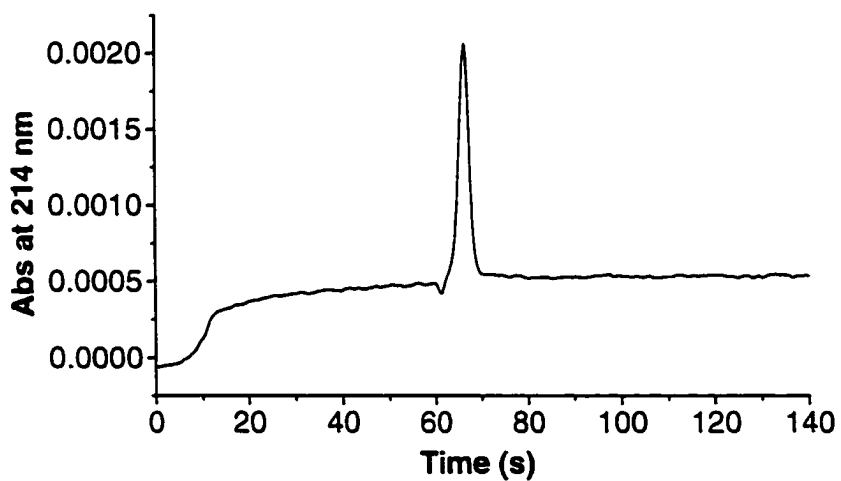


Figure 3.4 Electropherogram of purified antibody eluted from PD-10 desalting.

Reproducibility of the recovery from the PD-10 column was excellent ($\pm 3\%$ RSD, $n=5$), when 0.5 M of sodium chloride solution was added to 20 mM borate buffer. When desalted mAb was diluted so that its final ionic strength was less than or equal to that of the running buffer, a Gaussian (symmetrical) peak was obtained, as shown in Figure 3.4. The monoclonal antibody recovered from the desalted column retained its biological activity. This was confirmed by the formation of the complex peak when ovalbumin was mixed with the antibody and the mixture analyzed by absorbance detection with CE (see Chapter 4, Figure 4.3). This test is imperative, and must be done prior to labeling the antibody.

The advantages of CE are both short run time and the need for less reagents to check whether the labeled antibody is active or not. ELISA is labor-intensive and time-consuming compared to CE and it is subject to nonspecific adsorption as source of error. As a result, the unlabeled antibody has to be used as a negative control to correctly interpret the ELISA data.

3.3.1 Calculation of dye to antibody ratio(D/P)

A simple method [29] for estimating D/P involves measuring antibody (mAb) absorbance at 280 nm and Cy5 dye absorbance at its absorption maximum (650 nm), as shown in eq. 3.3.

$$D/P = \frac{A_{dye} \epsilon_{dye, 650nm}}{(A_{280nm} - 0.1A_{dye, 650nm}) \epsilon_{Ab, 280nm}} \quad (3.3)$$

The extinction coefficient of the Cy5 dye was $250,000 \text{ M}^{-1} \text{ cm}^{-1}$ at 650 nm (Amersham) and the extinction coefficient of antibody at 280 nm was taken to be $202,500 \text{ M}^{-1} \text{ cm}^{-1}$. This value was calculated based on the assumption that the extinction coefficient of mAb for 1 mg/ml of mAb is $1.35 \text{ mg}^{-1} \text{ ml}^{-1}$ (Pharmacia Catalogue, 1999), while the molecular

weight of mAb (IgG1) that we determined by Matrix Assisted Laser Desorption Ionization (MALDI) was 150,000 Da. The 0.1 factor in the denominator accounts for the dye absorption at 280 nm, which we determined to be 10 % of the absorption of the dye at its maximum. Figure 3.5 shows the UV/Vis spectrum of Cy5-labeled antibody. Fixing the absorbance values at 280 nm and 650 nm for the labeled antibody to equation 3.3 yields D/P ratio 1.7.

3.3.2 Disadvantages of direct derivatization

By direct derivatization, we refer to a labeling procedure where a covalent bond is formed between the analyte (mAb) and the labeling reagent (Cy5 dye) by directly mixing the two reagents together.

Several experiments were performed for direct derivatization of mAb with Cy5 dye using the recommended protocol from the supplier (Amersham). Figure 3.6 shows the derivatization reaction of Cy5 and the antibody where a covalent bond (an amide bond) is formed between an amino group of the antibody and Cy5 dye. A hydrolysis reaction of Cy5 which competes with the derivatization reaction is also shown in Figure 3.5. Bifunctional Cy5 dye was used in this study instead of the monofunctional dye, which contains only one succinimidyl group, because the monofunctional dye was reported to be less efficient [30]. The molar ratio of D/P for the labeled antibody using direct derivatization was 3 – 7.

As shown in Chapter 2, direct derivatization results in inactive antibodies. Derivatization is a random process and because antibodies have several sites for reactivity including four N-terminal amino groups at their binding sites, its is likely

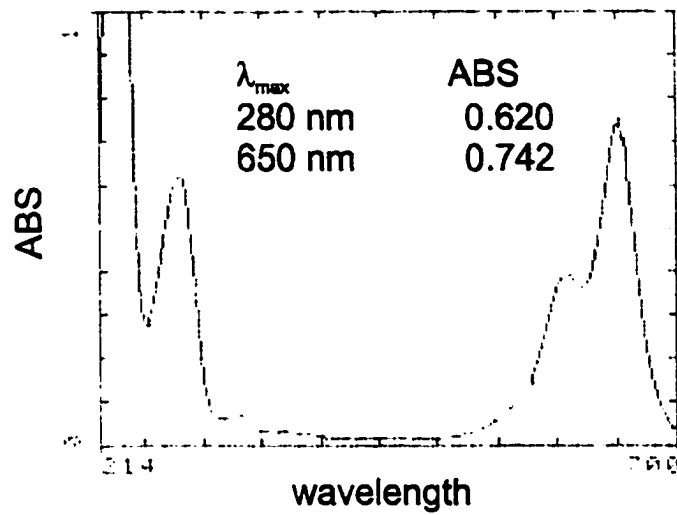


Figure 3.5 UV/Vis spectrum of Cy5-labeled antibody synthesized using affinity chromatography

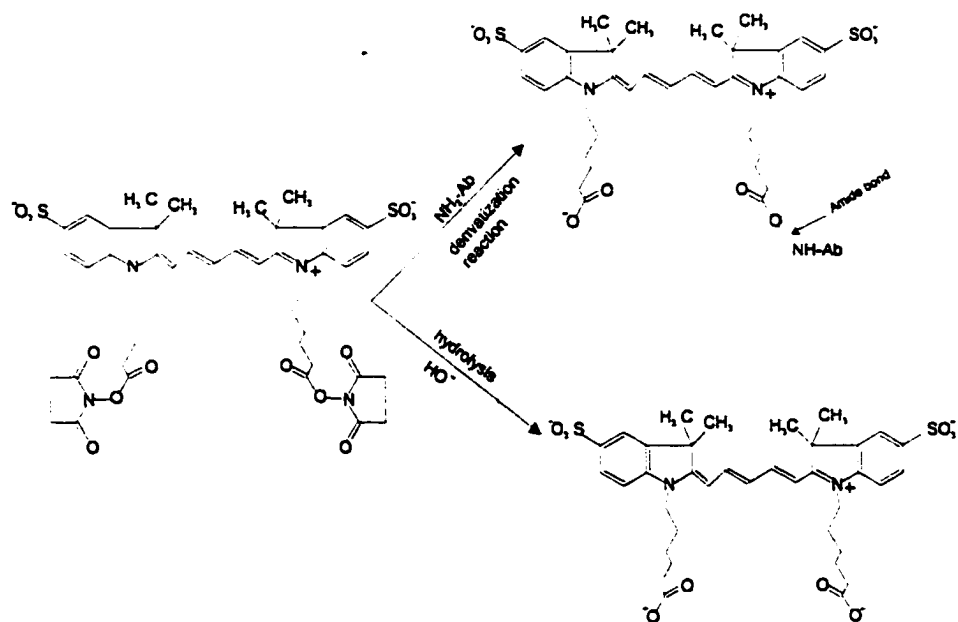


Figure 3.6 Structure of bifunctional Cy5 dye. A covalent bond (an amide bond) is formed between the antibody and Cy5 dye during labeling. Also, hydrolysis occurs simultaneously and competes with the labeling reaction.

that Cy5 dye will react with such groups, especially lysine free-amino groups that are at or near the binding site. Consequently, the tertiary structure of the mAb will change, and the antibody may become inactive.

ELISA results shown in Figure 3.7 confirm that direct derivatization can render the antibody inactive. A dark spot in the picture of the microtitre plate, Figure 3.7, indicates a positive reaction. We can see that column No.1 for the unlabeled anti-ovalbumin antibody is active at a concentration range *ca.* 16 pM-1.3 nM. For the labeled anti-ovalbumin antibody, a higher concentration was required to observe the activity of the antibody. For example, for a final product with D/P ratio of 2:1, the concentration range of labeled antibody that reacted with ovalbumin was from 0.125-1.3 nM. This concentration range decreased even further to 0.25 nM-1.3 nM for labeled antibody with D/P = 5:1. (Note: The concentration for column No. 1 is the actual concentration added). ELISA is an amplification technique wherein only active labeled mAb molecules bind to ov immobilized in the wells and show a positive result. The rest of the inactive mAb molecules would be washed away before adding the enzyme substrate. ELISA showed that derivatization had at least partially deactivated the antibody because only higher concentrates of labeled antibody reacted with the ovalbulmin, whereas the unlabeled antibody reacted at all concentration range. In contrast, CE is a separation tool which does not differentiate between active and non-active antibody. Furthermore, the complex formed from a low population of active mAB would not be amplified. When present at low concentration its signal would be lost in the background due to the high population of inactive labeled antibody.

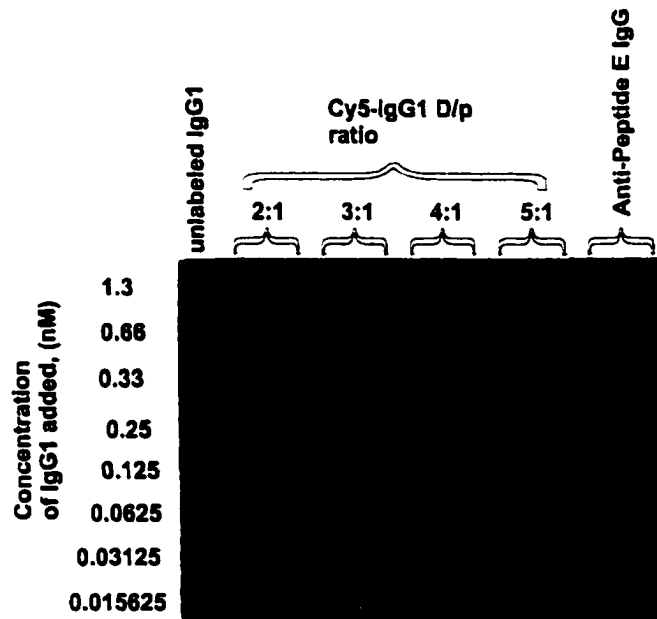


Figure 3.7 ELISA results for labeled and unlabeled monoclonal antibody. Dark spots represent antibody with affinity for the immobilized ovalbumin in the titre plate. Unlabeled antibody with different dilution showed better affinity than labeled antibody. As the D/P ratio increased, the affinity of labeled antibody for the ovalbumin decreased. (Results were obtained from Canada West Biosciences).

We performed a different set of experiments with the aim of controlling the derivatization process and therefore maintaining the activity of the antibody. In these experiments we used rabbit polyclonal antibody, and the factors we manipulated in the labeling procedure of antibody with Cy5 dye included antibody concentration, dye to protein ratio, and reaction time. We varied the dye to protein ratio and maintained the concentration of the polyclonal antibody at 1 mg/ml. The reaction time was not modified. Different aliquot volumes of Cy5 dye dissolved in DMF were added to 1 mg/ml of polyclonal antibody and incubated at ambient temperature for 30 min. The labeled polyclonal antibody was separated from the excess dye using a Sephadex G50 column and then was examined for activity and purity on a CE-based chip. Figure 3.8 shows the results of reaction of labeled antibody having different D/P ratios with ovalbumin. The left upper trace of Figure 3.8 shows labeled antibody with a D/P of 4. The right upper trace of Figure 3.8 displays the electropherogram of a mixture of labeled antibody with ovalbumin. This electropherogram does not contain the complex peak. A shoulder peak in the right electropherogram of the middle trace in Figure 3.8 indicates that labeled antibody with a D/P of 1.6 exhibited little activity. The right bottom electropherogram of Figure 3.8 displays that labeled antibody with a D/P of 0.9 shows some activity for ovalbumin. Because labeled polyclonal antibody can recognize different binding sites on the ovalbumin, labeled polyclonal antibody showed some activity with labeled antibody having a D/P ratio from 0.9-1.6. Using this labeling procedure, a large amount of ov (molar ratio, ov/ab =5:1) was required to react with the labeled antibody to form a complex peak. Therefore, results were not satisfactory for trace analysis of ovalbumin. In Figure 3.8, The signal to noise ratio (S/N) observed were 116, 78, and 34

for D/P 4, 1.6, and 0.9 respectively. The S/N are consistent with the decrease in dye to protein ratio.

In one experiment, a synthesis of directly Cy5-labeled monoclonal antibody yielded a product that gave results somewhat better than shown in the bottom trace of Figure 3.8. However, this product could never be synthesized again by such a procedure. A variety of D/P ratios were synthesized by CWB for our testing, however the results with different synthetic batches of the labeled polyclonal and monoclonal antibodies were quite irreproducible. Lower D/P ratios did give some active material, but the extent of activity varied greatly and a repeat synthesis rarely gave the same results. Further, the complexes formed by the products synthesized were usually poorly resolved from the free labeled antibody and the antibody activity seemed to be low. Therefore, we focused on another approach to label the antibody, with the goal of improving performance and reproducibility.

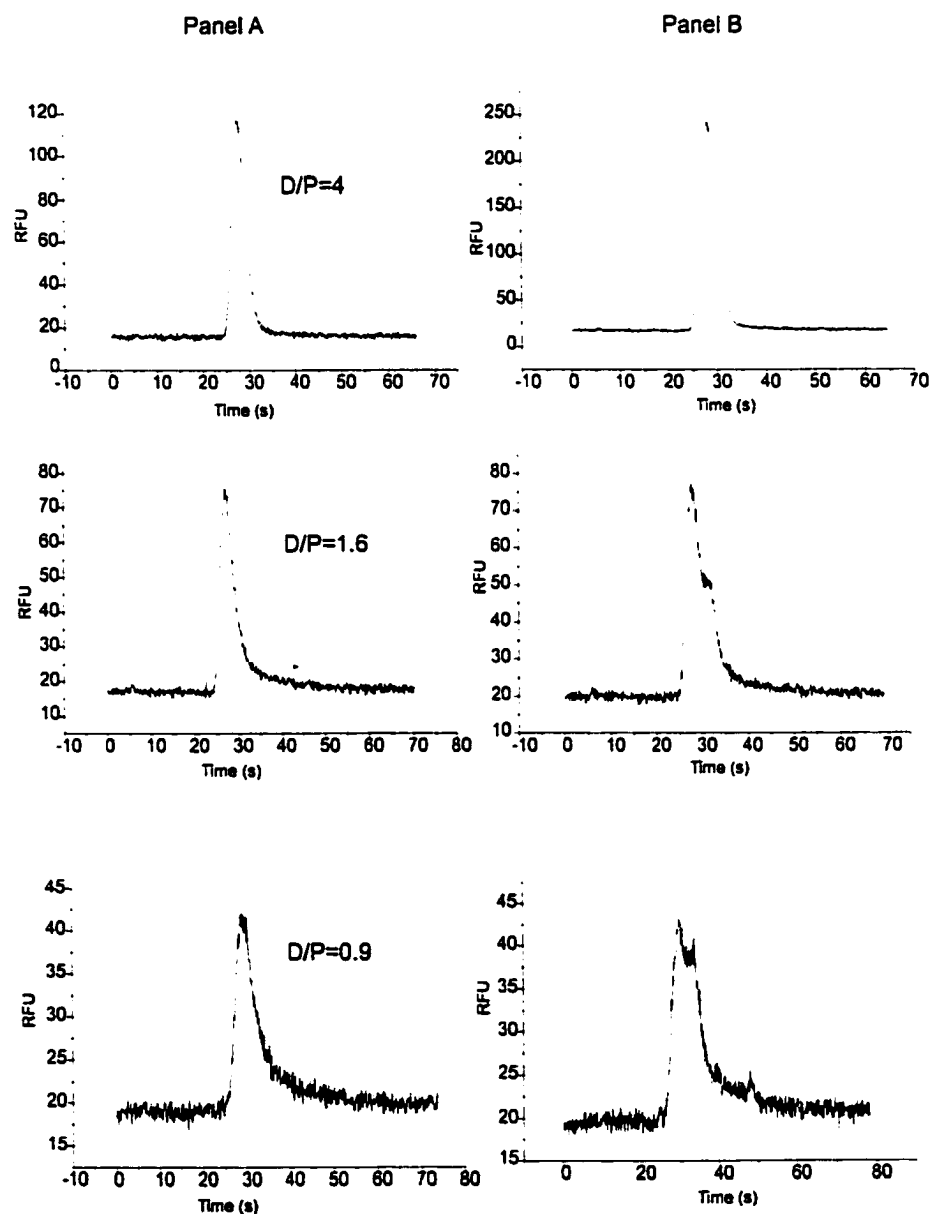


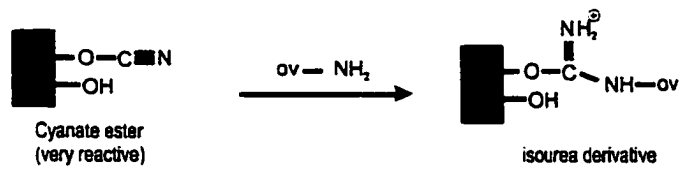
Figure 3.8 Electropherograms of Cy5-labeled rabbit polyclonal antibody with various D/P ratios. (Panel A). The D/P ratio is indicated next to the labeled antibody. Electropherograms of binding of ovalbumin to labeled antibody, (Panel B). Results were obtained using the DARPA chip. CE conditions: 10 mM borate buffer, pH 8.5; injection voltage 1500 V for 15 s; separation voltage 6 kV; concentration of labeled antibody was 300 nM; molar ratio of ovalbumin to labeled antibody was 5:1.

3.3.3 Affinity protection chromatography

The above results demonstrated that antibody binding sites had to be protected prior to derivatization with Cy5 dye, in order to have an active labeled antibody. We developed an affinity chromatography protection method for labeling the antibody without sacrificing its activity. We termed this method affinity protection chromatography (APC). In this method, we employed CNBr-activated Sepharose 4B beads as a support to prepare an immunosorbent column involving covalent coupling of ovalbumin to the CNBr. The reaction proceeds through the interaction of the amino groups of ovalbumin with the cyanate ester group on the matrix, as shown in Figure 3.9A. We added mAb, which selectively binds to immunosorbent (CNBr-ov). The Cy5 dye was then added to the CNBr-ov-mAb column to label the antibody and, after an incubation period, the labeled antibody was eluted by changing the pH of the CNBr-ov-mAb column from alkaline to acidic. Figure 3.9B depicts the protocol of the labeling procedure using affinity chromatography. APC safeguarded the antibody's binding sites, which were bound to the immobilized ovalbumin on the CNBr matrix. Therefore, when Cy5 dye molecules were added they labeled lysine residues or other free amino groups away from the active site.

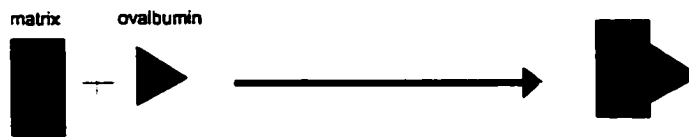
The first step in the proposed APC involved immobilizing ov on a gel bed. Various gels have been used for protein immobilization. Coupling of ov to a gel has been reported in studies determining the efficacy of various gels for protein binding. Ovalbumin was found to bind with 90 % coupling efficiency to carbolink gel and with 52 % coupling efficiency to aminolink gels [31].

A



B

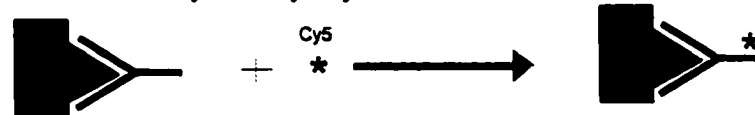
1- Couple ovalbumin to CNBr matrix



2- Apply sample containing antibody



3- Label antibody with Cy5 dye



4- Elute labeled antibody

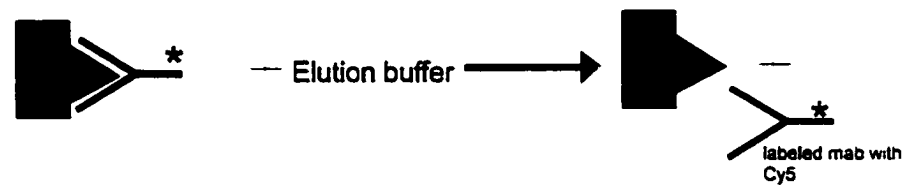


Figure 3.9 (A) Coupling reaction of ovalbumin to CNBr-activated Sepharose 4B beads. (B) Schematic diagram for affinity protection chromatography (APC).

In another study, ovalbumin was used as a linking agent to create a concanavalin A affinity column. A 32-56 % coupling efficiency was found to bind to cellulose beads activated with adipic acid hydrazide [32]. We considered Ultralink™ Biosupport medium (product No. 53110) from Pierce, and CNBr-activated Sepharose 4B from Pharmacia. These are very frequently used gels.

Two important parameters that we used to characterize CNBr-activated sepharose 4B as the immobilizing phase are the coupling efficiency and percentage of antibody bound. The coupling efficiency (%) is the ratio of the moles of the antigen coupled to the polymer matrix to the moles of antigen offered to the matrix and is calculated using eq. 3.1. Percentage of bound antibody is given by eq. 3.2 and reflects the amount of antibody bound to the immunosorbent (CNBr-ov bead). The usefulness of an immunosorbent will be determined by the values of these two parameters.

TABLE 3.1 SUMMARY OF RESULTS FROM AFFINITY PROTECTION COLUMN

ovalbumin			antibody			molar ratio ov/ab	recovery %	
input (mg/g)	bound (mg/g)	coupling efficiency %	input (mg/g)	bound (mg/g)	bound %		total	bound
17.5	16.8	96	11.1	7.3	66	7.7	1.3	1.9 ^a
17.5	16.8	96	8.8	6.15	70	9.1	5.0	7.1 ^b
17.5	16.8	96	11.7	8.37	72	6.7	4.4	6.3 ^b
33.3	24.6	74	2.3	2.11	95	38.9	13.0	13.2 ^a
50.0	48.5	97	1.8	1.8	100	89.8	50.0	50.0 ^a

^a labeled monoclonal antibody

^b rabbit polyclonal antibody

As shown in Table 3.1 the coupling efficiency of ovalbumin to the CNBr matrix was 74-97%. The coupling efficiencies obtained in this study were better than those reported before [32]. Columns 6 and 7 indicate that the amount of antibody bound to the matrix increased with the increasing amount of ov on the matrix and a decreasing amount of

mAb in solution. Because immobilization of ovalbumin on the matrix is a random (stochastic) process, deactivation of some ovalbumin is likely [33]; hence saturating the matrix with ovalbumin should maximize the amount of active ovalbumin in the matrix. We mean by saturation exceeding the recommended range of ligand (ov) added to the gel, which is 18-35 mg/ml according to the manufacturer (Pharmacia). Recovery of antibody per total antibody added or per total antibody bound (columns 8 and 9) showed an increase as molar ratio of ov/ab stepped up from 7.7 to 89.9. For nearly the same amount of ov on the matrix, the percentage of bound polyclonal antibody was larger than that of monoclonal antibody. This suggests that the polyclonal antibody is more active than the monoclonal antibody.

3.3.3.1 Recovery and D/P ratio of labeled antibody

Mujumdar et al. [29] reported that at pH 8.5, Cy5 dye loses 70 % of its activity after *ca.* 12 min. Therefore, in order to minimize the fast hydrolysis of Cy5 dye at pH 8.5, we did not dissolve the dye in buffer before adding it to the gel (CNBr-ov-mAb). We took approximately one ml of the gel slurry and added it to the vial containing solid Cy5 dye. This improved the D/P ratio of product from 0.3 to 1.7. The labeled antibody was eluted after incubating the gel with 0.1 M glycine buffer, pH 2.8, for 10 min. The process of incubation was repeated and fractions were pooled. The absorbance of the fractions was measured at two wavelengths, 650 nm (to measure the concentration of the dye) and 280 nm (to measure the concentration of mAb). From these two values, the D/P ratio was calculated according to eq. 3.3. The recovery of labeled monoclonal antibody from CNBr-ov gel was between 35-50% with a D/P ratio of 1.7, as shown in UV/Vis spectrum of labeled antibody (Figure 3.5). Fractions with D/P ratios less than 1 implied that the

antibody was under-labeled and those fractions were discarded. The recovered mAb* was tested on chip for purity and reactivity. Figure 3.10A shows the electropherogram of mAb* with D/P of 1.7. As shown in Figure 3.10A, only a single peak was obtained for mAb*, with a migration time *ca.* 22 s. No excess Cy5 dye was observed in the background of the electropherogram, denoting that the Cy5-labeled mAb was 100% pure. We analyzed a mixture of ov and labeled antibody (molar ratio of ov/mAb* = 3.1) using CE-based microchip and the results shown in Figure 3.10B demonstrate that the labeled antibody was active and therefore, a complex peak with migration time of 26 s was observed.

Cy5-labeled antibody was successfully synthesized more than five times using affinity protection chromatography, showing reproducibility of the affinity protection method. The synthesized-labeled antibody was used by other members in our group and by people at DRES either to determine ovalbumin immunoassay or affinity constant of labeled antibody.

3.3.3.2 Thermodynamics factors affecting amount of mAb bound to CNBr-ov column

As shown in Table 3.1, at low loading of ovalbumin onto the column (17.5 mg of ovalbumin per gram of matrix) 66-72% of the antibody was bound to the column, whereas at a high loading (*ca.* 35-100 mg of ovalbumin per gram of matrix) 92-100% of antibody was bound to the matrix. The direct benefit of having high antibody concentration bound to the ov immobilized on the matrix is a high recovery for labeled antibody during elution.



Equation 3.4 represents the binding reaction of ovalbumin with antibody assuming a single site interaction between ov and mAb. The equilibrium or affinity constant of the above reaction is equal to $[Ab-Ag]/[Ab][Ag]$. The affinity constant will control the amount of bound antibody. Table 3.1 shows that an increased antibody binding efficiency results in better recovery.

The relative yield for bound mAb is equal to $K[ov]/(1+K[ov])$, where K is the affinity constant for anti-ovalbumin. The derivation of this equation will be given in Chapter 4 (see eq. 4.3). It should be noted that the concentration of mAb does not appear on the right-hand side of the equation and, hence does not affect the yield. The maximum amount of the ov is limited by two factors. First, there is a limit to the amount of ov bound per particle of the matrix. Secondly, there is a limit to the number of particles per unit volume. Because the affinity constant of mAb is low (see Chapter 4) the amount of ov must be increased in order to improve the yield. This was achieved by increasing the percentage of bound ov, as indicated in column 3 of Table 3.1. When we started developing methods for labeling the antibody, the affinity constant for binding of ov and antibody was not available. As a result, the amount of ov put on the matrix was not enough to react with the added antibody and therefore, the recovery of antibody from the affinity protection column was very low, 1.9-7.1%). Later, we determined the affinity constant of the interaction of ov and mAb (see Chapter 4) to be $K_a = 0.33 (\pm 0.02) \times 10^6 M^{-1}$. Therefore, we repeated the

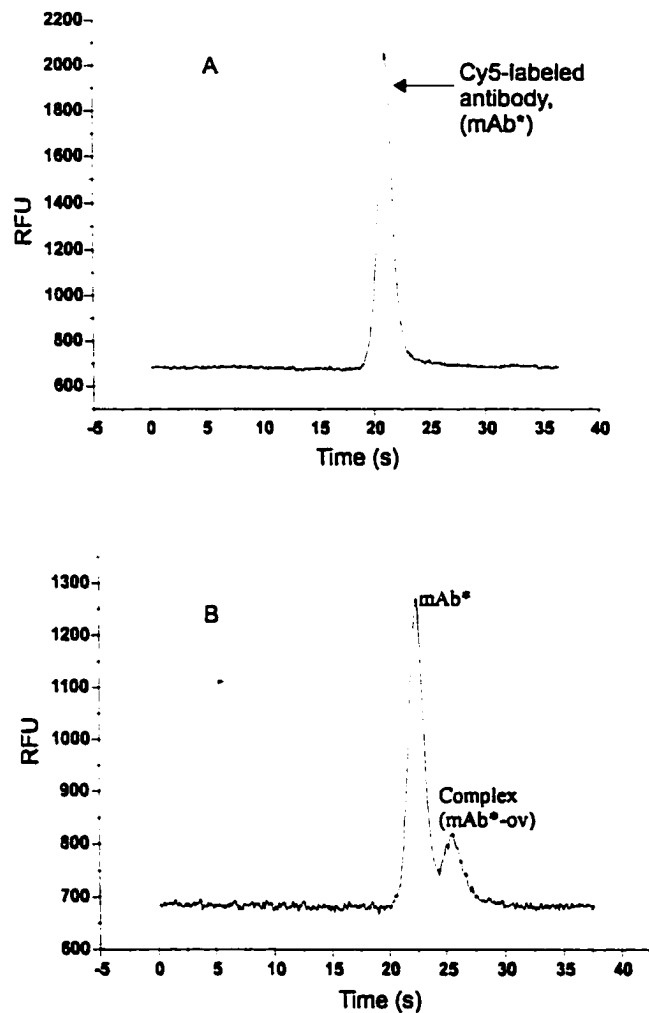


Figure 3.10 Electropherograms Cy5-labeled mAb (mAb*) using affinity protection chromatography (A) and separation of mAb* from its complex (B). CE conditions: DARPA chip; 5 mM Borate buffer/10 mM NaCl, pH 8.5; injection voltage 1500 for 15 s; separation voltage 6 kV; LIF detection. He-Ne laser with excitation wavelength 632.5 nm. emission was at 675 nm; molar ratio of ovalbumin to mAb* was 3:1. Concentration of mAb was 200 nM.

experiments and the amount of ovalbumin immobilized on the affinity protection column was in substantial excess of compared to antibody added (molar ratio of ov/mAb \geq 89:1). The yield of the labeled antibody was improved from 1.3 to 50%.

Recovery values in column 9 of Table 3.1 were expected to be constant and not increasing. The fact that the increase with increasing ov loading may indicate the ov is more efficient at passivating functional sites on the gel than ethanolamine. Incubation for 15 h or more did remove further labeled antibody from the gel, giving $102 \pm 10\%$ yield. However, multiple product peaks seen in the CE indicate that chemical changes of the labeled antibody had occurred. Previous studies of exposure of labeled antibody to ImmunoPure[®] IgG elution buffer (pH 2.8) for an hour showed the antibody was permanently deactivated. T. Dickinson, at DRES, used a high enough concentration of ov to consume all the labeled antibody and showed that all labeled antibody that was incubated for 30 min with ImmunoPure[®] IgG elution buffer (pH 2.8) was active.

3.3.3.3 Alternative gel matrices

Desirable matrix characteristics are: (1) loose, porous structure; (2) structurally stable spherical beads of uniform porosity and size; (3) easy derivatization; (4) polar but uncharged surface; and (5) mechanical and chemical stability [34,35].

CNBr-activated Sepharose gel meets many of these criteria, however, the gel has several drawbacks. For example, coupling of amines to activated polysaccharides introduces N-substituted isourea bonds that are not completely stable, particularly in the presence of a nucleophile [36]. The isoureas are positively charged at physiological pH ($pK_a = 9.4$) and as a result such matrices exhibit ion-exchange properties that can give rise to non-specific interactions. Based on these facts we did not try to employ the ov-

treated CNBr activated-Sepharose 4B column to purify the monoclonal antibody from mouse ascites fluid. The matrix was only used for affinity protection column.

We tried another solid immunosorbent matrix (Ultralink Biosupport medium) from Pierce. Ultralink™ Biosupport medium was strongly recommended by the supplier. It is composed of beads of a bis-acrylamide/Azolactone copolymer. The advantage of this matrix over CNBr activated beads is that the reaction of N-hydroxysuccinimide-activated beads with the amino groups gives a stable N-alkylcarbamate (Urethane) linkage, devoid of additional charged groups over a wide range of pH (ca. pH 2-10) [37]. We followed the protocol of the manufacturer to immobilize ovalbumin on the matrix. In our first trial, coupling efficiency of ov was 86% and the final yield for labeled antibody using the same procedure for CNBr-activated Sepharose was 50 %. Subsequent trials were not successful and we could not again obtain high coupling efficiency for ovalbumin on this matrix. Even with 5 ml of gel, we obtained poor coupling efficiency for ovalbumin (2%), therefore, we decided not to use the matrix and continued working with CNBr beads.

3.4 Conclusions

We employed protein G affinity chromatography to purify mouse monoclonal antibody (IgG1) from ascites fluid. A high recovery of purified antibody (> 95%) was achieved. Direct derivatization with Cy5 dye resulted in inactive or poorly active antibody, when measured by CE. If the reagents are to be used for affinity CE, then ELISA data should be interpreted with caution. The saturation test in affinity CE can identify whether any inactive material is present or not. Affinity CE appears to be a better way to test activity than is ELISA. The Affinity protection chromatography (APC) method offers great potential for saving a considerable amount of time and labor in

developing a labeled antibody that does not become inactivated by labeling. With purified antibody as a starting reagent, APC can be performed in about 1 day. The APC method could also be used to label the antigen, by covalently binding the antibody to the gel matrix.

3.5 References

- 1 K.H. Bannefeld, H. Stass and G. Blaschke, *J. Chromatogr. B*, 692 (1997) 453.
- 2 G.S. Wynia, G. Windhorst, P. C. Post and F. A. Maris, *J. Chromatogr.*, 773 (1997) 339.
- 3 Y.F. Cheng and N. J. Dovichi, *Science*, 242 (1988) 562.
- 3 A.J.G. Mank, N.H. Velthorst, and C. Gooijer, *J. Chromatogr.*, 695 (1995) 165.
- 5 A.J.G. Mank, N.H. Velthorst, and C. Gooijer, *J. Chromatogr.*, 695 (1995) 175.
- 6 A.J.G. Mank, H. Lingeman and C., Gooijer, *Trends in Anal. Chem.*, 11 (1992) 210.
- 7 U.A.Th. Brinkman, R.W. Frei and H. J. Lingeman, *J. Chromatogr.*, 492 (1989) 251.
- 8 I.S. Krull, Z. Dely and H. Lingman, *J. Chromatogr. B*, 659 (1994) 1.
- 9 M.E. Szulc and I.S. Krull, *J. Chromatogr.*, 659 (1994) 231.
- 10 P. Beyer Hietaps and A.G.-Ewing, *J. Liq. Chromatogr.*, 18 (1995) 3557.
- 11 Peter R. Bank, *Trends in Anal. Chem.*, 17 (1998) 612.
- 12 R.W. Frei and K. Zech (Eds.), *Selective Sample Handling and Detection in High Performance Liquid Chromatography*, Parts A and B, Elsevier, Amsterdam, 1988, 1989.
- 13 K. Blau and J. Halket (Eds.), *Handbook of Derivatives for Chromatography*, 2nd Ed., Wiley, New York, 1993.
- 14 A.J.G. Mank and E.S. Yeung, *J. Chromatogr.*, 708 (1995) 309.
- 15 G.-D. Li, I.S. Krull and S.A. Cohen, *J. Chromatogr.*, 724 (1996) 147.
- 16 R.A.Evangelista and F.T.A. Chen, *J. Chromatogr.*, 680 (1994) 587.
- 17 T.M. Phillips, N.S. More, W.D. Queen and A. M. Thompson, *J. Chromatogr.*, 327 (1985) 205.

- 18 T.R. Burkot, R.A. Wirtz and J. Lyon, *J. Immunol. Methods*, 64 (1985) 25.
- 19 K. Shimura and B.L. Karger, *Anal. Chem.*, 66 (1994) 9.
- 20 I.S. Krull, R. Strong, Z. Sasic, B.-Y. Cho, S.C. Beale, C.-C. Wang and S. Cohen. *J. Chromatogr. B*, 699 (1997) 173.
- 21 S.R. Fahnestock, P. Alexander, J. Nagel and D. Filipula, *J. Bacteriol.*, 167 (1986) 870.
- 22 K. Ernest-Cabrera and M. Wilchek, *J. Chromatogr.*, 397 (1987) 187.
- 23 P. Cassulis, M.V. Magasic and V.A. DeBri, *Clin. Chem.*, 37 (1991) 882.
- 24 R. Axen, J. Porath and S. Ernback, *Nature*, 214 (1967) 1320.
- 25 Monoclonal antibody purification handbook, Pharmacia Biotech, Code No. 18-1037-46.
- 26 Th. Trenynck and S. Avrameas, *Immunoenzymatic Techniques*. Vol. 1. Elsevier Science Publishers B.V. (Biomedical Division), Amsterdam, Netherlands (1990).
- 27 P.D. Grossman, J.C. Colburn, H.H. Lauer, R.G. Nielsen, R.M. Riggan, G.S. Sittampalam and E.C. Rickard, *Anal. Chem.*, 61 (1989) 1186.
- 28 R. Weinberger, *Practical capillary electrophoresis*, Academic Press Inc., San Diego, (1993).
- 29 B.R. Mujumdar, A.L. Ernst, R.S. Mujumdar, J.C. Lewis, and S.A. Waggoner, *Bioconjugate Chem.*, 4 (1993) 105.
- 30 P.L. Southwick, L.A. Ernest, E.W. Tauriello, A.R. Parker, R.B. Mujumdar, H.A. Clever and A.S. Waggoner, *Cytometry*, 11 (1990) 418.
- 31 P.L. Domen, J.R. Nevens, A.K. Mallia, G.T. Hermanson, and D.C. Klenk, *J. Chromatogr.*, 510 (1990) 290.

- 32 J. Turková, L. Petkov, J. Sajdok, J. Káš and M.J Beneš, *J. Chromatogr.*, 500 (1990) 585.
- 33 R.L. Wimalasena and G.S. Wilson, *J. Chromatogr.* 572 (1991) 85.
- 34 P. Cuatrecasas, M. Wilchek and C.B. Anfinsen, *Proc. Natl. Acad. Sci. USA*, 61 (1968) 636.
- 35 C.R. Lowe and P.D.G. Dean, *Affinity Chromatography*, Wiley, London, 1974, p. 13.
- 36 M. Wilchek, T. Oka and Y.J. Topper, *Proc. Natl. Acad. Sci. USA*, 72 (1975) 1055.
- 36 G.S. Bethell, J.S. Ayers, W.S. Hancock and M.T.W. Hearn, *J. Biol. Chem.*, 254 (1979) 2572.

Chapter 4

Measurement of affinity constant of anti-ovalbumin using CE

4.1 Introduction

The measurements of affinity or dissociation constants are of tremendous importance in biochemistry. More specifically, in health related fields affinity constants are relevant to: (1) predict nonlinear pharmacokinetic processes [1], (2) investigate drug displacement phenomena [2-6], and (3) study the inter-individual binding variability due to different physiological or pathological factors (age, disease, genetic aspects, etc.) [7-10]. When developing immunoreagents it is important to select antibodies with a high affinity constant. There are several categories of methods used to measure the binding affinity between a receptor and ligand: (1) Conventional, (2) Chromatographic, (3) Spectroscopic, (4) Other methods, and (5) Capillary Electrophoresis.

(1) Conventional methods: These methods include equilibrium dialysis, ultrafiltration and ultracentrifugation, and have mainly been used to study drug-protein interactions. Each of these methods has specific drawbacks. For example, equilibrium dialysis requires a long time for equilibrium to be established [11,12] and suffers from Donnan effects [13] that hinder the passage of free ligands, and from non-specific adsorption to the dialysis apparatus [14]. The main problem associated with ultrafiltration is the stability of the binding equilibrium during the separation process. Therefore, it is advisable to validate a method using a complementary technique, especially with low-affinity interactions [15]. Ultracentrifugation is an alternative to both equilibrium dialysis and ultrafiltration, since it eliminates the problems associated with the membrane effects. However, the shortcomings of ultracentrifugation are the error in estimating the

free ligand concentration due to physical phenomena such as sedimentation and back diffusion [16].

(2) Chromatographic methods: these include numerous variants of high performance size-exclusion chromatographic techniques for studying binding interactions, including frontal analysis [17], the vacancy peak method [18], retention analysis [19], and the Hummel-Dryer method [20,21]. Separations using high performance size-exclusion chromatography, equilibrium dialysis, ultrafiltration and ultracentrifugation methods are based on size differences between molecules. The size difference requirement limits their usefulness for antibody-antigen interactions, since for haptens or small antigens the antibody and the complex are of similar size.

(3) Spectroscopic methods: Spectroscopic techniques include ultraviolet, visible, fluorescence and ^1H NMR, -(proton nuclear magnetic resonance) [22-24]. These techniques can be used to monitor protein binding by titration if the molecule undergoes a shift in its spectral properties upon binding [25]. Advantages to spectroscopic methods include the ability to collect larger numbers of data points more efficiently than membrane dialysis and ultrafiltration; however, spectroscopic techniques are limited by the inherent physical properties of the molecules being studied.

(4) Other methods: Occasionally, other methods used in ligand-protein studies have been based on the unique features of the ligand, which reveal specific qualitative or quantitative aspects of the protein–ligand interactions. Examples include the use of polarography [26], calorimetry [27] or stopped-flow experiments for evaluating binding kinetics [28], as well as fluorescence polarization immunoassay [29]. The analytical

potential of field flow fractionation (FFF) for characterization of binding interactions should also be mentioned [30,31], although it is not yet in common practice.

(5) Capillary electrophoresis (CE): Capillary electrophoresis and its family of related techniques, including those utilizing microchips, have experienced a tremendous growth in the last decade due to the high speed of analysis, small sample size requirements, and high efficiency of separation. One of the most attractive features of CE is its ability to simultaneously separate a wide variety of analytes, including those that form complexes through molecular interactions. This area of research is known as affinity capillary electrophoresis (ACE) [32]. Figure 4.1 is a schematic diagram of the main modes of affinity capillary electrophoresis. As shown in Figure 4.1, ACE can be classified into three modes: (a) dynamic equilibrium affinity electrophoresis, (b) affinity-based CE or CEC separations on an immobilized selector, and (c) nonequilibrium electrophoresis of equilibrated sample mixtures.

(a) Dynamic equilibrium affinity electrophoresis:

When this mode is employed the sample to be tested may contain receptor proteins and the separation buffer contains the ligand, Figure 4.1A. Experimentally, first, a fixed concentration of receptor and neutral marker (neutral marker is added to measure electroosmotic velocity) is injected into a capillary filled with buffer (but no ligand) to determine the electropherogram of the mixture as a control sample. Secondly, the capillary is filled with a known concentration of ligand, L_1 . Then, the mixture of receptor and neutral marker of the same concentration is injected again, and the receptor binds to the ligand in the separation buffer. A shift in the migration time of the receptor is observed. The experiment is repeated with increasing concentrations of ligand, but a

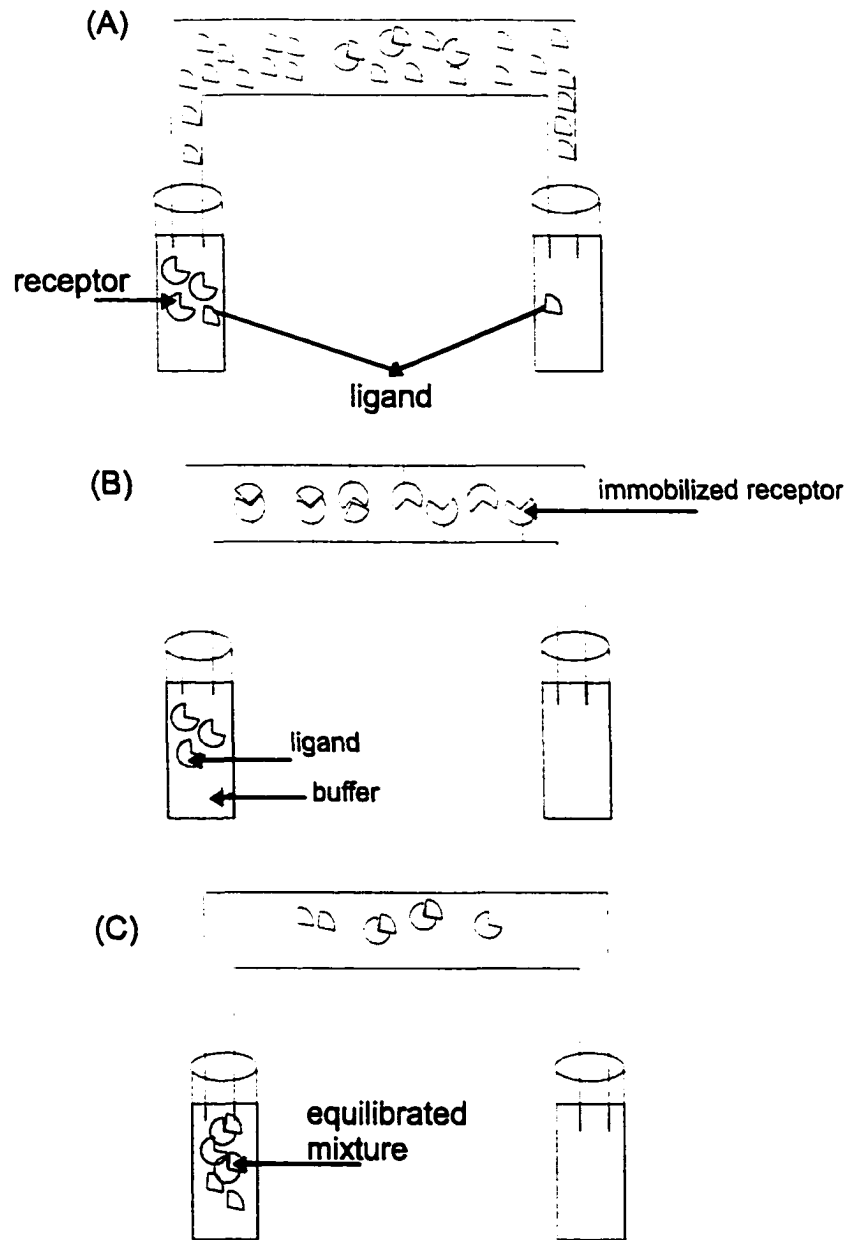


Figure 4.1 Schematic diagram showing the three modes of Affinity Capillary Electrophoresis (ACE). (A) Dynamic equilibrium electrophoresis. (B) Affinity-based CE. (C) Nonequilibrium electrophoresis of equilibrated mixtures of ligand and receptor.

fixed concentration of the receptor. As a result, the receptor peak gradually shifts as a function of the ligand concentration in the separation buffer. This technique can be used to derive binding parameters of the ligand-receptor interaction such as the affinity constant K_a of the receptor and the number of binding sites. This type of affinity electrophoresis has been used for some time in native gel electrophoresis [33-36], but its applicability has increased with its adaptation to the CE format [37-64].

The equilibrium method is suitable for rapidly equilibrating complexes with high forward and reverse reaction rates. Therefore, to use this approach for valid binding constant determination, it is required that the dissociation rate constant (off-rate), k_{off} , be much shorter than the receptor peak migration time. As a rule of thumb, the complex dissociation half-time, expressed as $\ln 2/k_{off}$ must be less than 1% the migration time [65]. This means that the receptor will always be in one form, which is its electrophoretic free state; its bound state should not be observed. The considerations for using such methods have been discussed elsewhere [66,67].

(b) Affinity-based CE or CEC separations on immobilized selectors:

Figure 4.1B shows the schematic diagram for affinity-based CE. Receptor proteins can be immobilized on various substrates such as a portion of the capillary wall [68], microbeads [69], membranes [70], or microchannels [71]. The ligand, present in a diluted solution or a complex mixture, is affinity-captured on the receptors and unwanted matrix components are washed away. The specific ligand is subsequently released from its adsorbed state and separation is performed by capillary electrophoresis.

(c) Nonequilibrium electrophoresis of equilibrated sample mixtures:

As shown in Figure 4.1C, equilibrated, pre-mixed samples consisting of a known amount of receptor and ligand concentration at different ratios are analyzed using CE. In this case, CE is simply a tool to separate and quantitate bound and free molecules. In this chapter, we will explore this approach to determine anti-ovalbumin antibody binding parameters. This method has been previously reported [72-77]. The binding experiments for antibody and antigen using this approach can be carried out as follows: (A) generation of a calibration curve of peak heights versus concentrations for ovalbumin (ov), by injecting various concentrations of ovalbumin in CE; (B) experiments under the same conditions as in (A), but where the samples are pre-equilibrated with a fixed concentration of antibody. Peak heights of free ovalbumin after incubation are used to obtain the amount of bound ovalbumin (i.e., complex) in each analysis of incubated samples; (C) data treatment involving the use of a Scatchard plot [80], which is a plot of bound versus free antigen, its slope yields $-K_a$. Binding parameters such as the affinity constant (K_a) and the average number of binding sites (n) for antibody-antigen interactions are obtained from such binding experiments.

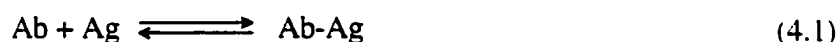
These binding parameters are very important for the detectability of an antigen, which increases with larger affinity constants. The specificity increases with greater differences in affinities of antibodies for specific and non-specific antigens.

In this chapter we explore the use of CE-UV based immunoassays for determining the K_a of a native antibody. Also, we report on two observations made by my colleagues, A. Jemere and S.B. Cheng, who used the labeled antibody in their experiments. Jemere obtained a detection limit for an ovalbumin assay of *ca.* 200 nM, while the detection limit for the same instrument was 0.24 nM for standard Cy5 dye solution. Cheng had to mix

ovalbumin in the micromolar concentration range with labeled antibody in the nanomolar range in order to observe the (mAb*-ov) complex using a chip with LIF detection. Data obtained by T. Dickinson for evaluating the affinity constant of Cy5-labeled anti-ovalbumin will also be presented and compared with the value obtained for nonlabeled antibody.

4.2 Data Analysis:

Scatchard plots are a common graphical representation of binding data. The Scatchard plot can be derived from the classical law of mass action for a 1:1 binding of an antigen (Ag) to an antibody (Ab) to form an immune complex (Ab-Ag) according to equation 4.1



The affinity constant K_a for the above reaction can be defined by equation 4.2

$$K_a = \frac{[\text{Ab-Ag}]}{[\text{Ab}][\text{Ag}]} \quad (4.2)$$

where $[\text{Ab}]$, $[\text{Ag}]$ and $[\text{Ab-Ag}]$ are the molar concentration of free antibody and antigen and the complex, respectively.

The Langmuir isotherm, eq. 4.3, can be derived from eq. 4.2 [81].

$$\frac{[\text{Ab-Ag}]}{[\text{Ab}_t]} = \frac{K_a[\text{Ag}]}{1 + K_a[\text{Ag}]} \quad (4.3)$$

$[\text{Ab}_t]$ is the total antibody concentration, and K_a is the intrinsic association constant for binding one epitope of one antigen molecule to one antibody binding-site. The antibody (IgG1) has two ligand binding sites per molecule. The antigen also may have one or more antigenic determinants of the same or different types [81, 82-84]. Therefore, complexes other than Ab-Ag and Ab-Ag₂ are possible. Schumaker et al. [84] introduced

a mathematical model and presented a detailed analysis for a special case of interactions where both antigen and antibody are bivalent. Eq. 4.3 can be extended to antibodies with multiple binding sites [82] and re-written in the form:

$$\frac{[\text{bound Ag}]}{n[\text{Ab}_t]} = \frac{K_a[\text{free Ag}]}{1 + K_a[\text{free Ag}]} \quad (4.4)$$

Equation (4.4) can be linearized into the Scatchard form as follows:

$$\frac{[\text{bound Ag}]}{[\text{free Ag}]} = -K_a[\text{bound Ag}] + n[\text{Ab}_t]K_a \quad (4.5)$$

where n is the average number of combining sites per antibody molecule used for binding the antigen and $[\text{bound Ag}]$ is the concentration of antigen reacted and bound to the antibody. A plot of $[\text{bound Ag}]/[\text{free Ag}]$ versus $[\text{bound Ag}]$ gives a straight line whose slope is $-K_a$, with an intercept of $n[\text{Ab}_t]K_a$. This plot is known as the Scatchard plot. The average number of binding sites (n) can be calculated from the intercept of the Scatchard plot, according to eq. 4.5. The product of $n[\text{Ab}_t]$ is called B_{max} which is the total binding site concentration. Equation 4.5 is useful because by simple inspection certain information about the binding reaction can be obtained. For example, if a plot from eq. 4.5 gives a straight line, then the binding sites are identical and independent (independence means the occupancy of one site does not affect the probability of binding to any other site). If sites are identical and dependent, that is, the binding is cooperative, then a curve line will result. A curved line could also be obtained if the binding sites are different. Cooperative binding refers to the case when one site on the receptor or antibody is occupied by the ligand (the antigen) so that the binding probability of the ligand at the other site might increase (positive cooperation) or decrease (negative

cooperation). Cooperativity has been previously observed in antibody-antigen binding [85-87].

In this chapter, we will also determine the binding parameters (K_a and n) by means of nonlinear least-squares curve fitting of bound ovalbumin versus free ovalbumin concentrations (eq. 4.4); using the Levenberg-Marquardt algorithm provided by Origin (MicroCal Software Inc., Northampton, MA, USA). Values obtained from the nonlinear least-squares curve fitting will be compared with the transformed values obtained from a Scatchard plot.

4.3 Experimental

4.3.1 Chemicals

Monoclonal anti-ovalbumin (8.1 mg/ml, 0.5 ml) and ovalbumin (grade V) were purchased from Sigma (St. Louis, MO, USA). Other chemicals were previously described as in Chapter 2. Purification and labeling procedures for anti-ovalbumin have been described in Chapter 3.

4.3.2 Apparatus

A Beckman CE system with UV detection was used in the analysis of binding experiments for native protein species. T. Dickinson at DRES, also employed a Beckman CE equipped with LIF detection for the evaluating the binding constant of Cy5-labeled anti-ovalbumin. A detailed description of the instrumentation was given in Chapter 2.

4.3.3 Procedure

A 22 μ M stock solution of ovalbumin was prepared in 5 mM borate buffer/10 mM NaCl (pH 8.5). To create a calibration curve of ovalbumin relating peak height to

concentration, 22 μM ovalbumin stock solution was diluted with 5 borate buffer/10mM NaCl, pH 8.5 to give 100 μl of solution with concentrations ranging from 0 and 7.8 μM . Mixtures containing different ratios of ovalbumin (ov) to a fixed concentration of purified anti-ovalbumin (IgG1) were prepared in 5 mM borate buffer (pH 8.5), containing 10 mM of NaCl, and were equilibrated at room temperature for a period of 5 min before CE. Each sample in a series contained the same amount of 333 nM purified antibody while the ovalbumin concentration was varied from 555 nM to 7.8 μM . In a typical experiment, 5 μl of 1 mg/ml of antibody was added to a microcentrifuge tube, followed by 85 μl of buffer and 10 μl of ovalbumin, so that the final volume was 100 μl . Therefore, for this particular binding experiment, the final molar concentration ratio of ovalbumin to antibody was 6.7. The microcentrifuge tube was vortexed for 30 s and then incubated at ambient temperature for 5 min, unless otherwise stated. The other sample mixtures had the following molar ratios of ([ov]/[mAb]): 1.67, 3.33, 6.67, 10, 13.33, 16.67 and 23.33.

CE was utilized to separate pre-equilibrated sample mixtures. The conditions for electrophoretic separation of each sample, using an uncoated capillary, were as follows: length to the detector 20 cm, total capillary length 27 cm, applied voltage 16 kV, measured current 30 μA . The running buffer was 5 mM boric acid adjusted to pH 8.5 with 1 M NaOH, containing 10 mM NaCl unless otherwise reported. The same buffer was used as a diluent for the incubation mixtures. All buffer solutions were filtered through a 0.22 μm pore size sterile filter prior to analysis. Binding experiments of native species were detected on-column with UV detection at 214 nm. Each sample was analyzed in five replicates to check the reproducibility of migration times.

4.3.4 Data handling

Electropherograms were acquired using P/ACE software version 2 and exported as ASCII data files using DDE (Dynamic Data Exchange) to Microsoft Excel. Then, the data were copied into Igor pro (WaveMetrics Inc., Lake Oswego, Oregon, USA) Version 3.12 for peak analysis. Figure 4.2 demonstrates the multiple curve fitting using Igor pro. For labeled anti-ovalbumin, electropherograms were acquired and analyzed using P/ACE Version 2 (Beckman, Fullerton, CA, USA). Peak heights of either ovalbumin peak using UV detection, or labeled antibody peak with LIF detection were utilized to calculate the concentration of free and bound ovalbumin.

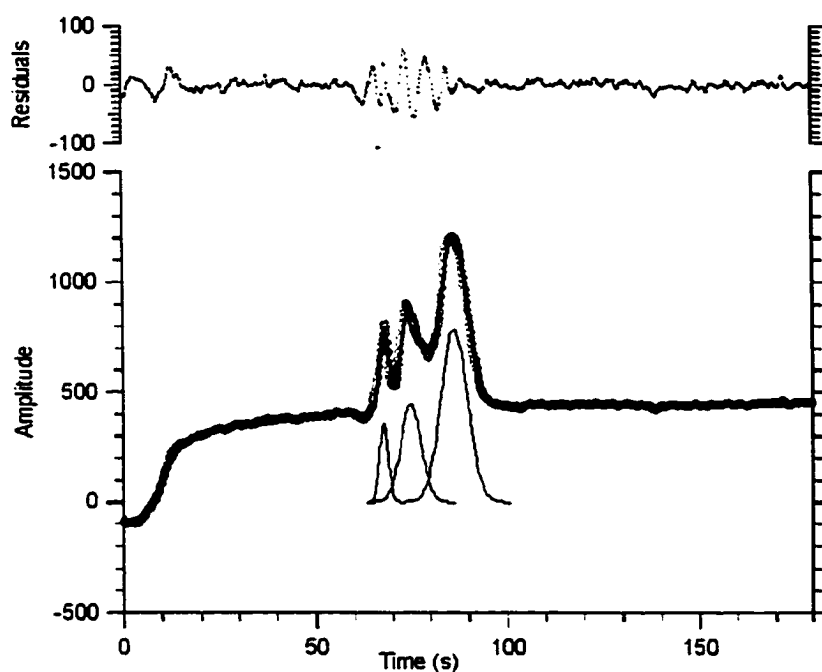


Figure 4.2 Multiple curve fitting for an electropherogram of a binding experiment using Igor pro. Solid line represents the fitting peaks to the data represented by open circles. Lower peaks illustrate the amount of overlap between fitted peaks. Residues are scattered as shown from residual plot.

4.4 Results and Discussion

4.4.1 Reaction time required to reach equilibrium

The equilibration time of the binding reaction between the native antibody and ovalbumin was estimated by incubating 50 $\mu\text{g/ml}$ of antibody with 250 $\mu\text{g/ml}$ of ovalbumin (final volume: 100 μl) in a microcentrifuge tube. Samples were injected into Beckman CE system at different times: 5 min, 30 min, 5 h, 17 h and 22 h. After 5 min the peak height was constant. Accordingly, all samples were incubated at ambient temperature for 5 min.

4.4.2 Measurements of association constant between ovalbumin and antibody in their native states.

Figure 4.3 shows the electropherograms from the binding experiments of native species in which the molar concentration of mAb was fixed and ovalbumin (ov) concentrations were increased. The mAb peak height progressively decreased, whereas the complex peak increased as ovalbumin was added. A saturation of mAb occurred at a molar ratio ($[\text{ov}]/[\text{mAb}]$) of 23.33 as shown in Figure 4.4. The mAb used in the binding experiments was purified using protein G, as described in Chapter 3. A purification step was necessary because the non-purified antibody showed a contaminant peak, which co-eluted with ovalbumin, as illustrated in Chapter 2.

The association constant of ovalbumin with antibody was calculated from a Scatchard plot according to eq. 4.5. The plotted parameters were equilibrium molar concentrations of free and bound ovalbumin in solution. The molar concentrations of free ovalbumin were readily obtained using the calibration curve of ovalbumin. Then the molar concentration of bound ovalbumin was calculated as the difference between the

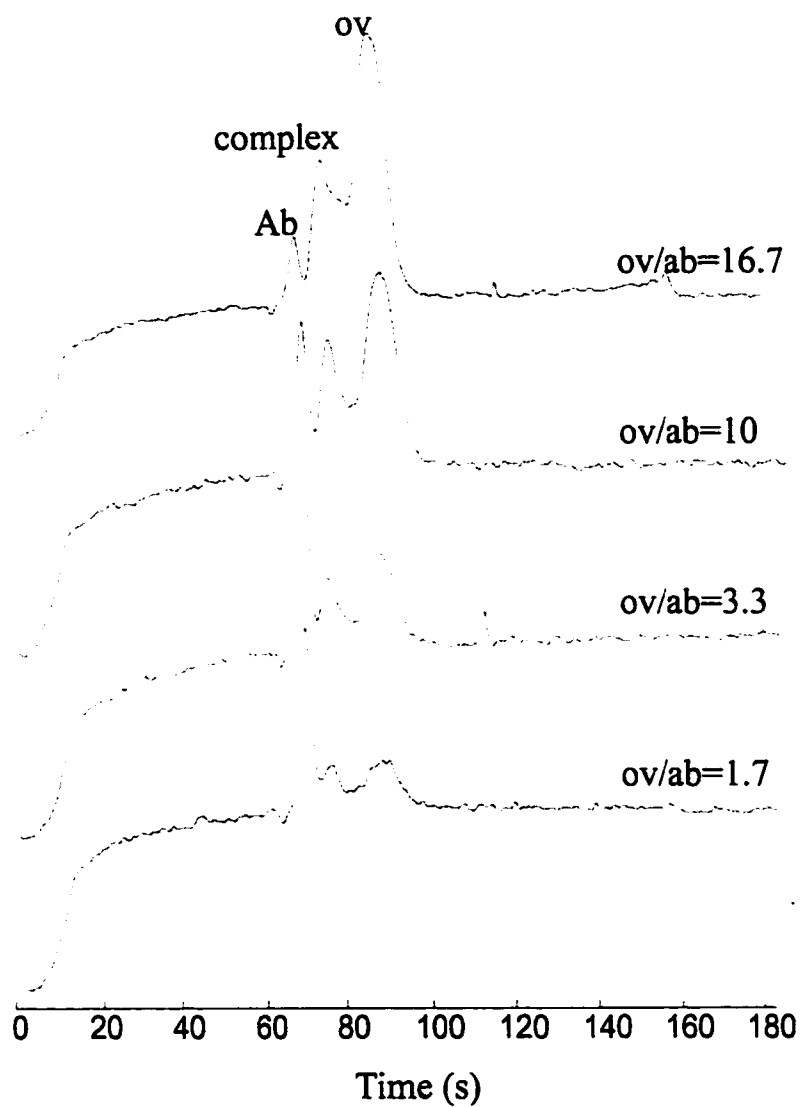


Figure 4.3 Electropherograms of mixtures of native ovalbumin and its monoclonal antibody. Molar ratios of ov/Ab are indicated next to each electropherogram. Antibody concentration was fixed at 333 nM. All experiments were performed on Beckman CE with UV detection at 214 nm. The capillary was uncoated fused silica 50 μm i.d. and 365 μm o.d. The effective separation length of the capillary was 20 cm; voltage: 16 kV. Electrophoresis was performed 5 min after the reagents were mixed.

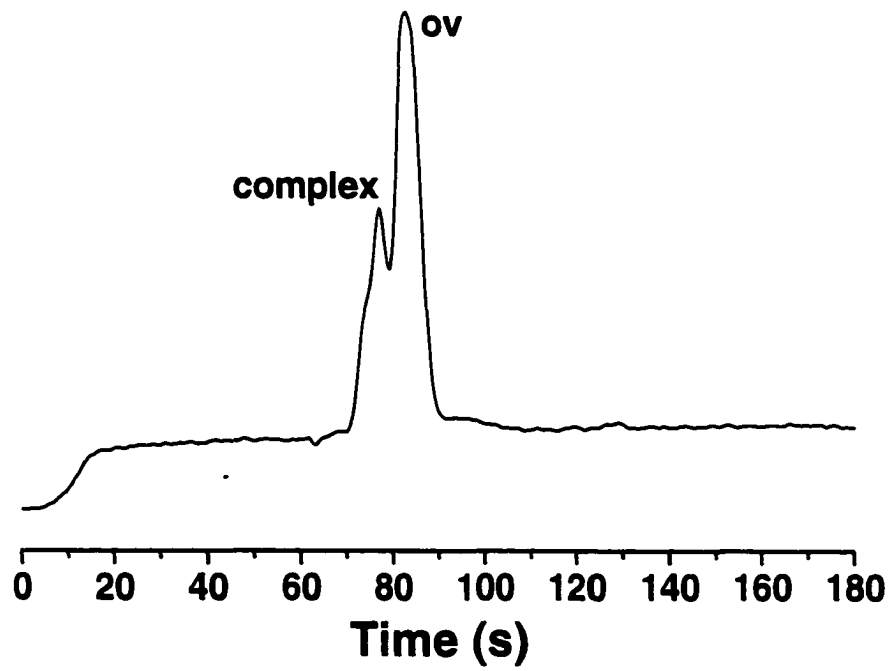


Figure 4.4 Electropherogram showing saturation of antibody. Molar ratio of [ov]/[mAb] was 23.33. The concentration of mAb was 333 nM. Separation conditions were the same as in Figure 4.3.

total ovalbumin concentration added to the sample mixture and free ovalbumin concentration in the equilibrium mixture. In this approach, we assumed that adsorption of ovalbumin or antibody on the capillary wall is negligible. Figure 4.5 shows the Scatchard plot for the data calculated as described above. The association constant of mAb calculated from the slope of the best fit straight line (correlation coefficient $R^2 = 0.996$) was $0.31 \pm 0.01 \times 10^6 \text{ M}^{-1}$. The average binding sites (n) per molecule of antibody used in this study can be determined from the x-intercept of the Scatchard plot according to eq. 4.5, giving a value of 0.96 ± 0.01 . This suggests that the stoichiometry of antibody (IgG1):ovalbumin is 1:1. The linearity of the Scatchard plot also implies that the antibody binding sites are the same and can be treated independently, without considering cooperativity effects .

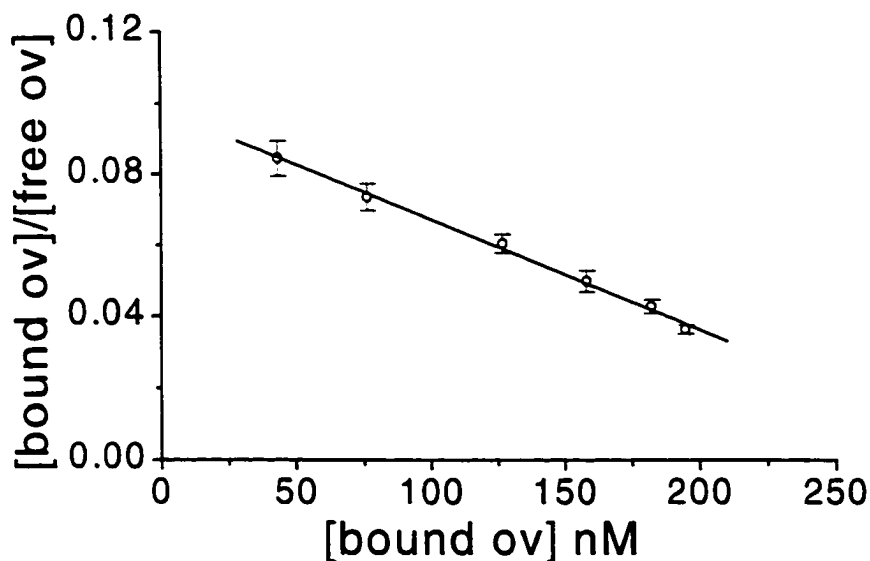


Figure 4.5 CE-derived Scatchard plot for the interaction of ovalbumin and nonlabeled antibody. Data was fit using linear regression.

4.4.3 Measurements of Cy5-labeled anti-ovalbumin affinity constant

T. Dickinson (at DRES) determined the affinity constant of Cy5-labeled anti-ovalbumin (mAb*) using the same methodology adopted for nonlabeled antibody. The concentration of labeled antibody was fixed, whereas the concentrations of nonlabeled ovalbumin were varied from 0.56-3.34 μM . To create a calibration curve relating peak height to concentration, mAb* stock solution (1.45 μM) was diluted with borate buffer (pH 8.0) to give 20 μl of solution with concentrations between 0 to 0.67 μM . The incubation time for the binding reaction between labeled antibody and nonlabeled ovalbumin was 5 min.

A P/ACE (Beckman Instruments, Fullerton, CA, USA) was used with a 635 nm solid state laser at 2.5 mW was used as a fluorescence excitation source and a detection at 675 nm wavelength. Silica capillaries (Polymicro Technologies, Phoenix, Az, USA) with 50 μm i.d., 365 μm o.d, and a total length 27 cm (20 cm to the detector) were used. Data acquisition (5 Hz) and control and peak analysis were performed using P/ACE software v. 2. Conditioning the capillary was the same as described in chapter 2. Between runs the capillary was washed for 2 min with borate buffer pH 8.0 containing 16 mM NaCl. Injection of samples was for 3 s with a pressure of 0.5 p.s.i.

For this study T. Dickinson varied the concentration of ovalbumin in the sample mixtures and the concentration of labeled antibody was fixed at 167 nM. Only labeled species (i.e., free mAb* and mAb*-ov complexes) could be observed with LIF detection. The peak heights of the complex increased as the amount of ovalbumin increased. To determine the affinity constant using the Scatchard equation, the concentrations of both bound and free ovalbumin must be known. The concentration of free mAb* was

determined from the calibration curve of mAb* peak heights versus the concentration of mAb*, ranging from 0 to 0.67 μM . The concentration of bound antigen could be determined by subtracting the total concentration of mAb* from the concentration of free mAb*. To construct a Scatchard plot, the concentrations of both free and ovalbumin must be determined, yet the label gives us mAb* concentrations.

The following equations were used to determine the concentrations of bound and free ov. A key assumption must be made, that $n = 1$, or some other specific value to make conversions. However, since $n = 1$ for the unlabeled mAb there must be no difficulty with this assumption for labeled antibody.

Since,

$$[\text{Ag}]_t = \text{known,}$$

$$[\text{Ab}]_t = \text{known,}$$

$$[\text{Ab-Ag}] = [\text{Ab}]_t - [\text{Ab}]_f$$

where, $[\text{Ab}]_f$ was measured using the calibration curve for mAb*,

then, $[\text{bound Ag}] = n [\text{Ab-Ag}]$, and assuming $n = 1$,

$$[\text{bound Ag}] = [\text{Ab-Ag}]$$

Therefore, $[\text{Ag}]_f = [\text{Ag}]_t - [\text{Ab-Ag}]$, or

$$[\text{Ag}]_f = [\text{Ag}]_t - [\text{Ab}]_t + [\text{Ab}]_f$$

The Scatchard equation then becomes,

$$\frac{[\text{Ab}]_t - [\text{Ab}]_f}{[\text{Ag}]_t - [\text{Ab}]_t + [\text{Ab}]_f} = -K_a ([\text{Ab}]_t - [\text{Ab}]_f) + n[\text{Ab}]_t K_a \quad (4.6)$$

The subscripts t and f stand for total and free species. The bound ov/free ov ratio is given by the left hand-side of eq. 4.6, while bound ov is given by $([\text{Ab}]_t - [\text{Ab}]_f)$.

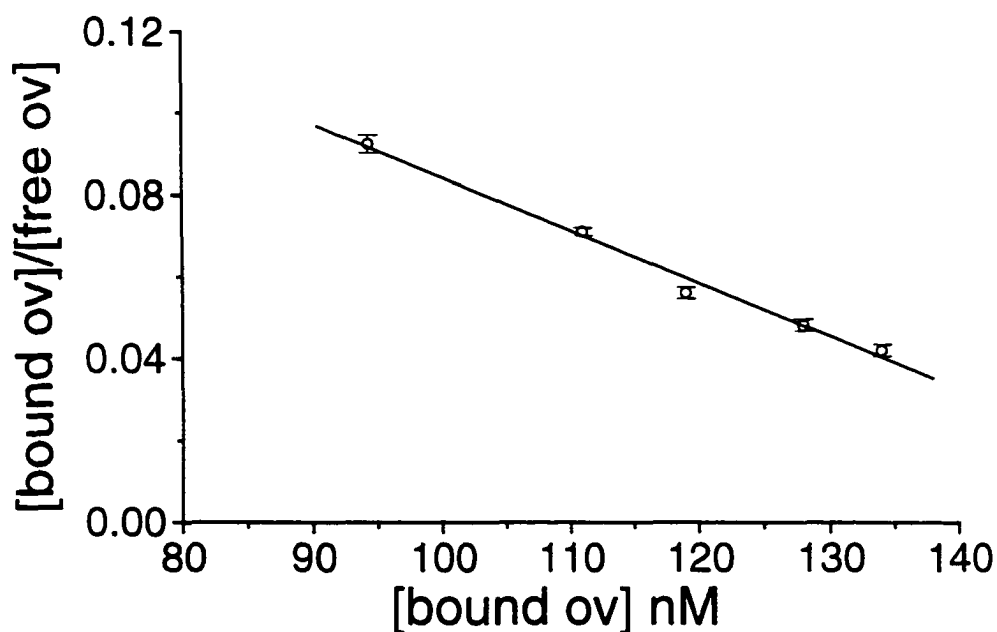


Figure 4.6 CE-derived Scatchard plot of Cy5-labeled antibody and native ovalbumin. Concentration of labeled antibody was 167 nM. Experimental conditions were in Section 4.4.3.

The Scatchard plot for the mAb* is shown in Figure 4.6. The solid line obtained with linear regression analysis gave a slope of $1.14 (\pm 0.16) \times 10^6 \text{ M}^{-1}$ and $R^2 = 0.961$. The estimated value of n from the x-intercept is 0.95 ± 0.02 . According to eq. 4.6, the affinity constant of Cy5-labeled antibody is then $1.14 (\pm 0.16) \times 10^6 \text{ M}^{-1}$. This result is reasonably close to the measured affinity constant of nonlabeled antibody, although apparently not the same.

4.4.4 Non-linear least square analysis (NLLS)

The usual approach of ligand binding studies is to fit the experimental data to eq. 4.5 and to plot them in the form of a Scatchard plot. The most important limitations

concerning this approach have been reviewed recently [88-91]. One problem arises from forcing a linear fit to the data. Another is that simple least squares fitting does not account for error in both variables, X and Y.

The graphical and statistical analysis of raw (i.e., untransformed binding data) have become an appropriate quantitative approach for ligand-protein binding studies. Non-linear least squares analysis (NLLS) fits the data to any equation that defines y (bound) as a function of x (free ligand) and finds the values of those variables that generate the curve that comes closest to the data. The parameters K_a and n were determined by iterative nonlinear least-squares regression of eq. 4.4, using the LM algorithm of Origin software to find the best fit of the [bound ov] versus the [free ov] at a constant antibody concentration. A typical curve is illustrated in Figure 4.7a for nonlabeled antibody and Figure 4.7b for labeled antibody. The binding parameters determined for the nonlabeled antibody were $K_a = 0.33 (\pm 0.02) \times 10^6 \text{ M}^{-1}$ and $n = 0.94 \pm 0.06$, and for labeled antibody $K_a = 1.00 (\pm 0.01) \times 10^6 \text{ M}^{-1}$ and $n = 0.98 \pm 0.02$. The binding parameters obtained for both labeled and nonlabeled antibody were in reasonable agreement, considering the fact that the results were reported by two different laboratories.

From the determined value of n in the curve fit, the total concentration of binding sites ($n[\text{Ab}]_t$) was $311 \pm 7 \text{ nM}$ for the nonlabeled antibody, whereas, the expected value was 333 nM . The difference could be attributed to the uncertainty in measuring the initial concentration of nonlabeled antibody by UV absorbance at 280 nm . However, for labeled antibody, the expected value for the total binding site concentration (167 nM) agrees with the value (164 nM) obtained for NLLS.

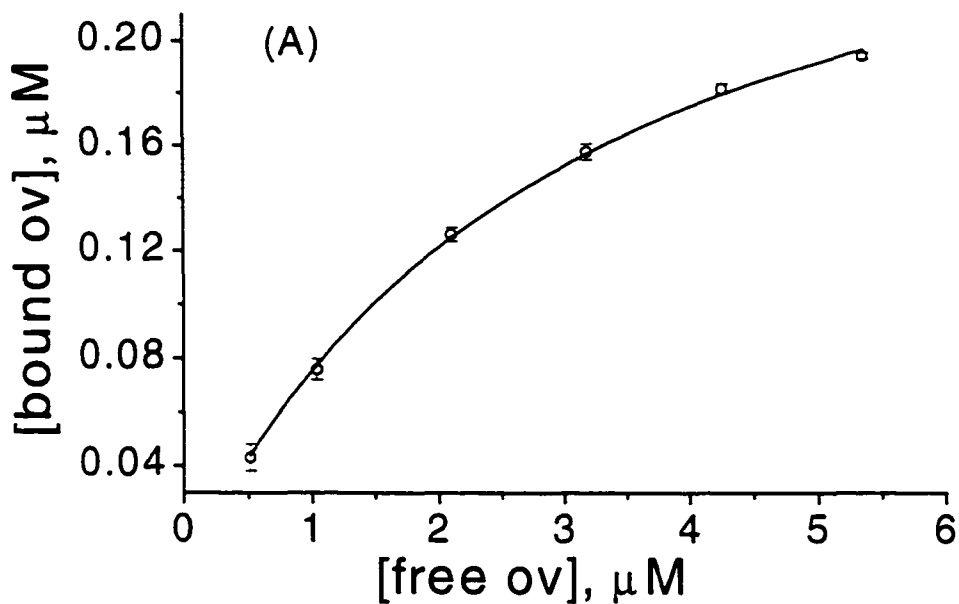


Figure 4.7 Non-linear least squares analysis of the interaction of ovalbumin and antibody. Data was fitted using eq. 4.4. CE-derived data were shown as open circles and fitted points by a solid line. (A) Interaction of native ovalbumin and antibody. (B) Interaction of Cy5-labeled antibody and ovalbumin.


Although the binding parameters (i.e., K_a and n) obtained from either the Scatchard or NLLS were in close agreement we report the values obtained from NLLS fitting, since the non-linear fit is generally agreed to be more reliable.

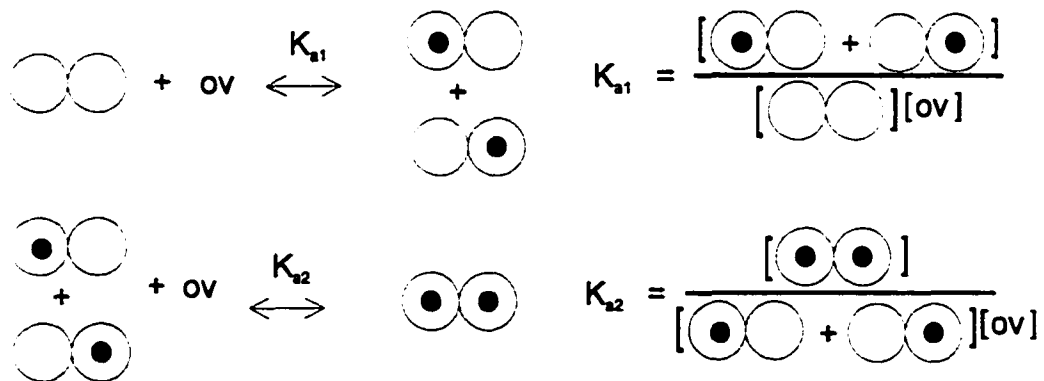
4.4.4.1 Fitting the binding data to two binding sites

In deriving eq. 4.6, we assumed a 1:1 interaction of ovalbumin and the antibody. Equation 4.7 represents the situation where two binding sites are involved in the interaction of ov with the antibody [92].

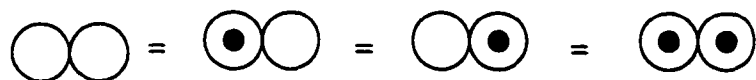
$$[\text{bound Ag}] = \frac{n_1 [\text{Ab}]_{\text{total}} K_{a1} [\text{free Ag}]}{1 + K_{a1} [\text{free Ag}]} + \frac{n_1 [\text{Ab}]_{\text{total}} K_{a2} [\text{free Ag}]}{1 + K_{a2} [\text{free Ag}]} \quad (4.7)$$

When the two binding sites are the same and noncooperative K_{a1} equals 4 K_{a2} . This can be proved as follows:

If two binding sites can be represented as  then we can represent the equilibria as follows:



For noncooperative binding and at 50% saturation, the four population must be equal.



Calling each concentration C gives $K_{a1} = (C+C)/(C)[\text{ov}]$ and $K_{a2} = (C)/(C+C)[\text{ov}]$ or

$$K_{a1}/K_{a2} = \{2C/C(ov)\} / \{C/2C(ov)\} = 4.$$

Attempts to fit the binding data for labeled antibody using nonlinear least squares method for a two binding sites model (i.e., $n = 2$) gave $K_{a2} = 2 \times 10^3 \text{ M}^{-1}$ and $K_{a1} = 0.99 \times 10^6 \text{ M}^{-1}$. This is essentially equivalent to saying the K_{a2} term is irrelevant (in this case, $K_{a1} = 496$ times K_{a2}), in the sense that a two site binding model with equivalent sites predicts $K_{a1} = 4 \times K_{a2}$. So the single binding site model fit the data best, in that if a second site really present it has a much lower affinity constant. We did not fit the data for nonlabeled antibody to two binding sites model since both antibodies seem to behave similarly.

4.5 Effect of affinity constant (K_a) on the detection limit

Table 4.1 shows the calculations of the concentration of antigen required to saturate 253 nM antibody and the dependence of the reaction on the K_a . The values in Table 4.1 were obtained from eq. 4.4, which has the form of a Langmuir adsorption isotherm. For simplicity, all molecules are considered monovalent. For example, the concentration of unbound Ag at 50% saturation of 253 nM antibody with affinity constant (K_a) 10^7 M^{-1} is 100 nM. Therefore, the total concentration of antigen required to saturate 50% of the total concentration of the antibody is, *ca.* 227 nM. It is evident from Table 4.1 that a large amount of antigen is required to obtain a reasonable degree of antibody saturation, if $K_a[\text{Ab}]_{\text{total}} < 1$.

Two important conclusions can be drawn from Table 4.1. First, the affinity of the antibody strongly influences the amount of antigen reacted; for example, to saturate 5% of the antibody with a $K_a = 10^8 \text{ M}^{-1}$, requires 11 times less antigen than is needed when the antibody has an affinity constant of $K_a = 3.3 \times 10^5 \text{ M}^{-1}$.

Table 4.1 The concentration of antigen required to saturate 253 nM antibody and the dependence on the K_a of the reaction

saturation level %	[bound Ag] (μM)	[Ag] _{total} (μM) required if				
		$K_a = 10^5$	$K_a = 3.3 \times 10^5$	$K_a = 10^7$	$K_a = 10^8$	$K_a = 10^9$
5	0.013	0.539	0.172	0.018	0.013	0.013
10	0.025	1.136	0.362	0.036	0.026	0.025
20	0.051	2.551	0.808	0.076	0.053	0.051
30	0.076	4.362	1.375	0.119	0.080	0.076
40	0.101	6.768	2.121	0.168	0.108	0.102
50	0.127	10.127	3.157	0.227	0.137	0.128
60	0.152	15.152	4.697	0.302	0.167	0.153
70	0.177	23.510	7.248	0.410	0.200	0.179
80	0.202	40.202	12.324	0.602	0.242	0.206
90	0.228	90.228	27.500	1.128	0.318	0.237

A. Jemere (in our group) estimated the detection limit of ovalbumin to be *ca.* 200 nM using 253 nM Cy5-labeled antibody and LIF detection with the DARPA box. As shown in Table 4.1, the total antigen required to bind 5% of antibody (assuming an affinity constant = $3.3 \times 10^5 \text{ M}^{-1}$) was 172 nM. This value was close to the detection limit of 200 nM. Binding of 5% of the mAb is likely to be within a factor of 2 of the detection limit, given a $\pm 3\%$ peak height standard deviation. So the prediction of % bound in Table 4.1 are consistent with the observed detection limit. In contrast, our group reported a detection limit 0.24 nM for standard Cy5 dye using the same detection method. The difference is attributed to the chemistry of the assay rather than the detection limit of the instrument.

The other feature the table shows is that an increasingly larger excess of antigen is required to bind very much of the antibody when using a low affinity antibody. We observed that considerable excess ovalbumin was required to obtain a complex peak, thus

demonstrating the low affinity constant of the antibody. Clearly a better antibody would be useful. Unfortunately, an antibody with a higher affinity value was not available commercially to our knowledge.

4.6 Conclusions

The present study demonstrates that free solution CE provides a rigorous and efficient means of accurate measurements of binding parameters. Added attractions for CE are: (1) simplicity, (2) speed, (3) direct quantification, and (4) small amounts of samples. The binding constant for the native anti-ovalbumin is $0.33 (\pm 0.02) \times 10^6 \text{ M}^{-1}$. This value is in reasonable agreement with the value of $1.00 (\pm 0.02) \times 10^6 \text{ M}^{-1}$ obtained with Cy5-labeled anti-ovalbumin measured in a different lab. We employed nonlinear least squares curve fitting in order to deduce these parameters.

4.7 References

- 1 W.R. Gillespie, *J. Pharmacokin. Biopharm.*, 21 (1993) 99.
- 2 G.T. Tucker and M.S. Lennard, *Pharmac. Ther.*, 45 (1990) 309.
- 3 S.D. Nelson, *J. Med. Chem.*, 25 (1982) 753.
- 4 J.J. MacKichan, *Clin. Pharmacokin.*, 9 (Suppl. 1) (1984) 32.
- 5 J.J. MacKichan, *Clin. Pharmacokin.*, 16 (1989) 62.
- 6 P.E. Rolan, Br.J., *Clin. Pharmacol.*, 37 (1994) 125.
- 7 S.M. Wallace and R.K. Verbeek, *Clin. Pharmacokin.*, 12 (1987) 41.
- 8 R. Zini, P. Riant, J. Barre and J.-P. Tillement, *Clin. Pharmacokin.*, 19 (1990) 147.
- 9 R. Zini, P. Riant, J. Barre and J.-P. Tillement, *Clin. Pharmacokin.*, 19 (1990) 218.
- 10 F. Herve, E. Gomas, J.C. Duche and J.P. *J. Clin. Pharmacol.*, 36 (1993) 241.
- 11 H. Kurz, H. Trunk and B. Weitz, *Drug Res.*, 27 (1977) 1373.
- 12 W.F. Bowers, S. Fulton and J. Thompson, *Clin. Pharmacokin.*, 9 (suppl 1) (1984) 49.
- 13 W.W. Mapleson, *J. Pharmacol, Meth.*, 17 (1987) 231.
- 14 J.A. Henry and S.N.Br. Mitchell, *J. Clin. Pharmacol.*, 11 (1981) 119.
- 15 D.L. Parson and H.F. Fan, *Res. Commun. Clin. Pathol. Pharmacol.*, 54 (1986) 405.
- 16 M. Oellerich and H. Muller-Vahl, *Clin. Pharmacokin.*, 9 (suppl 1) (1984) 61.
- 17 B. Sebille, N. Thuaud and J.-P. Tillement, *J. Chromatogr.*, 167 (1978) 159.
- 18 B. Sebille, N. Thuaud and J.-P. Tillement, *J. Chromatogr.*, 180 (1979) 103.
- 19 B. Sebille and N. Thuaud, *J. Liq. Chromatogr.*, 3 (1980) 299.
- 20 N. Thuaud, B. Sebille, M.H. Livertoux and J. Bessiere, *J. Chromatogr.*, 282 (1983) 509.
- 21 S.F. Sun, S.W. Kuo and R.A. Nash, *J. Chromatogr.*, 288 (1984) 377.

- 22 M.H. Rahman, T. Maruyama, T. Okada, K. Yamasaki and M. Otagiri, *Biochem. Pharmacol.*, 46 (1993) 1721.
- 23 N. Muller, F. Lopicque, E. Drelon and P. Netter, *J. Pharm. Pharmacol.*, 46 (1994) 300.
- 24 S. Narita, T. Tasaki and T. Kitagawa, *Chem. Pharm. Bull.*, 37 (1989) 1009.
- 25 C.F. Chignell, *Drug Fate and Metabolism, Methods and Techniques*, Marcel Dekker, New York (1977), Chapter 5.
- 26 M.H. Livertoux and J. Bessiere, *Biochem. Bioenerget.*, 17 (1987) 535.
- 27 A. Aki and M. Yamamoto, *J. Pharm. Pharmacol.*, 41 (1989) 674.
- 28 N. Shaklai, R.L. Garlick and H.F. Bunn, *J. Biol. Chem.*, 259 (1984) 3812.
- 29 B.H. Chen, E.H. Taylor and A.A. Pappas, *Clin. Chim. Acta*, 163 (197-87) 75.
- 30 J.C. Giddings, *Science*, 260 (1993) 1456.
- 31 M.H. Moon and J.C. Giddings, *J. Pharm. Biomed. Anal.*, 11 (1993) 911.
- 32 G. Rippel, H. Corstjens, H.A.H. Billiet and J. Frank, *Electrophoresis*, 18 (1997) 2175.
- 33 K. Takeo and S. Nakamura, *Arch. Biochem. Biophys.*, 153 (1972) 1.
- 34 K. Takeo and E.A. Kabat, *J. Immunol.* 121 (1978) 2305.
- 35 T.C. Bóg-Hansen and K. Takeo, *Electrophoresis*, 1 (1980) 67.
- 36 N.H.H. Heegaard and T.C. Bog-Hansen, *Appl. Theor. Electrophoresis*, 1 (1990) 149.
- 37 F.A. Gomez, J.K. Chen, A. Tanaka, S.L. Schreiber and G.M. Whitesides, *J. Org. Chem.* 59 (1994) 2885.
- 38 Y.-H. Chu, L.Z. Avila, H.A. Biebuyck and G.M. Whitesides, *J. Med. Chem.* 35 (1992) 2915.

- 39 L.Z. Avila, Y.-H. Chu, E.C. Blossey and G.M. Whitesides, *J. Med. Chem.* 36 (1993) 126.
- 40 Y.-H. Chu, W.J. Lees, A. Stassinopoulos and C.T. Walsh, *Biochemistry* 33 (1994) 10616.
- 41 K. Shimura and B.L. Karger, *Anal. Chem.*, 66 (1994) 9.
- 42 N.H.H. Heegaard and F.A. Robey, *J. Liq. Chromatogr.*, 16 (1993) 1923.
- 43 L. Valtcheva, J. Mohammad, G. Pettersson and S. Hjerten, *J. Chromatogr.* 638 (1993) 263.
- 44 R. Vespaleck, V. Sustacek and P. Bocek, *J. Chromatogr.*, 638 (1993) 255.
- 45 S. Busch, J.C. Kraak and H. Poppe, *J. Chromatogr.* 608 (1993) 257.
- 46 G.E. Barker, P. Russo and R.A. Hartwick, *Anal. Chem.*, 64 (1992) 3024.
- 47 F.A. Gomez, L.Z. Avila, Y.-H. Chu and G.M. Whitesides, *Anal. Chem.*, 66 (1994) 1785.
- 48 S. Busch, J.C. Kraak and H. Poppe, *J. Chromatogr.*, 635 (1993) 119.
- 49 R. Kuhn, R. Frei and M. Christen, *Anal. Biochem.*, 218 (1994) 131.
- 50 S. Honda, A. Taga, K. Suzuki, S. Suzuki and K. Kakehi, *J. Chromatogr.*, 597 (1992) 377.
- 51 J. Liu, K.J. Volk, M.S. Lee, M. Pucci and S. Handwerger, *Anal. Chem.*, 66 (1994) 2412.
- 52 S. Handwerger, M. Pucci, K.J. Volk, J. Liu and M.S. Lee, *J. Bacteriol.*, 176 (1994) 260.
- 53 D.M. Goodall, *Biochem. Soc. Trans.*, 21 (1993) 125.

- 54 J.L. Carpenter, P. Camilleri, D. Dhanak and D. Goodall, *J. Chem. Soc. Chem. Commun.* (1992) 804.
- 55 Y.-H Chu and G.M. Whitesides, *J. Org. Chem.*, 57 (1992) 3524.
- 56 Y.-H Chu, L.Z. Avila, H. A. Biebuyck and G.M. Whitesides, *J. Org. Chem.*, 58 (1992) 648.
- 57 N.H.H. Heegaard, F.A. Robey, *Anal. Chem.*, 64 (1993) 2479.
- 58 M. Mammen, I.J. colton, J.D. Carbeck, R. Bradley and G.M. Whitesides, *Anal. Chem.* 69 (1997) 2165.
- 59 S.A.C. Wren and R.C. Rowe, *J. Chromatogr.*, 603 (1992) 235.
- 60 E.-S. Kwak and F.A. Gomez, *Chromatographia*, 43 (1996) 659.
- 61 M. Mammen, F.A. Gomez and G.M. Whitesides, *Anal. Chem.* 67 (1995) 3526.
- 62 M.H.A. Busch, J.C. Kraak and H. Poppe, *J. Chromatogr.*, 777 (1997) 329.
- 63 Y.-H Chu, L.Z. Avila, J. Gao and G.M. Whitesides, *Acc. Chem. Res.*, 28 (1995) 461.
- 64 F.A. Gomez, J.N. Mirkovich, V.M. Dominguez, K.W. Liu and D.M. Macias, *J. Chromatogr.*, 727 (1996) 291.
- 65 V. Horejsí, M. Tichá, *J. Chromatogr.*, 178 (1979) 1.
- 66 V. Horejsí, *J. Chromatogr.*, 376 (1986) 49.
- 67 V. Matousek and V. Horejsí, *J. Chromatogr.*, 245 (1982) 271.
- 68 K. Ensing and A. Paulus, *J. Pharm. Biomed. Anal.*, 14 (1996) 305.
- 69 N.A. Guzman, M.A. Trebilcock, J.P. Advis, *J. Liq. Chromatogr.*, 14 (1991) 997.
- 70 A.L. Tomlinson, N.A. Guzman and S. Naylor, *J. Cap. Elec.*, 2 (1995) 247.
- 71 N.A. Guzman, *J. Liq. Chromatogr.*, 18 (1995) 3751.
- 72 L. Tao, R.T. Kennedy, *Electrophoresis.*, 18 (1997) 112.

- 73 H. C. Nghia and D. Jed Harrison, *Electrophoresis*, 19 (1998) 3040.
- 74 K. Shimura and B.L. Karger, *Anal. Chem.*, 66 (1994) 9.
- 75 N.M. Schultz and R.T. Kennedy, *Anal. Chem.*, 65 (1993) 3161.
- 76 N.M. Schultz, L. Huang and R.T. Kennedy, *Anal. Chem.*, 67 (1995) 924.
- 77 D. Schmalzing, W. Nashabeh, X.W. Yao, R. Mhatre, F.E. Regnier, N.B. Afeyan and M. Fuchs, *Anal. Chem.*, 67 (1995) 606.
- 78 F.T. Chen and S.L. Pentoney, *J. Chromatogr.*, 680 (1994) 425.
- 79 F.T. Chen and R.A. Evangelista, *Clin. Chem.*, 40 (1994) 1819.
- 80 G. Scatchard, *Ann. NY Acad. Sci.*, 51 (1949) 660.
- 81 M.W. Steward, J. Steensgaard, *Antibody Affinity: Thermodynamic Aspects and Biological Significance*, CRC press, Boca Raton, FL, 1983.
- 82 A. Nisonoff, D. Pressman, *J. Immunology*, 80 (1958) 417.
- 83 M. Sela, *The Antigens* Academic Press, N.Y. (1974) 71.
- 84 V.N. Schumaker, G. Green, R. Wilder, *Immunochemistry*, 10 (1973) 521.
- 85 D. Lancet and I. Pecht, *Biochem.*, 16 (1977) 5150.
- 86 A.L. Zidovetzki, I. Pecht, *Proc. Natl. Acad. Sci. USA*, 76 (1979) 5848.
- 87 R. Zidovetzki, A. Light and I. Pecht, *Mol. Immunol.*, 18 (1981) 491.
- 88 I.M. Klotz, *Science*, 217 (1982) 1247.
- 89 I.M. Klotz, *Science*, 220 (1983) 981.
- 90 K. Zierler, *Trends Biochem. Sci.*, 14 (1989) 314.
- 91 J.C. Kermode, *Biochem. Pharmacol.*, 38 (1989) 29.
- 92 D. Freifelder, "*Physical biochemistry: Application to Biochemistry and Molecular Biology*", 2nd edition, W.H. Freeman and Company, N.Y., 1982.

Chapter 5

Automation of sample introduction into microchip-based CE

5.1 Introduction

Continuous monitoring of a chemical process, usually by determining the concentration of some species, is gaining increasing attention in biotechnology [1], process control [2,3], and the environmental [4,5], and medical sciences [6,7]. For example, those continuously monitoring an industrial process will be informed of a change in conditions or a chemical event very soon after its actual occurrence, thus they can immediately undertake steps to correct the situation should it be damaging to the process.

For monitoring purposes, the instrument needs to be fully automated. The key analysis elements are sample introduction, sample pretreatment, reactions, separation and detection. With conventional instrumentation it is possible to couple techniques such as flow injection analysis (FIA) to chromatographic systems or other techniques. This allows continuous sample monitoring in applications such as process control. Miniaturization of such systems using micromachining should provide an exciting route to complex analysis systems on scale of a microchip. The rapid analysis time possible on-chip allows essentially real time decisions. The low volume of reagent consumption allows for long term operation without intervention at remote sites, and reduces the cost of assays involving expensive biochemical reagents. The ability to integrate sample processing with the analysis removes the requirement for a highly trained practitioner of manually performed chemical analysis. A number of examples of on-chip chemical analysis such as immunoassay [8,9], enzymatic assay [10], chemical reaction [11-13],

pre- and post chemical reaction [14-16] have been demonstrated. In these examples electroosmotic pumping was employed to mix, and separate the reaction products.

A key missing analytical element is automated sample introduction; we are unaware of a simple and disposable microchip interface to an external fluid system that allows automation of sample introduction. ACLARA and CALIPER Co. (Mountain View, CA, USA) use a robot for sample introduction into microfluidic chips. In this chapter, we describe two microchip devices, Faster and DARPA, which contain 1 mm wide and 300 μm deep sample introduction channels (SIC) for introducing the sample into the chip using pressure-driven flow. Electric fields were applied across narrow channels, 36-68 μm wide and 10-13 μm deep, so that electroosmotic pumping was used for quantitative injection of reagents and liquid transport on the chip. The sample introduction channel (SIC) was designed to have the least resistance to flow, so that during loading the sample with a pressure driven flow, the main flow would be in the SIC and would not perturb the electrophoresis channels.

In this chapter, we used Faster devices to evaluate the SIC for rapid sample exchange of fluorescein isothiocyanate (FITC)-labeled phenylalanine and FITC-labeled arginine used as test compounds. We demonstrated that 12 μl of sample (added in two consecutive additions of 6 μl each) and ca. 25 s were required to condition the chip and acquire the electropherogram of the next sample. Thus increasing the throughput of sample analysis on chip. We also demonstrate for the first time a fluidic interface assembly for coupling a microchip to external reservoir containing fluorescein. The assembly allowed for real-time analysis of a continuously changing concentration of fluorescein. A linear calibration curve for fluorescein was obtained. The SIC was

incorporated onto a microchip (DARPA device) with a manifold channel for mixing, reaction and separation, to produce a fully automated microchip. The evaluation of the SIC for continuous monitoring using the DARPA device will be presented in this chapter as well.

5.2 Experimental

5.2.1 Materials and Reagents

The separation and dilution buffer was prepared from 100 mM Tris (tris(hydroxymethylamino)methane, Sigma)/ 20 mM boric acid (Baker, Phillipsburg, NJ, USA) and adjusted to pH 9 using 1 M NaOH solution. Fluorescein-5-isothiocyanate (FITC), amino acids, and fluorescein di-sodium salt were purchased from Sigma (St. Louis, MO, USA). We prepared 10 mM FITC in 95% acetone and 5% water. Stock solutions of 10 mM of phenylalanine (Phe) and arginine (Arg) were prepared in tris/boric acid, pH 9. Each amino acid was labeled with FITC as described before [17]. Briefly, we added 1 volume of 10 mM FITC to 5 volumes of 10 mM amino acid. The mixture was allowed to react overnight at room temperature. The solutions were diluted to a final concentration of 10 μ M, using tris/boric acid pH 9. A 1 mM stock solution of fluorescein di-sodium salt (Sigma) was prepared in tris/boric acid buffer (pH 9). Bifunctional Cy5 dye was purchased from Amersham. A 200 nM stock solution of Cy5 dye was prepared in 5 mM borate buffer adjusted to pH 8.3 using 1 M NaOH. All solutions were prepared in doubly-distilled, de-ionized water and filtered through 0.22- μ m pore size Millipore-GV sterile filter units (Millipore, Bedford, MA, USA) before being injected into the capillaries on the chip in the manner previously described [18, 19].

5.2.2 Instrumentation

The instrument set up was described in Chapter 2. In this chapter we used a 488 nm air cooled Argon ion laser (Uniphase, 2014, San Jose, CA, USA), operated at 4.1 mW as source of fluorescence excitation for studying sample exchange of FITC-labeled amino acids and for continuous monitoring of changing concentration of fluorescein. Bifunctional Cy5 dye (Amersham) was used as a test compound to study the SIC of DARPA microchips. Thus, a 632.5 nm He-Ne (red laser) was utilized as a source of excitation and a band pass filter 675 nm as an emission filter.

5.2.3 Device fabrication

A single-mask micromachining process has been described before (see Figure 1.1 Chapter 1). Since both Faster and DARPA devices had two channel depths, fabrication of such devices was performed using either a modified single mask process or two-mask process. In early studies, we used the Faster chip, the fabrication of shallow electrophoresis channels and the SIC, using a single-mask process, was performed as follows:

1- Starting with 3 or 4 inch squares of 0211 Corning glass wafer a 200Å chromium film (acting as an adhesive layer) and 1000 Å gold layer (used as a protective layer during glass etching) were sputter coated.

2- A positive photoresist layer (Waycoat HPR 504, Ollin Hunt) was spin coated onto the substrate (for 65 s at 2000 rpm) with a photoresist coater/developer (Solitec Wafer Processing, San Jose, CA USA); the wafer was soft baked at 110 °C for 30 min to improve photoresist adhesion

3- Illumination of a chrome photomask of the Faster chip, designed using L-edit (Tanner Research, Pasadena, CA, USA), with UV light was realized with a contact mask aligner (Karl Süss, Garching, Germany).

4- The exposed photoresist was removed using Microdeposit 354 developer (Shipley, Newton, MA, USA). The wafer was hard baked for 30 min at 110 °C. The Cr and Au layers were removed with a commercial Cr etch (KTI Chemicals, Sunnyside, CA, USA) and an aqueous potassium iodide/iodine solution (Alberta Microelectronic Center), respectively.

5- Then, to etch the SIC to 300 µm deep, the whole chip was carefully masked-off by black tape except for the SIC region. The glass was etched using a mixture of HF:HNO₃:H₂O (20:14:66) for 2.5 h at an etching rate of ca. 2 µm/min. Then, for etching the narrow channel to 36 µm, the black tape was removed and the chip was dipped again in the etching solution for 18 min.

5- Finally, the photoresist was stripped off with acetone and the wafer was, then, rinsed with piranha etch and distilled water.

Later on, the AMC modified the fabrication of devices by using a two-mask process. In the first mask, shallow channels were patterned into a 0211 wafer, followed by the second mask process wherein the SIC channel was patterned onto the same wafer. The drawback of this approach is that the metal mask (i.e., Cr/AU) layer is not resistive enough to the etching solution. Therefore, the SIC can not be reproducibly etched to 300 µm.

To solve this problem, the SIC were patterned in one wafer and the narrow channels on another wafer. Then the two wafers were thermally bonded after drilling 1.5 mm

holes in the wafer containing the SIC. Before bonding, the SIC must be aligned so that it intersects with the narrow channel and the holes meet the ends of the shallow channels.

5.2.4 Sample exchange

For fast sample exchange, glass tubing (5 mm o.d., 2 mm i.d., and 1.3 mm long) was glued with epoxy onto both sides of the SIC to form reservoirs. One reservoir was connected to a 3-way valve (Chromatographic Specialities Inc, Ontario, CA) via plastic tubing (8 mm o.d. and 3 mm i.d.). The valve in turn was connected to a house vacuum line. Figure 5.1 illustrates the sequence of the sample exchange of Phe-FITC. The 3-way valve was switched to atmosphere and 6 μl of Phe-FITC was loaded into the SIC using an Eppendorff pipet. The electropherogram of Phe-FITC was obtained by applying -1.5 kV between reservoir 1 and 3 (reservoir 1 at ground) for 15 s and then applying -3 kV between reservoir 4 and 5 (reservoir 4 at ground). The 3-way valve was again switched to vacuum to drive out the Phe-FITC into the vacuum trap. With an Eppendorf pipet, 6 μl of the next sample (10 mM Arg-FITC) were used to flush the SIC. Then, the 3-way valve was again switched to atmosphere and another 6 μl of Arg-FITC was introduced into the SIC for analysis. An estimated time of 3 s and volume of 12 μl of Arg-FITC, 6 μl to flush the SIC and 6 μl to measure the electropherogram of the Arg-FITC were used for sample exchange experiment. The injection channel was then flushed with Arg-FITC by applying -3 kV for 20 s between reservoirs 1 and 3 (1 at ground).

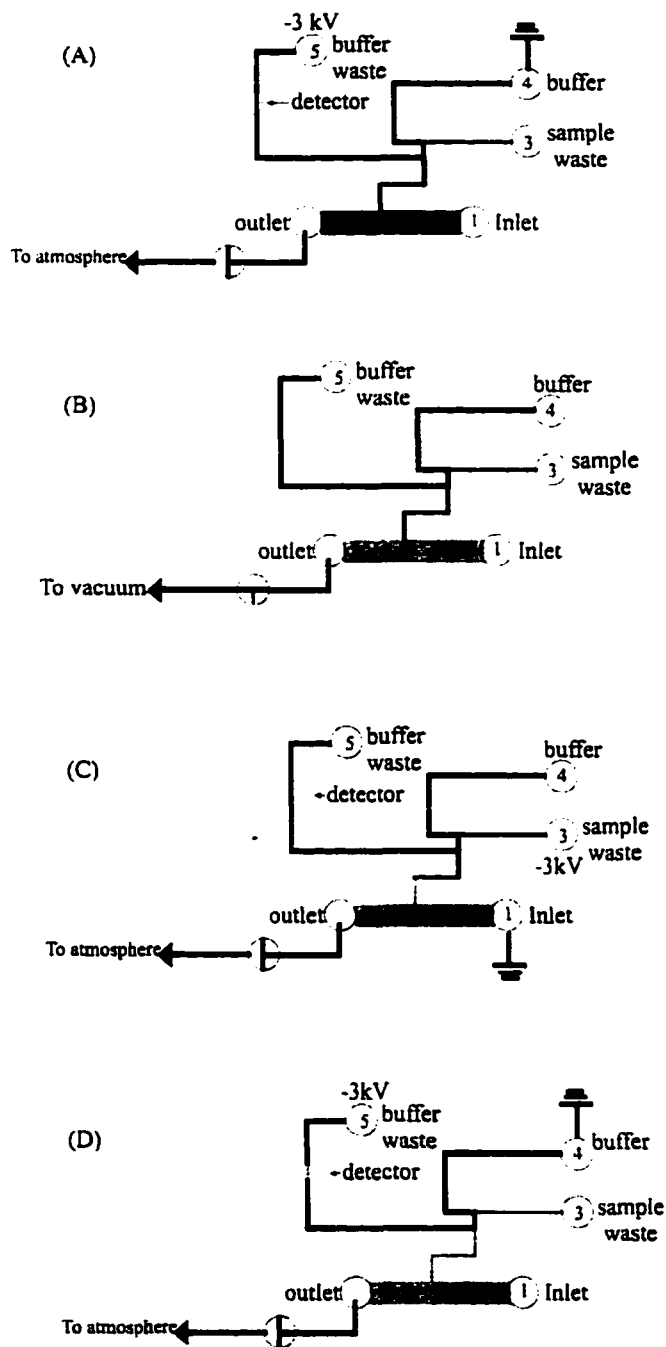


Figure 5.1 Sequence of sample exchange of Phe-FITC and Arg-FITC on Faster chip. Sequence of sample exchange on Faster chip. (A) switching the 3-way to atmosphere and applying -3 kV, between buffer and buffer waste reservoirs to move the sample plug into the separation channel. (B) switching the 3-way valve to vacuum to pull out the Phe-FITC in SIC and then adding 6 μ l of Arg-FITC for rinsing the SIC. (C) loading another 6 μ l of Arg-FITC for CE analysis; applying -3 kV for 20 s to rinse injection channel so that Arg-FITC filled the channel. (D) employing separation voltage (-3 kV) between buffer and buffer waste reservoirs and recording the electropherogram of the Arg-FITC.

Because there was some leakage of sample from the injection channel into the separation channel during this step, the separation channel was then flushed using -3 kV applied to reservoir 5 and reservoir 4 (reservoir 4 at ground). Separate studies (*vide infra*) demonstrated that these potential programs properly flushed the injection and separation channels.

5.2.5 On-line Monitoring

Figure 5.2 illustrates the fluidic interface plate designed to facilitate connection of the chip to an external fluid system. Five threaded holes were drilled in the upper plexiglass plate, 8 mm thick. The holes can accommodate flangeless fittings and 1.6 mm male nut, from Upchurch Scientific (Oak Harbor, WA, USA). To tighten the upper and lower plexiglass plates with screws, flow through holes were drilled in both plates. The device, was then sandwiched between two plexiglas plates so that the five reservoirs of the device were aligned with the fitting holes drilled in the upper plate. Then we tightened the two plates together. As long as the holes are distributed equally around the plexiglass plates the device will not break during tightening the two plates. As shown in Figure 5.2, part of the device was left uncovered by plexiglass to allow the Ar ion laser to be directly focused into the separation channel.

Connection to a beaker containing the buffer via a peristaltic pump was achieved with teflon tubing (0.8 mm i.d. and 1.6 mm o.d.). Reservoir 1 was connected to the outlet of the peristaltic pump and the effluent from reservoir 2 was returned to the same external beaker.

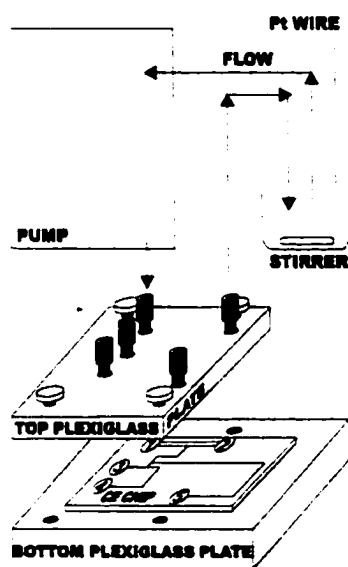


Figure 5.2 Leak-free assembly for continuous monitoring. The flow rate of the pump was 1 ml/min or 5 cm/s.

This method provided a leak free interconnection to the chip, with a total dead volume of 160 μL , about 0.2 % of the total volume (70 ml of tris/boric acid buffer pH 9) in the sample beaker. A Platinum wire, 8 cm long, was located in the sample beaker to provide the electrical grounding contact required by the chip's reservoir 1. The sample beaker containing 70 ml of tris/boric acid buffer, pH 9, and a magnetic stirring bar was placed on an insulating Styrofoam pad on a magnetic stir motor. Fluorescein sample concentration was increased stepwise by adding 10 μL of 1 mM fluorescein in the same buffer. To ensure proper mixing, the sample was stirred for 2 min and the peristaltic pump was run at a flow rate of 1 ml/min, driving solution through the sample introduction channel. We applied -3 kV between the beaker and reservoir 3 for 30 s to flush the injection channel with the solution in the SIC. We made two consecutive injections and separations, using a 3 s injection time, and the data from the second and subsequent separations were analyzed. A separation voltage of -6 kV was applied between reservoir 5 and reservoir 4 (reservoir 4 at GND) to elute the fluorescein sample.

5.2.6 Investigations of SIC of the DARPA device

We used the same setup as in section 5.2.5 to investigate the SIC of the DARPA device. The sample in the beaker was 200 nM Cy5 dissolved in tris/boric acid (pH 9). A 632.5 nm He-Ne laser was used and the emission was monitored at 675 nm. Two sets of experiments were performed, one in which the pump was on and the other when the pump was off. When the pump was run at a flow rate of 0.7 ml/min the Cy5 sample was injected by applying an injection voltage of -1.5 kV between reservoir 1 and reservoir 3 (reservoir 1 at GND) for 10 s; the layout of DARPA device is shown in Figure 5.6A. Then, the sample plug in the double T-injector was eluted by applying -6 kV between

reservoir 4 and reservoir 5 (reservoir 4 at GND). The electropherograms were acquired at a sampling rate of 10 Hz and peak area and peak heights were measured using Igor Pro V. 3 (Wavemetrics, Lake Oswego, OR, USA). Before turning the pump on, the separation channel was rinsed with buffer by applying a voltage of -6 kV between reservoirs 4 and 5 (reservoir 4 at ground). We repeated the same experiments except that the pump was not run.

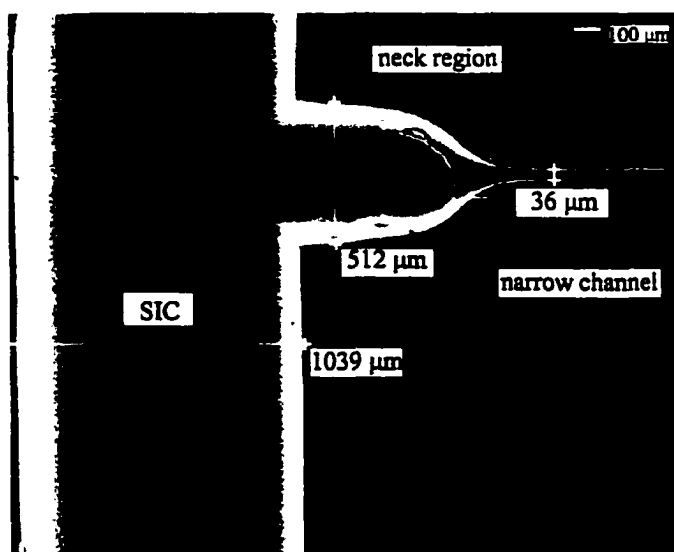


Figure 5.3 Electron micrograph of Faster device showing sample introduction channel etched to ca. 1 mm wide and 300 μm deep intersecting with injection channel etched to 36 μm wide and 10 μm deep. Triangle-like channel is the neck region.

5.3 Results and Discussion

The narrow channels were 10 μm deep and 36 μm wide, whereas the SIC was 300 μm deep and 1 mm wide. Such a drastic difference in channel dimensions means channels have radically different resistance to solution flow, so that the pressure required to drive the sample into the injection channel should be much larger than that required to drive flow through the SIC. In this way, it should be possible to use pressure to exchange sample on-chip in one region without contaminating the fluid within the rest of the chip.

Figure 5.3 shows electron micrograph of the etched SIC, with the injection channel leading off to the side. Mask under etching effects produced the short neck region that joined the two channels.

5.3.1 Theory

The linear flow rate of liquid in a rectangular channel [20] is given by eq. 5.1.

$$U = \frac{ab}{\eta} \frac{\Delta P}{L} F \quad (5.1)$$

where a , b , and L are the half width, half depth, and length of the channel, respectively. η is the viscosity (kg/m s) of the fluid. ΔP is the pressure difference. F is a constant [21] that depends on the ratio of a/b . The value of F can be obtained from Figure 5.4 with ($b \leq a$).

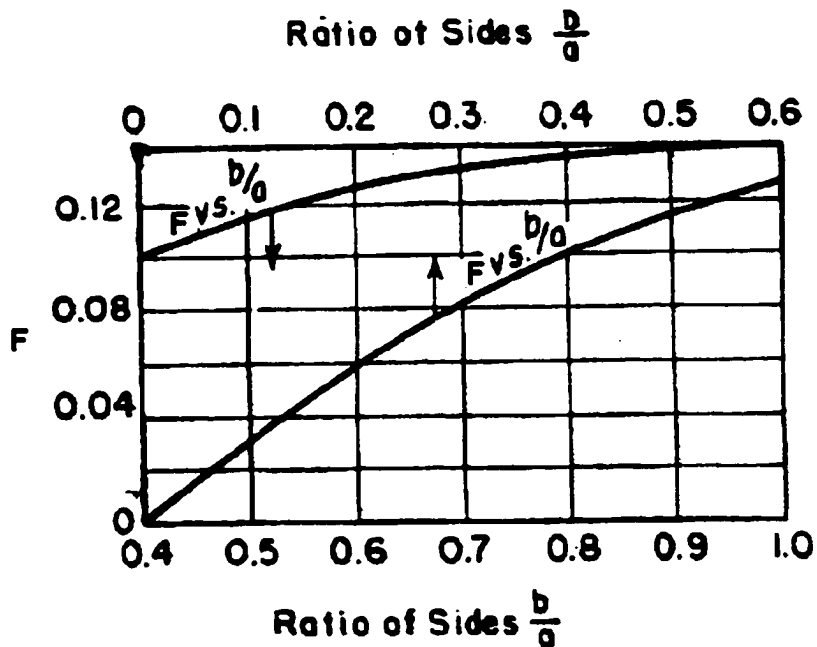


Figure 5.4 Relation between F and ratio of half width and depth. (Adapted from Ref. [21]).

Equation 5.1 can be re-arranged as follows:

$$\Delta P = U \left(\frac{\eta L}{abF} \right) \quad (5.2)$$

There is an analogy between the flow in a tube and flow of electricity through a wire.

Since Ohm's law for electricity is

$$\Delta V = IR$$

then the parenthetic term in eq. 5.2 is analogous to resistance and its reciprocal is analogous to conductance. Thus the resistance to flow (r) in the channels can be defined by eq. 5.3

$$r = \frac{\eta L}{abF} \quad (5.3)$$

The fluid resistance of each channel is proportional to the length of channel and its cross-sectional areas, just as it is for electrolyte resistivity [18]. However, there is an additional geometric factor.

For devices used in this study (i.e., Faster and DARPA devices), some segments were either 240 or 275 μm wide at the top surface of the channel (see Table 2.1 and 2.2, Chapter 2); other channels were either 36 μm or 68 μm wide at the top surface. In order to easily compare the fluid resistance of channels with different cross sections, we expressed the wider segments as an equivalent length (l_{eq}) using eq. 5.4

$$l_{eq} = \frac{l_{true} A_{eq} F_{eq}}{A_{true} F_{true}} \quad (5.4)$$

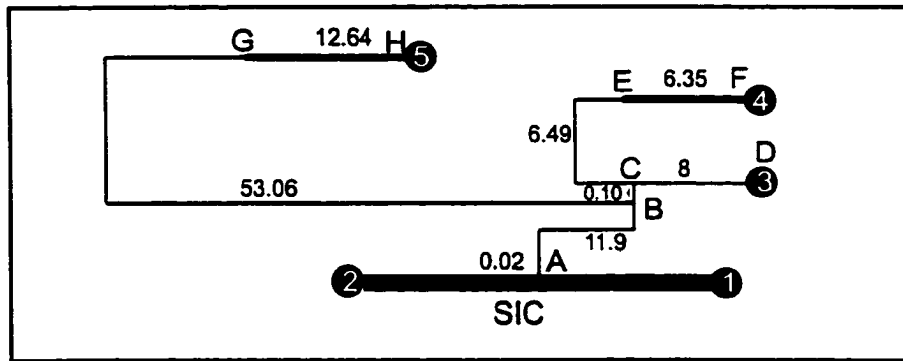
where A_{eq} is the cross-sectional areas of the 36- μm wide and 10- μm deep channel in the case of the Faster chip, or the 68- μm wide and 13- μm deep channel in the case of the

DARPA chip. A_{true} is the cross-sectional area of the channel after etching. F_{eq} is the geometric factor for the reference cross section. F_{true} is the geometric factor for the true half width and half depth of the larger channels after etching.

5.3.2 Preferential flow design and device testing

Figure 5.5A shows the layout of the Faster chip, showing the equivalent lengths of the wider channels (thicker lines) calculated using eq. 5.4. The dimensions of the channels were given in Table 2.2 (see Chapter 2). In order to compare the resistance to flow of the electrophoresis channels with the SIC, the total equivalent length of the electrophoresis channels should first be estimated. Therefore, we represented the electrophoresis channel of Faster chip as a network of resistors connected in series and in parallel as shown in Figure 5.5B. The estimated equivalent length of electrophoresis channels ($F_{\text{eq}} = 0.07638$, $F_{\text{true}} = 0.01352$) was 16.53 mm. Since the SIC of the Faster chip was 1 mm wide, 300 μm deep, and 20 mm long, the equivalent length of the entire SIC using eq. 5.4 ($F_{\text{SIC}} = 0.08109$, $F_{\text{eq}} = 0.07638$) was 0.0229 mm. Then, the resistance to flow of the narrow channels of Faster chip using eq. 5.3 was $2.14 \times 10^6 \text{ kg/m}^2 \text{ s}$ and for the SIC it was $2.97 \times 10^3 \text{ kg/m}^2 \text{ s}$. A value of 0.000891 kg/m.s was used for the viscosity at 298 K [22]. When sample comes to the branch point A in the SIC (Figure 5.5A) it will have a choice of directions. The fluid resistance associated with traversing the remaining of the SIC will be $1.48 \times 10^3 \text{ kg/m}^2 \text{ s}$. To enter the electrophoresis channels, the fluid faces a resistance of $2.14 \times 10^6 \text{ kg/m}^2 \text{ s}$.

(A)



(B)

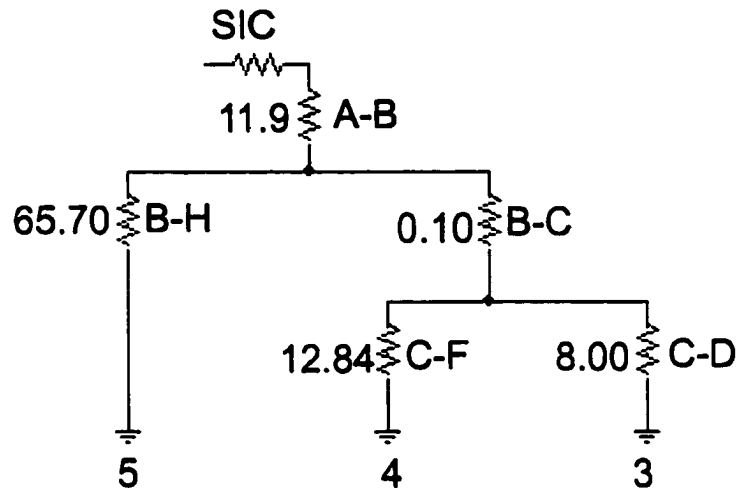


Figure 5.5 (A) Equivalent lengths of Faster layout. True lengths were given in Table 2.2 (see chapter 2). Thick lines were $240\ \mu\text{m}$ at the top and thin lines were $36\ \mu\text{m}$ at the top. SIC was $1000\ \mu\text{m}$ wide at the top and $300\ \mu\text{m}$ deep (B) Equivalent fluid resistance network of the shallow channels on the Faster chip. Channel lengths were converted to equivalent length of $36\ \mu\text{m}$ wide and $10\ \mu\text{m}$ deep channel using the equation $L_{\text{eq}} = L_{240} A_{36} F_{36} / A_{240} F_{240}$. Dimensions were given in mm.

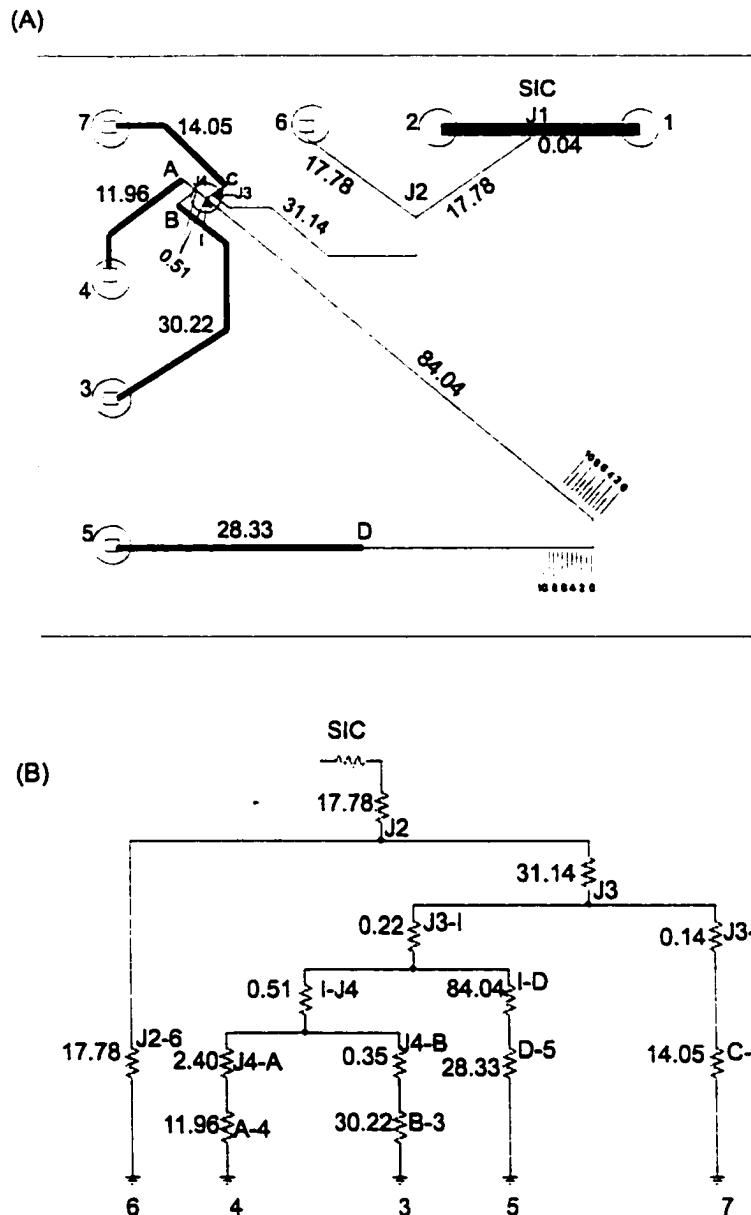


Figure 5.6 (A) DARPA layout. The feature lengths that define the lengths on the photomask were given in Table 2.1 (see Chapter 2). Thin lines were 68 μm wide and thick lines were 275 μm at the top surface. Channel lengths were converted to equivalent lengths of 68- μm wide and 13 μm deep channel using the formula $L_{\text{eq}} = L_{275} A_{68} F_{68} / A_{275} F_{275}$. Dimensions were in mm. (B) Equivalent fluid resistance network of the shallow channels on the DARPA chip.

The equivalent lengths of the DARPA chip are shown in Figure 5.6A. The electrophoresis channels of the DARPA chip were represented as a network of resistors, as shown in Figure 5.6B. The total equivalent length ($F_{eq} = 0.05604$, $F_{trac} = 0.01528$) of the electrophoresis channels was 29.76 mm. For the SIC of the DARPA chip, the equivalent length ($F_{eq} = 0.05604$, $F_{SIC} = 0.08109$) was 0.0387 mm. With these two values into eq. 5.4, the resistance to flow of electrophoresis channels of DARPA device was $2.14 \times 10^6 \text{ kg/m}^2 \text{ s}$ and for the SIC it was $2.78 \times 10^3 \text{ kg/m}^2 \text{ s}$. Again the SIC resistance to flow at point J1 is $1.39 \times 10^3 \text{ kg/m}^2 \text{ s}$. As we can see, the resistance to flow for the separation channels of the two devices were almost the same and much larger than that of the SIC. Hence, the fluid should preferentially flow through the SIC during sample loading, and only a minute amount should enter the segment A-B (the neck region) of the Faster design.

In a first simple experiment, we flushed 0.1 M KMnO_4 through the SIC channel of Faster device using a plastic syringe fitted into the channel via a trimmed Eppendorf pipet tip and applied the maximum thumb pressure to the syringe. Under a microscope, the dye was seen to extend into the neck region without entering the $36 \mu\text{m}$ wide region of the injection channel.

An earlier device design had the same layout as that shown in Figure 5.5A, but the SIC depth was the same as all the other channels ($10 \mu\text{m}$) and the width of the SIC was only $520 \mu\text{m}$ wide at the top surface. This gave an equivalent length ($F_{SIC} = 0.0063$, $F_{eq} = 0.07638$) for the SIC of 14.83 mm versus the 16.53 mm for the electrophoresis channels. The resistance to flow of the SIC was estimated as $1.92 \times 10^6 \text{ Kg/m}^2 \text{ s}$ and the resistance to flow of the SIC from point A was $0.96 \times 10^6 \text{ Kg/m}^2 \text{ s}$. In the same simple test, the dye quickly entered the entire injection channel as well as the remainder of the microchip.

While these experiments are not quantitative they do illustrate that manipulating the ratio of flow resistance on-chip can be used as a tool to control flow directions.

5.3.3 Exchanging of Phe-FITC and Arg-FITC solutions into the chip

Solutions of fluorescein isothiocyanate labeled arginine (Arg-FITC) and phenylalanine (Phe-FITC) were alternately loaded into the SIC and analyzed for cross-contamination. Figure 5.7 shows the results for switching between a Phe-FITC then an Arg-FITC sample solution. A single 6 μ l flush with the Arg-FITC solution was followed by a second 6 μ l loading of the same solution to fill the sample channel. Complete exchange is evidenced by the absence of any peak for Phe-FITC at 31 s in the subsequent Arg-FITC. Exchange back to Phe-FITC was also complete after one 6 μ l flush and one 6 μ l sample for loading. Attempts to remove the previous sample under vacuum and introduce a new sample without a rinse step produced 30 % contamination in the next electropherogram.

An effort was also made to reduce the length of time required to flush the narrow injection channel along the segment A-B, i.e., the loading from the SIC to the sample injection region. To increase the fluid velocity, the flushing voltage was increased to -3 kV. The effect of flush time was evaluated in a series of experiments in which first Phe-FITC then Arg-FITC was introduced into the SIC between each injection channel flush. A single sample channel flush, followed by a 6 μ L sample plug was used for each exchange. Separation was performed with a field of 476 V/cm, with -3 kV applied between reservoirs 4 and 5 (reservoir 4 at ground).

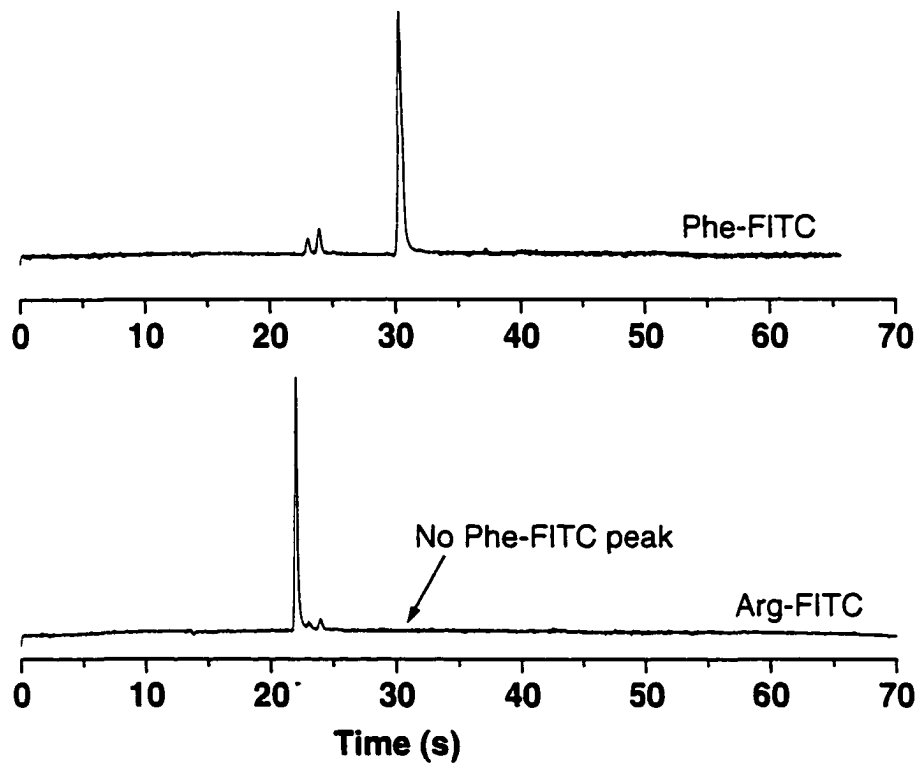


Figure 5.7 Electropherograms of Phe-FITC and Arg-FITC acquired from the sequence in Figure 5.1. The exchange was evidenced by the absence of Phe-FITC in the Arg-FITC electropherogram.

A series of experiments were carried out for which the injection channel flush times varied from 5 to 20 s. The Phe-FITC peak was reduced to about 16 % of its initial value after only 5 s, while a 20 s flush ensured complete elimination of Phe-FITC solution from the injection channel path. It must be noted that the electrically driven flush of the injection channel suffers from some leakage into the separation channel, so that the first sample plug to be separated was always excessively large. For this reason a second plug formation, obtained by applying -3 kV between reservoir 1 and 3 (reservoir 1 at ground) for 2 s was always performed, and the electropherogram of that plug was analyzed.

The observed mobility of Phe-FITC was $3.1 \times 10^{-4} \text{ cm}^2 \text{ V/s}$. Therefore, with an electric field strength of 1500 V/cm along the injection channel, the time required to flush the injection channel was estimated to be ca. 5 s. This time is considerably shorter than that actually required, 20 s. It is likely that the dead volume in the neck region at the interface between the sample and injection volume accounts for this discrepancy.

The reproducibility of the sample introduction and injection procedure was also evaluated. The two labeled amino acid solutions were alternately exchanged using the single 6 μL sample channel flush procedure, -3 kV for 20 s between reservoirs 1 and 3, followed by two injections and separations, with evaluation of the data for the second separation. For 5 replicate exchanges of each solution the relative standard deviation of the peak heights was $\pm 4\%$.

5.3.4 Calibration curve of fluorescein using on-line monitoring setup

A continuous on-line monitoring system was set up as described in the Experimental section. Fluorescein was added step-wise to an external beaker, and the solution was continuously pumped through the SIC. The flow rate was 1 ml/min, corresponding to a flow rate of ca. 5 cm/s inside the SIC.

Figure 5.8 shows the calibration curve for the peak area of fluorescein with the increase in the beaker's fluorescein concentration from 0.15 to 0.9 μM . The calibration curve gave a slope of $5.0 (\pm 0.2) \times 10^3 \text{ mV}/\mu\text{M}$ and a y-intercept of $-63 \pm 126 \text{ mV}$ with $R^2 = 0.996$. The results clearly indicate that the microchip with a SIC channel can continuously monitor changing concentrations over time in an external vessel.

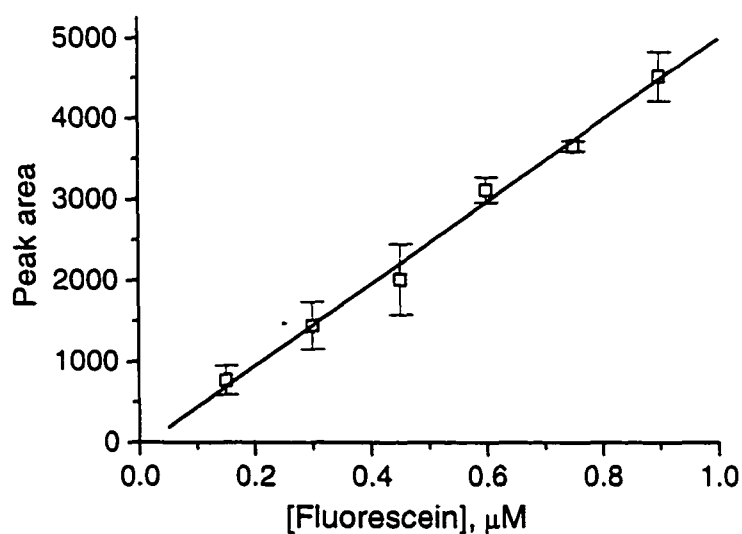


Figure 5.8 Calibration curve of fluorescein. Experimental conditions are given in the Experimental section.

5.3.5 Testing the SIC of the DARPA device

The DARPA device is an ideal μ TAS device since it combines all the elements required for an automated chemical analysis. We tested the performance of the SIC in the DARPA design for any leakage into the separation channels, using the same setup as in Figure 5.2. Since Cy5 dye was used, the 632.5 He-Ne laser was employed as a source of excitation. The emission signal was measured by a photomultiplier tube (PMT) using a 675 nm band pass filter. Cy5 solution (200 nM) was driven at a flow rate of 0.7 ml/min into the SIC for 3 min, and then the pump was stopped. The Cy5 sample in the SIC was injected by applying 1500 V for 15 s and then separated by using -6 kV applied between reservoir 5 and 3 (reservoir 3 at ground). The electropherogram is displayed in Figure 5.9A. We then turned the pump on at a flow rate 0.7 ml/min and Cy5 samples were continuously injected and separated by applying -1.5 kV between reservoir 1 and 3 (reservoir 1 at ground) for injection and -6 kV for separation between reservoirs 4 and 5 (reservoir 4 at ground). Figure 5.9B shows the electropherogram when the pump was on. The difference in migration time of the peak marked with an asterisk (Figure 5.9) when the pump is on versus off is due to the drift in electroosmotic flow which results from adsorption of Cy5 dye on the channel wall. We have mentioned in the Experimental section that rinsing the separation channel with running buffer before switching the pump could assist in removing any adsorbed species from the previous experiment and refresh the surface of the capillary wall. Therefore, the asterisk peak migrates faster because of the increase of electroosmotic flow.

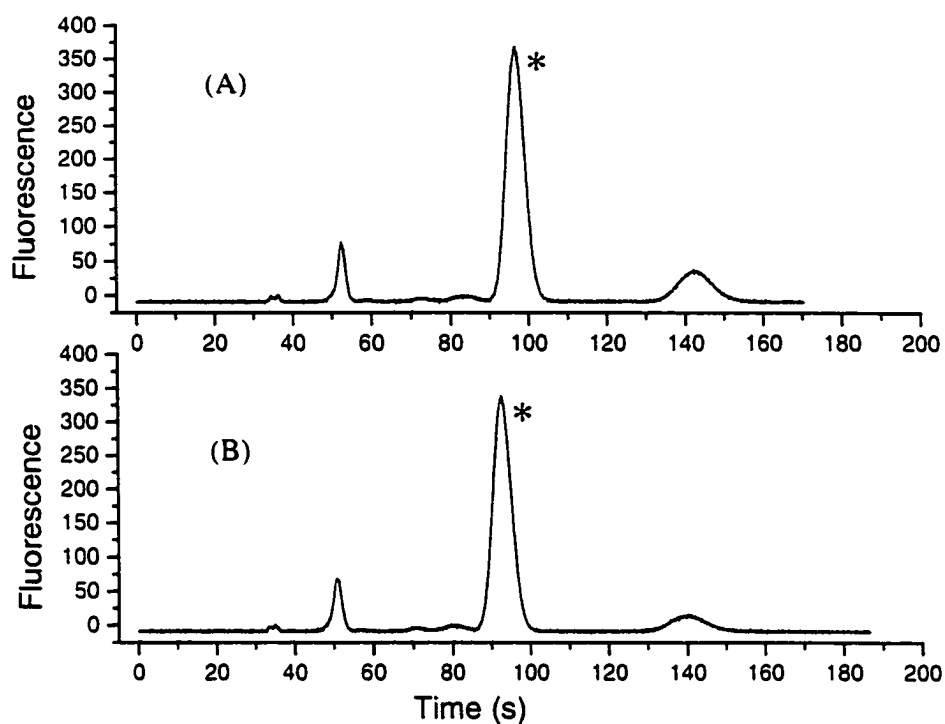


Figure 5.9 (A) Electropherogram of 200 nM bifunctional Cy5 dye when pump was off. The CE conditions: tris/boric acid (pH 9), injection voltage 1.5 kV for 10 s and separation voltage 6 kV, a 632.5 He-Ne red laser for excitation and 675nm emission filter. (B) Electropherogram of Cy5 dye when the pump was on under the same experimental conditions as (A). Peak analysis was performed on the peak marked with the asterisk.

When the pump was on, the average peak height of the asterisk peak (Figure 5.9A) of Cy5 was 358 ± 60 ($n = 7$); when the pump was off, the average peak height of the asterisk peak (Figure 5.9B) was 347 ± 42 ($n = 6$). We calculated Student's t-test at 95% confidence level to compare peak heights when the pump was on or off. For 11 degrees of freedom, the tabulated t-values (Table 4.2 Ref. 22) lie between 2.131-2.228 and the calculated value was 0.376. Therefore, the difference in peak heights with and without the pump on was not that significant. This data showed that the sample could be

continuously introduced by pressure-driven flow without significantly leaking into the device.

Poiseuille's law for a cylindrical cross section tubing is $U = \frac{\Delta p r^2}{8\eta L}$, where Δp is the pressure difference (dynes/cm²), and the length of tube is L (cm). U is the linear flow velocity in cm/s, r is the internal radius of the tube (cm), and η is in g/cm s. The length of the PEEK tubing (0.8 mm i.d., 1.6 mm o.d.) from reservoir 2 to the waste tube of the DARPA device was 40 cm, and the flow rate of the pump was 66 μ l/min. Then using Poiseuille's law for a cylindrical cross section tubing, pressure difference inside the tubing was 490 g/cm s². Assuming Δp for the electrophoresis channels with 29.76 mm equivalent length is 490 g/cm s², therefore the flow rate or leakage of Cy5 dye into the electrophoresis channels using eq. 5.1 becomes ca. 0.001 mm/s at a flow rate of 66 μ l/min within the SIC. The electroosmotic flow at a field strength of 208 V/cm for fluorescein with an observed electrophoretic mobility 3×10^{-4} cm V/s was 0.62 mm/s. Therefore, the back leakage from the pump was about 0.2% of the value of electroosmotic flow.

We received a series of bad batches of DARPA devices in which the SIC channel walls were not smooth when compared to SIC channels of the Faster device shown in Figure 5.3. As a result, an estimated 40% leakage of Cy5 dye solution into the narrow channels were observed. Although the SIC of the DARPA devices was rough its narrow channels were smooth. The roughness of the SIC in the DARPA device might be due to inefficiency of deep etching of SIC using the wet etching solution.

We expect that roughness of SIC could increase the resistance to flow of the SIC compared to the narrow channels, so that the leakage of fluid into the narrow channels may occur. Unfortunately the magnitude of the roughness on the resistance to flow could

not be estimated. Therefore, inspection of the SIC before employing it for continuous monitoring is essential.

5.4 Conclusions

We automated the microfluidic chip for sample loading by designing a microchip device in which one reservoir for sample loading was replaced by a 300 μm and 1 mm wide channel, called the sample introduction channel (SIC). Resistance to flow for the SIC was about 0.1% of the resistance to flow of the electrophoresis channels. As a result the sample could be continuously loaded using a pump without moving into the electrophoresis microchannels and contaminating them. Less than 30 s and 12 μl were required to remove Phe-FITC from the microchannels and obtain the electropherogram of Arg-FITC. However, this time could be further shortened either by eliminating the neck region connecting the SIC and injection channel or by increasing electric fields across the injection channel. We described a leak-free assembly in which the microchip can be easily interfaced with an external fluidic system and monitor the constant change in its concentration. Interfacing a microchip to the outside world is thus feasible.

5.5 References

- 1 H. Lüdi, M.B. Gran, P. Bataillard and H.M. Widmer, *J. Biotechnol.* , 14 (1990) 71.
- 2 G. Tschulena, *Phys. Scr.*, T23 (1988) 293.
- 3 N. Graber, H. Lüdi and H.M. Widmer, *Sens. Actuators*, B1 (1990) 239.
- 4 T.E. Edmonds, *Trends Anal. Chem.*, 4 (1985) 220.
- 5 G.G. Guilbault, *Anal. Chem Symp. Ser.*, 17 (1983) 637.
- 6 B.A. Shapiro, R.A. Harrison, R.D. Cane and R. Kozlowsky-Templin, *Clinical Application of Blood Gases*, Year Book Medical Publishers, Chicago, 1989.
- 7 K.E. Stinshoff, J.W. Freytag, P.F. Laska and L. Gill-Pazaris, *Anal. Chem.*, 57 (1985) 114R.
- 8 N. Chiem and D.J. Harrison, *Clin. Chem.*, 44:3 (1998) 591.
- 9 L.B. Koutny, D. Schmalzing, t.A. Taylor and M. Fuchs, *Anal. Chem.*, 68, (1996), 18.
- 10 A.G Hadd, D.E. Raymond, J.W. Halliwell, S.C. Jacobson and J.M. Ramsey, *Anal. Chem.*, 69 (1997) 3407.
- 11 D.J. Harrison, K. Fluri, K., Seiler, Z. Fan and C.S. and A. Manz, *Science* 61 (1993) 895.
- 12 D.J. Harrison, Z. Fan, K. Fluri, K. Seiler, in: Van den berg and A. Bergveld, (eds). *MESA Monographs: Micro Total Analysis System*, Kluwer Academic publishers, Dordrecht, 1995.
- 13 S.C. Jacobson, R. Hergenroder, J. Jr Moore, J. M. Ramesy, *Anal. Chem.*, 66 (1994) 4127.
- 14 C.L. Coyer, S.D. Mangru and D.J. Harrison, *J. Chromatogr.*, 781 (1997) 271.
- 15 K. Fluri, G. Fitzpatric, N. Chiem, D.J. Harrison, *Anal Chem.*, 68 (1996) 4285.

- 16 S.C. Jacobson, L.B. Kounty, R. Hergenroder, J. Jr. Moore, J.M. Ramesy. *Anal. Chem.*, 66 (1994) 3472.
- 17 J.V. Sweedler, J.B. Shear, H.A. Fishman, R.N. Zare, R.H. Scheller, *Anal. Chem.*, 63 (1991) 496.
- 18 K. Seiler, D.J. Harrison and A. Manz, *Anal. Chem.*, 65 (1993) 1481.
- 19 Z. Fan and D.J. Harrison, *Anal. Chem.*, 66 (1994) 177.
- 20 P.A. Longwell, *Mechanics of Fluid Flow*, McGraw Hill, New York, (1966) 140.
- 21 J.H. Perry, *Chemical Engineers Handbook*, 3 rd., McGraw Hill (1950) 3485.
- 22 P.W. Atkins, "*Physical Chemistry*", W.H. Freeman and Company, N.Y., 1994.

Chapter 6

Conclusions

One goal of this thesis was to develop a reproducible synthesis process for labeling an antibody without sacrificing its activity. The labeled antibody was used for the development of an ovalbumin assay on a glass electrophoresis chip. The other objective was to interface a glass chip to an external fluid, so that automated liquid delivery to and from the chip became feasible. The goals have been achieved and, based on the data obtained the single channel microchip-CE instrument (DARPA box) was developed. The purpose of this chapter is to summarize the main conclusions gained from this work and to suggest future directions of research projects involved in this thesis.

6.1 Summary

In Chapter 2, we briefly described the microchip-based CE instrument, the DARPA box (Figure 2.5) for biochemical analysis. We used CE to monitor the interaction of non-labeled polyclonal antibody and ovalbumin. The complex and the free affinity probes were separated by CE. A linear calibration curve for ovalbumin assay was obtained. However, labeled monoclonal antibody with Cy5 dye did not show any affinity for the ovalbumin when the experiments were repeated using CE with laser induced fluorescence (LIF) detection.

In Chapter 3, a critical development for performance of the ovalbumin assay was a scheme for labeling the antibody without sacrificing its active site; we used Affinity Protection Chromatography (APC). In this approach, we immobilized ov on activated CNBr-Sepharose 4B matrix. The coupling efficiency of ovalbumin on this matrix was >95%; the antibody was added to form an immobilized complex with the ovalbumin. In

this manner the antibody can be labeled without reacting with its recognition sites and labeling with Cy5 dye occurs elsewhere on the antibody. With this APC approach we synthesized homogenous and active labeled antibody. APC is reproducible and the synthesis takes 1 day using purified antibody as a starting reagent. The other important feature of APC is that it saves a considerable amount of time and labor in developing a labeled antibody.

We measured the affinity constant of the monoclonal antibody to ovalbumin (Chapter 4) using nonequilibrium CE. The results showed the native antibody had a low binding constant for the ovalbumin of $0.33 (\pm 0.02) \times 10^6 \text{ M}^{-1}$. Knowing about the low affinity constant of the antibody helped in improving the yield of labeled antibody using APC, and also explained the lower detection limit of ovalbumin using the DARPA instrument.

We addressed an important key element required for the μ TAS concept, which is sample introduction into the chip. We demonstrated a simple way to load the sample into the microchip. We used microchips that had channels 1 mm wide and 0.3 mm deep, for loading the sample. The electrophoresis channels, where the separation occurs, were 36 μm wide and 13 μm deep, or else 30 μm wide and 10 μm deep. We exploited the drastic difference in resistance to flow to manipulate the flow in the sample introduction channel without contaminating the electrophoresis channels. We utilized the SIC to exchange two test samples, Phe-FITC and Arg-FITC, into the chip. The results showed that the sample throughput is 1 sample/30 s. We interfaced the microchip to an external fluid reservoir to monitor the constant change from 0.15-0.9 μM in fluorescein concentration. A linear calibration curve was obtained. The interface is a leak-free assembly that

consists of the SIC, peristaltic pump, chromatographic fittings and plastic tubing and two plexiglass plates. Our results clearly showed that the concept of a lab-on-chip is within reach.

6.2 Future directions

6.2.1 APC for labeling antigens

It is important to further investigate the affinity protection chromatography demonstrated in this thesis. For example, labeling an antigen such as ovalbumin could be a good demonstration. Other antibodies or antigens with higher affinity constant than anti-ovalbumin could be labeled using APC using different labeling reagents such as fluorescein isothiocyanate (FITC) or rhodamine isothiocyanate (RITC), since these are less costly than Cy5 dye.

6.2.2 Preconcentration and labeling on microchips

Oleschuk et al. [1] have recently demonstrated the use of a solid phase extraction (SPE) concentrator on-chip for on-line preconcentration of BODIPY 493/503. The authors used a microchip design that had 200 μm wide sample cavity and two weirs, 9 μm high, for trapping octadecylsilane coated silica beads (1.5-4 μm diameter) as shown in Figure 6.1.

We propose a microchip design, Figure 6.2, that allow us to mix reagent and to load immunosorbent. The idea is to use a sample chamber containing immobilized antigen as a preconcentrator to selectively extract specific antibody from biofluid. By introducing labeling reagent into the solution buffer, the trapped antibody could be derivatized within the sample chamber. After a suitable period of time the excess

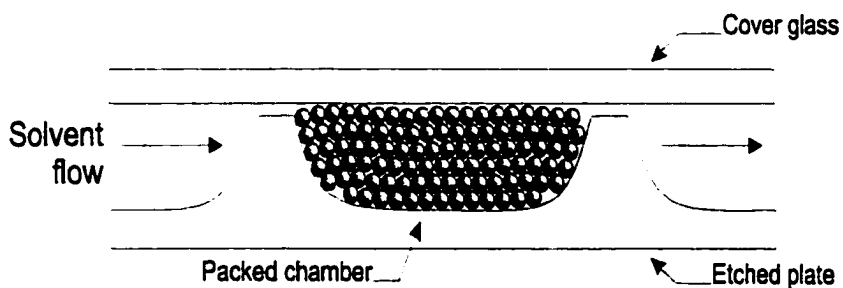


Figure 6.1 Drawing of cross-section of packed chamber, showing weir heights in relation to channel depth and particle size. Electroosmotic flow is driven by walls and by free groups on particles. Solvent flow direction is indicated for preconcentration step. (Adapted from Ref. 6.1).

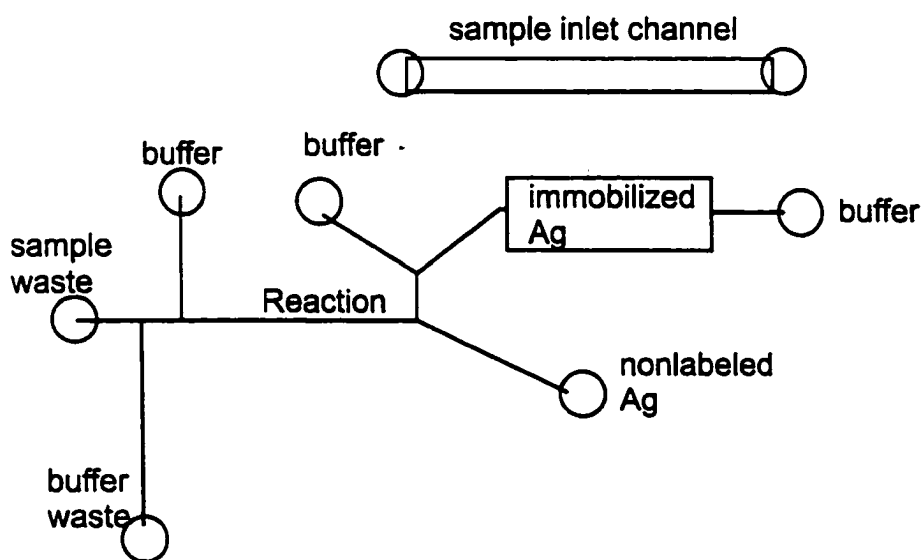


Figure 6.2 Proposed microchip design for preconcentration, derivatization, reaction, and detection of an antibody.

reagent could be eluted with a change in the ionic strength or pH of the elution buffer in order to release the now tagged antibody. The labeled antibody could then be mixed with nonlabeled antigen on chip for detection. This is potentially a solution to the generic problem of derivatization of proteins in biofluid at trace levels [2].

References

- 6.1 R.D. Oleschuk, L.L. Shultz-Lockyear, Y. Ning and D.J. Harrison, *Anal. Chem.*, in print.
- 6.2 I.S. Krull, R. Strong, Z. Sosic, B.-Y. Cho, S.C. Beale, C.-C. Wang and S. Cohen, *J. Chromatogr. B*, 699 (1997) 173.